Model-based Design, Operation and Control of Pressure Swing Adsorption Systems

A thesis submitted to Imperial College London

for the degree of Doctor of Philosophy

by

Harish Khajuria

Center for Process System Engineering, Department of Chemical Engineering, Imperial College London, United Kingdom

November, 2011

Declaration of Originality

I hereby declare that this is my own work and any published and unpublished work used here has been cited in the text, and the list of references in the bibliography section at the end of thesis.

Harish Khajuria

Abstract

This thesis is concerned with the design, operation and control of pressure swing adsorption (PSA) systems, employing state of the art system engineering tools. A detailed mathematical model is developed which captures the hydrodynamic, mass transfer and equilibrium effects in detail to represent the real PSA operation.

The first detailed case study presented in this work deals with the design of an explicit/multi-parametric model predictive controller for the operation of a PSA system comprising four adsorbent beds undergoing nine process steps, separating 70 % H_2, 30 % CH_4 mixture into high purity hydrogen. The key controller objective is to fast track H_2 purity to a set point value of 99.99 %, manipulating time duration of the adsorption step, under the effect of process disturbances. To perform the task, a rigorous and systematic framework is employed comprising four main steps of model development, system identification, the mp-MPC formulation, and in-silico closed loop validation, respectively. Detailed comparison studies of the derived explicit MPC controller are also performed with the conventional PID controllers, for a multitude of disturbance scenarios.

Following the controller design, a detailed design and control optimization study is presented which incorporates the design, operational and control aspects of PSA operation simultaneously, with the objective of improving real time operability. This is in complete contrast to the traditional approach for the design of process systems, which employs a two step sequential method of first design and then control. A systematic and rigorous methodology is employed towards this purpose and is applied to a two-bed, six-step PSA system represented by a rigorous mathematical model, where the key optimization objective is to maximize the expected H_2 recovery while achieving a closed loop product H_2 purity of 99.99 %, for separating 70 % H_2, 30 % CH_4 feed. Furthermore, two detailed

comparative studies are also conducted. In the first study, the optimal design and control configuration obtained from the simultaneous and sequential approaches are compared in detail. In the second study, an mp-MPC controller is designed to investigate any further improvements in the closed loop response of the optimal PSA system.

The final area of research work is related to the development of an industrial scale, integrated PSA-membrane separation system. Here, the key objective is to enhance the overall recovery of "fuel cell ready" 99.99 % pure hydrogen, produced from the steam methane reforming route, where PSA is usually employed as the purification system. In the first stage, the stand-alone PSA and membrane configurations are optimized performing dynamic simulations on the mathematical model. During this procedure, both upstream and downstream membrane configuration are investigated in detail. For the hybrid configuration, membrane area and PSA cycle time are chosen as the key design parameters. Furthermore, life cycle analysis studies are performed on the hybrid system to evaluate its environmental impact in comparison to the stand-alone PSA system.

Acknowledgements

I would like to sincerely thank my PhD supervisor Professor Stratos Pistikopoulos for providing consistent support and feedback during the course of my PhD. His passion for work, sharp research acumen and great leadership qualities have always inspired me to strive for extra and make my own mark. I am also grateful to him for motivating me to actively participate in several collaborative research projects, inside and outside the department, helping me to acquire new skill sets.

I would also like to acknowledge the financial support received from the Royal Commission for the Exhibition of 1851, ParOS Ltd., EPSRC and the EU project Hy2SEPS.

My sincere gratitude to the dedicated staff members of CPSE - Senait, Christina, and Graham, who were always ready to help and made things easier at work. Special thanks to Terrence for helping me with my gPROMS-MATLAB experiments.

My lab friends made my stay at the Imperial a memorable one. I would like to thank all of them, especially Kostas, Pei, Martina, Romain, Anna, Jerry, and Waqas, for all those moments.

I would like to express my deepest gratitude to my parents for always motivating me from an early age to try out new things. I could not have reached this stage without their support and encouragement. Finally, a special thanks to my wife Himani and my little hero Aarnav. You mean everything to me.

Contents

List of Tables

List of Figures

Nomenclature

Physical and Mathematical Quantities

A_{bed}	Bed area	m^2
C	Gas phase molar concentration	mol/m^3
C_p	Gas phase molar specific heat at constant pressure	J/mol K
C_v	Gas phase molar specific heat at constant volume	J/mol K
C_{p_s}	Adsorbent phase specific heat	J/kg K
C_{p_w}	Column wall specific heat	J/kg K
CV	Valve Cv coefficient	
d_P	Process design decision variables	
d_c	Controller design decision variables	
d_p	Particle diameter	mm
D	Bed diameter	m
D_m	Molecular diffusion coefficient	m^2/s
D_z	Axial dispersion mass transfer coefficient	m^2/s
H_p	Prediction horizon for the MPC optimization problem	
H_u	Control horizon for the MPC optimization problem	
K_{LDF}	LDF rate constant	1/s
k	Sampling instant	

Kc	Proportional gain for PI controller	
K_g	Gas phase thermal conductivity	W/K m
L	Bed Length	m
MW	Molecular weight	kg/mol
P	Bed Pressure	Pa
Q^*	Adsorbed phase concentration in equilibrium with bulk gas	mol/kg
$\overline{Q}$	Volume averaged adsorbed phase concentration	mol/kg
Q^{max}	Maximum adsorbed phase concentration in equilibrium with bulk gas	mol/kg
R	Ideal gas constant	J/mol K
RU	Weight constant for the MPC ΔU term	
t	Time	s
Δt_s	Sampling interval	
T	Gas or solid phase temperature	K
u	Controller output or process input variables	
U	Superficial velocity	m/s
v	Operational decision variables	
$\dot{xd}$	Differential variables	
xa	Algebraic variables	
y	Controlled or process output variable	
z	Axial position	m
Δd_w	Column wall thickness	
ΔH	Heat of adsorption	J/mol

Greek notations

γ	Lagrange multiplier	
ϵ_b	Bulk phase porosity	
ϵ_p	Particle phase porosity	
ε_d	Design tolerance	
ε_c	Control tolerance	
ε_{CSS}	CSS tolerance	
θ	Parametric uncertainty	
λ	Axial heat dispersion coefficient	W/m K
μ	Gas phase viscosity	kg/m s
τ_I	Integral time constant for PI controller	s
ρ_p	Particle density	kg/m^3
ρ_w	Column wall density	kg/m^3

Subscripts

i	Gaseous species
ads	Adsorption step of PSA cycle
$blowdown$	Blowdown step of PSA cycle
$codep1$	First co-current depressurization step of PSA cycle
$codep2$	Second co-current depressurization step of PSA cycle
$codep3$	Third co-current depressurization step of PSA cycle
f	Final value
$feed$	Feed step of PSA cycle or feed conditions
$purge$	Purge step of PSA cycle
$pe1$	First pressure equalization step of PSA cycle
$pe2$	Second pressure equalization step of PSA cycle
$repress$	Re-pressurization step of PSA cycle
s	Solid phase property

Chapter 1

Introduction

Pressure swing adsorption (PSA) is at the forefront of gas separation technology. Since its commercial inception in late 1950s, PSA technology has evidenced substantial growth in terms of size, versatility and complexity [137, 174]. Modern PSA systems, used widely in the gas separation industry can vary from two adsorbent bed separating air, to sixteen bed system producing pure hydrogen in excess of 100,000 Nm^3/hr [170]. However, despite the sharp growth and technological developments, PSA design process is still strongly dependent upon experimental procedures [146] to test and evaluate the impact of various design and operational decisions on its real time performance. The primary reason for this is the level of complexity a PSA exhibits during the operational stage while on the other hand also offering great flexibility at both design and operational stages, requiring careful selection of important decision variables.

PSA inherent dynamic nature is attributed to its periodic operation, where each bed in the PSA assembly undergoes a fixed sequence of processing steps, repeated in a cyclic fashion for achieving desired product purity (high pressure) as well as adsorbent regeneration (low pressure), simultaneously. The dynamic transition from one processing step to another for a given bed is performed by a

network of bed-interconnecting switch valves, whose active status keeps changing over the period of time. Consequently, the timing of these valves in turn controls the duration of process steps that each PSA bed undergoes in one cycle.

The dynamic operation also has a profound effect on the gas-solid hydrodynamics inside the packed bed. The strong interplay between the equilibrium and kinetic mechanisms is significantly effected by the changing bed pressure levels and transient boundary conditions. From the modeling point of view, variables vary both in spatial and time coordinates leading to a partial differential algebraic equation (PDAE) system.

A further manifestation of the periodically operating steps is that the PSA system never attains a true steady state. This is in sharp contrast to other kind of dynamic processes, where steady state is reached after the system runs for certain amount of time. In comparison, PSA exhibits the characteristic of cyclic steady state (CSS), which refers to a state in time when the system variables are same at the start and end of a cycle. The computation of CSS, which often requires the simulation of hundreds of cycles incorporating a rigorous nonlinear PSA model, poses an extra challenge towards the design, optimization and control of PSA.

A key aspect of the usage of model based methods for the optimal design and control of process systems is the associated trade-off between the design method and model complexity vs. the relative ease of obtaining solution. In this regard, the application of rigorous optimization based approaches to inherently dynamic and highly nonlinear systems like PSA still remains a challenging task, and is the main focus of this thesis. In this work, advanced and rigorous system engineering tools are employed for obtaining better operation and control of PSA systems, while simultaneously providing useful insights about the PSA systems.

It is important to note that the real time performance of PSA is usually evaluated in terms of product recovery achieved, while maintaining the system to

operate at the desired purity levels under the effect of disturbances and uncertainties. From the operational perspective, the main product losses during the PSA cycles, which reduces the system recovery, happens during the adsorbent regeneration stages of cycle. The fact that off-gas stream leaving the PSA system, in addition to containing impurity components, also has significant amount of product component, points towards the possibility of PSA integration with other separation devices such as membranes to improve the overall product recovery. Therefore, in addition to the optimal design and control of stand alone PSA configurations, process integration schemes towards the design of hybrid PSA-membranes systems are also investigated in detail. In the next section, a short summary of the thesis is provided.

1.1 Thesis Outline

- In Chapter 2, the basics of PSA operation are introduced. The key performance indicators are defined, followed by discussion on different types of PSA configurations, involving various combination of beds and processing steps. Next, the significance and role played by various cyclic steps of a multi-bed PSA cycle are described in detail. Finally, a brief overview of alternative gas separation methods such as membrane and cryogenic distillation separation is provided.

- Chapter 3 describes the important features of the rigorous mathematical model of PSA considered in this work for optimization and control purposes. The underlying assumptions are clearly stated and various methods towards the mathematical evaluation of CSS are also defined.

- Chapter 4 presents a detailed case study towards the design of an explicit/multi-

parametric MPC (mp-MPC) controller design for the PSA purity control. To start with, the concept of multi-parametric model predictive control (mp-MPC) extending from the MPC optimization framework is explained. The main steps involved in the functioning of both controller modes are also discussed. Next, the mp-MPC controller design procedure following a step by step framework is explained. Finally, the results obtained from the comparison of closed loop performance of mp-MPC with the standard PID controllers are demonstrated.

- In Chapter 5 a simultaneous optimization and control strategy for PSA operation under uncertainty is presented. First, a detailed literature overview of historical as well as the current state-of-the-art optimization based methodologies for simultaneous design and control of process systems under uncertainty is presented. Furthermore, detailed comparisons are also drawn among the key PSA optimization methodologies. Next, details of the key challenges involved in design, operation and control of PSA system are provided and incorporated into a simultaneous design and control optimization framework. Furthermore, detailed comparisons are also drawn with the conventional sequential design and control approach and explicit/multi-parametric MPC as the controller mode.

- Chapter 6 provides design heuristics for the integration of PSA-membrane system for improving hydrogen overall recovery as compared to stand-alone PSA system. Here, details of stand alone membrane and PSA configurations are discussed first, which eventually assist in preparing a good base case for the hybrid. Finally, life cycle analysis of hybrid process is also performed to evaluate its environmental impact.

- In Chapter 7 important conclusions and potential future directions from

this thesis are presented.

Chapter 2

Pressure Swing Adsorption Processes

2.1 Introduction

A search in the Chemical Abstract Services (CAS) database for "Pressure Swing Adsorption" results in 5200 articles, including including patents and research journals. Figure 2.1 shows the time evolution of the annual number of such contributions from the year 1966 to 2010. The plot clearly highlights the rapid growth this technology is evidencing since its commercial inception, while also indicating the strong interest shown by both industry and academia in this field. The primary reason for such a dramatic growth appears to be widely varying application of PSA system for separation of numerous classes of gaseous mixture. Table 2.1 outlines a brief overview of the variety of PSA separations that has been reported in the previous literature studies. Here, in addition to providing bulk separation and high purity separation involving conventional gases, new and unique PSA applications are emerging in the field of beauty and performance chemical industries.

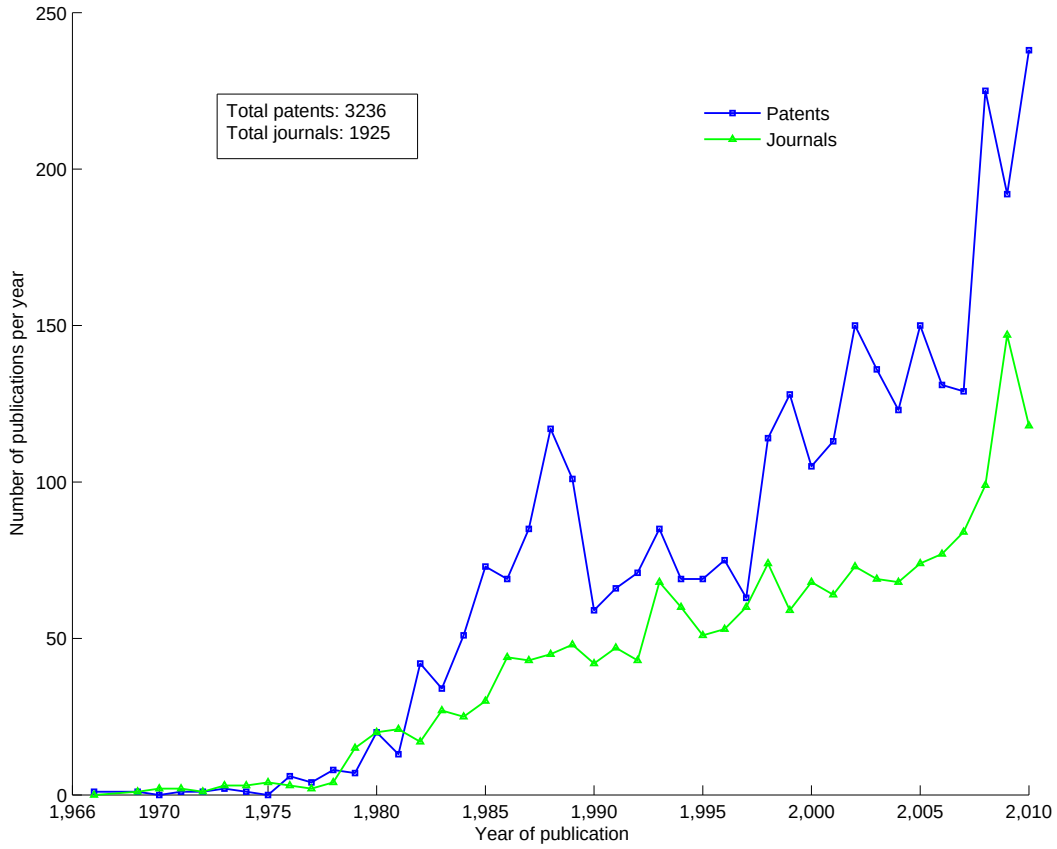

Figure 2.1: Yearly distribution of patent and research publications in the field of PSA technology

Table 2.1: A brief overview of PSA applications reported in the open literature

Authors	PSA applications
[77, 34, 54, 155, 101, 128, 65]	CO_2 recovery from industrial flue gas and CO_2 sequestration
[180, 179]	NO_x removal from exhaust gases
[11, 172, 94, 165, 176]	H_2 purification
[132, 127]	Air purification
[74, 46, 53, 109, 28]	Methane or natural gas recovery
[62, 147, 145]	Air separation - O_2 production
[27, 169, 4]	Air drying
[181]	CO purification from CO-CO_2-N_2
[31, 112]	Ethylene recovery
[126, 60]	Propylene recovery
[75, 76]	SO_2 recovery
[55, 140]	Citrus oil recovery (extraction) employing supercritical CO_2 as solvent
[115]	Volatile organic compounds (VOC) recovery from gasoline storage system
[166]	Separation and recovery of α-Tocopherol (anti-oxidant) and Squalene (emollient agent) employing super critical CO_2 as solvent

2.2 Separation Principle

The key separation principle used in a PSA operation is based on adsorption phenomena. Adsorption, in general can be defined as a process where the molecules or atoms of a single or multi-component fluid system in liquid, gas or even a super-critical phase tends to concentrate at the surface of a solid surface, under the effect of intermolecular interactions among the fluid (adsorbate) and solid phase (adsorbent). If the strength of interactive forces between the adsorbent and the fluid system is very strong, resulting in a electron transfer driven bonding, the phenomena is called chemisorption. On the other hand physisorption, or physical adsorption results when the surface forces between the adsorbent and the fluid system are rather weak and involve only weak natured electrostatic interactions. PSA processes are usually employed for gas-solid system exhibiting physisorption, where both fast adsorption and desorption at the adsorbent surface is realized by changing the pressure levels inside the bed.

In general, PSA separation processes are broadly classified in two categories, equilibrium based separation and mass transfer kinetics driven separation, depending upon which of these mechanism is playing the limiting role. Equilibrium based PSA separations exploits the equilibrium adsorbed phase concentration relationship of the impurity with its bulk phase partial pressure. The adsorbent material is designed to have the least affinity for the product component. The pressure during the adsorption step is kept at the highest level in order to increase the adsorbed amount of impurities, leading to enrichment of product component in the gas phase, while regeneration is performed at significantly lower pressure allowing the impurities to desorb back to the gas phase and be taken out of the bed. It is important to note that the mass transfer rate of all the species can be quite similar in pure equilibrium driven separation. On the other hand, in kinetic

driven separation, the mass transfer rates of the components from the bulk phase to the adsorption site are exploited through the suitable selection and design of adsorbent pore characteristics for the given gaseous species, in order to achieve an effective separation.

2.2.1 PSA performance indicators

A challenging task in comparing various process alternatives and design options for PSA systems is the quantification of their performance. In this regard, the knowledge of capital and operating costs provides an accurate account of the monetary value associated with the plant installation and operational features. An alternative approach, which does not require detailed information of the pricing and manufacturing data involves measuring other important performance indicators such as recovery, purity and productivity [136].

In past PSA studies, the combination of product recovery and purity, defined in equations 2.1 and 2.2, has been extensively used to benchmark different processes. Product purity is usually set by the customer requirements while recovery is to be maximized at the specified purity levels. In most of the PSA systems, this leads towards a trade-off situation as design changes to improve product recovery adversely effects the system purity.

$$\text{Product recovery} = \frac{\text{Amount of component in the product stream}}{\text{Amount of component in the feed stream}} \tag{2.1}$$

$$\text{Product purity} = \frac{\text{Amount of component in the product stream}}{\text{Total amount of product stream}} \tag{2.2}$$

It is to important to note that product recovery and purity have a strong effect on operating costs related to the production, as their definitions incorporates the information of both feed and the product streams. On the other hand, capital

cost due to the use of expensive adsorbents can also be quite significant. Towards this purpose, adsorbent productivity, defined in Eq. 2.3 is usually measured, which also captures the effective time utilization of the adsorbent under study.

$$\text{Adsorbent productivity} = \frac{\text{Amount of product component produced per cycle}}{(\text{Amount of adsorbent used})(\text{PSA cycletime})} \tag{2.3}$$

2.3 Types of PSA Cycle

A PSA system usually comprises of two or more adsorbent-filled beds interconnected to each other via a network of switch valves, which in turn controls the simultaneous operation of product purification and adsorbent regeneration steps. Therefore, a multiple bed assembly is used to ensure a constant supply of product, while the other beds are in the regeneration mode. The most commonly used PSA configurations are listed next with detailed description.

2.3.1 Skarstrom Cycle

This is perhaps one of the most commonly used PSA cycle in practice for small scale gas separation applications. In his original work, Skarstrom [137] employed this for equilibrium based air drying applications. The cycle involves only 2 beds performing the following four basic steps:

1. Cocurrent Pressurization with feed
2. Adsorption with feed
3. Countercurrent blowdown
4. Countercurrent purge with product

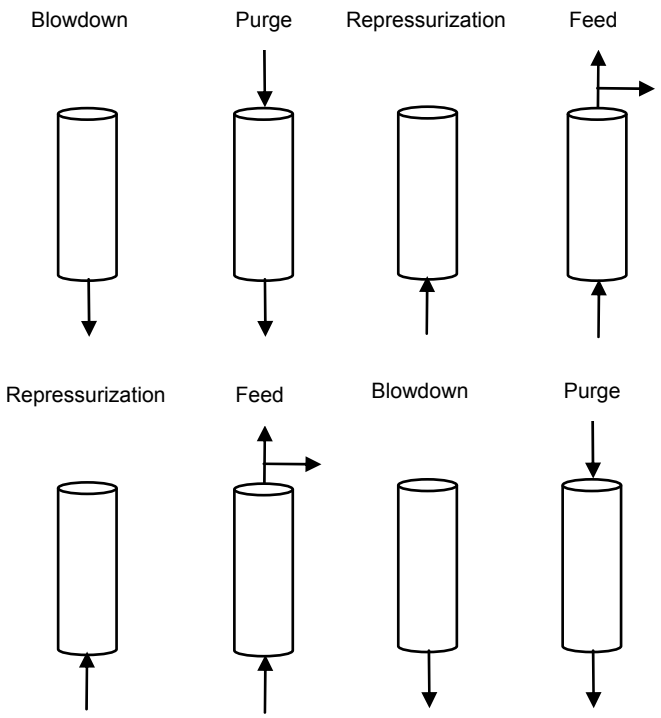

Figure 2.2: Two-bed, four-step Skarstrom cycle

In particular, the counter-current purge is provided by drawing off a product side stream undergoing adsorption step (see Figure 2.2), making the assembly self-sufficient in terms of any input from the external sources.

2.3.2 Vacuum Swing Cycle

A vacuum swing cycle (VSA) while employing exactly the same cyclic steps of Skarstrom cycle, differs from it in terms of using vacuum to regenerate the bed in the purge step, instead of the product itself. As shown in Figure 2.3, during the purge step, the product end remains closed while the feed end is connected to vacuum in order to remove the strongly adsorbed component. Furthermore, the omission of a dedicated product side stream for purging purpose, enhances the product recovery as well. However, this is only achieved at the expense of higher compression cost and is beneficial when the feed pressure is not significantly higher

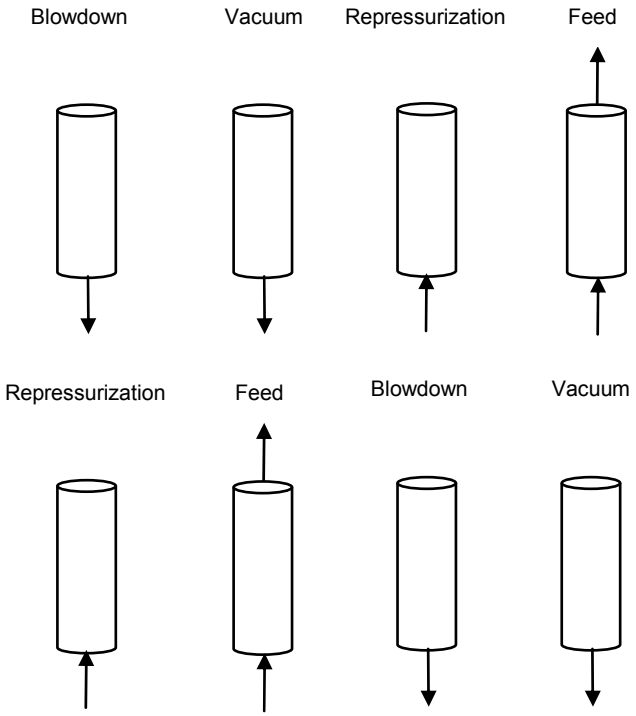

Figure 2.3: Two-bed, four-step vacuum swing adsorption cycle

than the atmospheric pressure.

2.3.3 Rapid Pressure Swing Cycle

Rapid pressure swing adsorption (RPSA) cycle is one of the simplest version of PSA cycle, and involves only a single bed undergoing the following two steps:

1. Cocurrent pressurization with feed - adsorption step

2. Depressurization step

The basic idea behind RPSA is to improve the adsorbent productivity (Eq. 2.3) by reducing the overall cycle time. In the first step, both repressurization with feed and adsorption with feed, are lumped together, leading to a overall shorter duration processing step in order to ensure desired product purity. In the next step, as shown in Figure 2.4 the product recovery continues along side the impurity removal at the feed end, as the pressure inside the bed reduces.

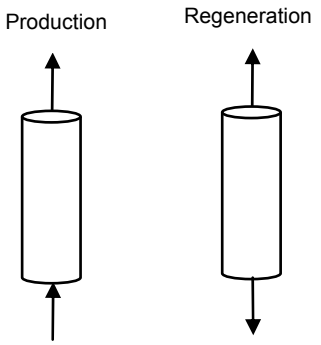

Figure 2.4: Two bed, four step, rapid pressure swing adsorption cycle

2.3.4 Multi-bed PSA

Most of the modern PSA systems, in addition to the four basic steps, also have extra depressurization steps (see Figure 2.5) between the end of adsorption step and start of the regeneration step, and the corresponding pressure equalization steps between the end of regeneration step and start of the re-pressurization step. The main purpose of these steps is to properly utilize the high pressure product towards the bed end for pressurizing other columns. The number of such steps is highly dependent on the number of beds involved in a given PSA cycle. Furthermore, there are also examples of PSA cycles, which contains an extra *idle* step [165] , in addition to the above mentioned steps. During this step, there is no inflow or outflow of fluid from the PSA bed. The most important reason for inclusion of this step is to allow necessary time to synchronize the multiple bed assembly. However, it is important to note that this will inevitably cause the PSA productivity to go down.

2.3.5 Rotary Valve Pressure Swing Adsorption

A recent addition to the PSA family is the rotary valve based PSA technology from Xebec Adsorption Inc [35], as depicted in Figure 2.6 [1]. In contrast to the

[1]Retrieved from http://www.chemicalprocessing.com/articles/2003/322.html

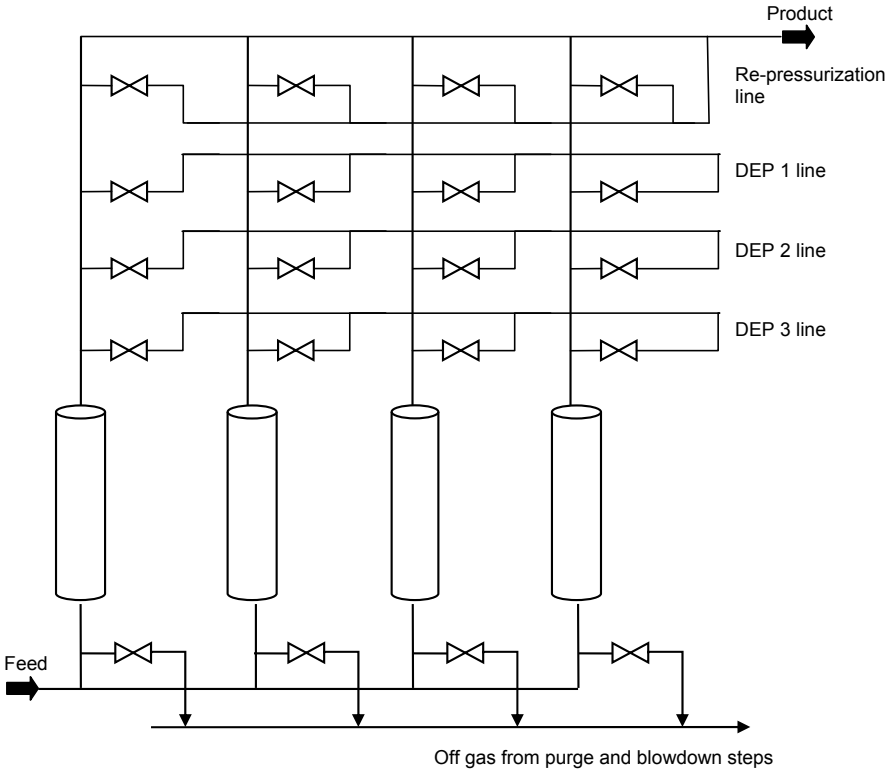

BED 1	FEED			DEP 1	DEP 2	DEP 3	Bd	Pu	PE 1	PE 2	REPRES
BED 2	PE 2	REPRES		FEED			DEP 1	DEP 2	DEP 3	Bd	Pu	PE 1
BED 3	Bd	Pu	PE 1	PE 2	REPRES		FEED			DEP 1	DEP 2	DEP 3
BED 4	DEP 1	DEP 2	DEP 3	Bd	Pu	PE 1	PE 2	REPRES		FEED		

Figure 2.5: Four-bed, 9-step multi-valve PSA configuration employed for this study. FEED: production step; DEP1: first co-current depressurization; DEP2: second co-current depressurization; DEP3: third co-current depressurization; Bd: counter-current depressurization or blowdown; Pu: counter-current purge; PE 1: first co-current pressure equalization; PE 2: second co-current pressure equalization; REPRES: counter-current re-pressurization with product.

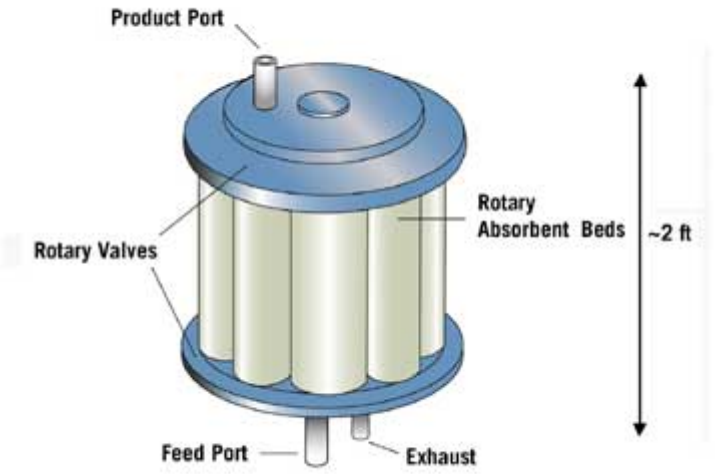

Figure 2.6: Rotary valve based pressure swing adsorption system from Xebec Adsorption Inc.

beaded adsorbent employed in the conventional PSA systems, this configuration uses structured adsorbents to allow very high fluid velocity across the packed bed. Consequently, hardware safety mechanism are installed to avoid fluidization. At the heart of the technology is the rotary valve system to direct flow between the beds during the PSA cycle, which is in sharp contrast to the switching valve method employed in the traditional PSA system. The combination of structured adsorbent and rotary valve set up paves the way for very fast PSA cycles, with a fraction of size of a more conventional PSA system.

2.4 Detailed Description of PSA Cyclic Operation

In order to gain further understanding of the PSA periodic operation, each processing step of the PSA cycle shown in Figure 2.5 is explained here in detail. The steps mentioned here are depicted in Figure 2.7, left to right, for further clarity.

1. Adsorption with feed:

   The feed gas mixture enters the feed of the column. The product gas con-

taining the desired pure component leaves the other end of column at product pressure, which is only slightly less than the inlet pressure. During this stage the impurities get adsorbed on the solid adsorbent, and the weakly adsorbed component comes out as a product. The time length of this step is very important as the impurity front keeps moving ahead from the feed end during this process step. If it advances too much towards the product end, then later on during the co-current depressurization steps, where the system pressure is decreasing and desorption happens as well, the impurities can breakthrough the column with the leaving product, bringing down its performance.

2. Adsorption with feed and product pressurization:

   At the start of this stage a side stream from the main product is taken out and is used to pressurize another bed undergoing re-pressurization with product step (step 10).

3. First co-current depressurization:

   During this stage the inlet flow to the bed is stopped and the outlet valve is opened to another bed undergoing second counter-current pressure equalization (step 9). As the pressure in the column reduces, the outlet stream containing pure product leaves the column and pressurizes other column. This efficient usage of the pure product gas left in the bed void space to pressurize other columns greatly improves the overall product recovery, as this not only minimizes the product losses during the counter-current depressurization stage but also reduces the system dependency on external sources for bed pressurization.

4. Second co-current depressurization:

In this stage the inlet to bed remain closed and outlet is now connected to another bed which has just finished counter current depressurization. The pure product coming out of the bed acts as an excellent source of purge stream for the other bed (step 7). Consequently, the system dependence on the external supply of product stream is further reduced.

5. Third co-current depressurization:

   The column continues to depressurize itself and is now connected to another column at lower pressure which has just finished purge step (step 8), in order to fully utilize the pure product gas at the product end to pressurize other columns.

6. Counter current depressurization:

   This is the blowdown stage, where the feed end is now opened to a lower pressure sink and the product is closed. During this stage the impurities, which are most concentrated near the feed end gets desorbed and leaves the column as an off gas, thus bringing adsorbent bed regeneration.

7. Counter current purge:

   The feed end still remains open to a low pressure sink, while the product end is now connected to a bed which has just finished first co-current depressurization (step 4). The pure product stream entering the bed at low pressure sweeps away the remaining impurities.

8. First counter-current pressure equalization:

   The column feed end is now closed and the product end is connected to another column undergoing step 5. Consequently, the pressure inside the bed starts rising.

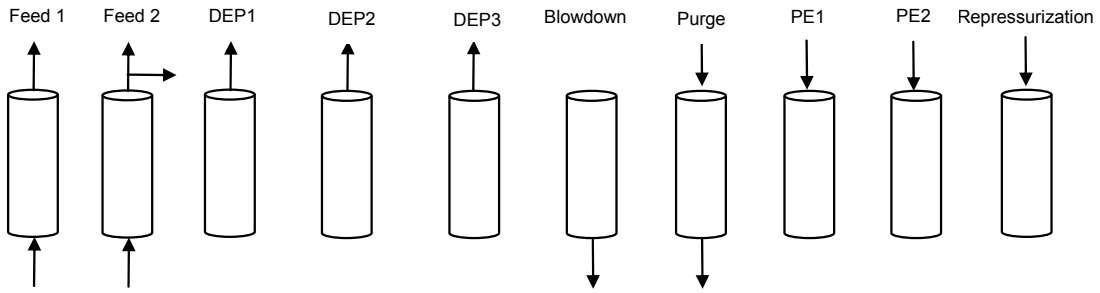

Figure 2.7: PSA processing steps transition for the first bed shown in Figure 4.3

9. Second counter-current pressure equalization:

   The pressure inside the column continues to rise as the product end is connected to another column undergoing step 3.

10. Counter-current re-pressurization with product:

    This is the final stage in the cycle where the column is pressurized with the product coming out of another bed in step2. By the end of this step, the pressure inside the column is at the same level as the feed pressure.

2.5 Alternative Options For Gas Separation and Purification

2.5.1 Temperature Swing Adsoprtion

In the case of PSA, the adsorbent regeneration operation is performed by lowering the bed pressure, as the impurities at lower pressure have less affinity for the adsorbent. An alternative way to perform desorption is to raise the bed temperature levels, as employed in the temperature swing adsorption (TSA) cycle. Figure 2.8, depicts the comparison between the PSA and TSA cycles for a given adsorption isotherm.

A TSA operation usually employs the following three basic steps.

1. Adsorption or production step at low temperature

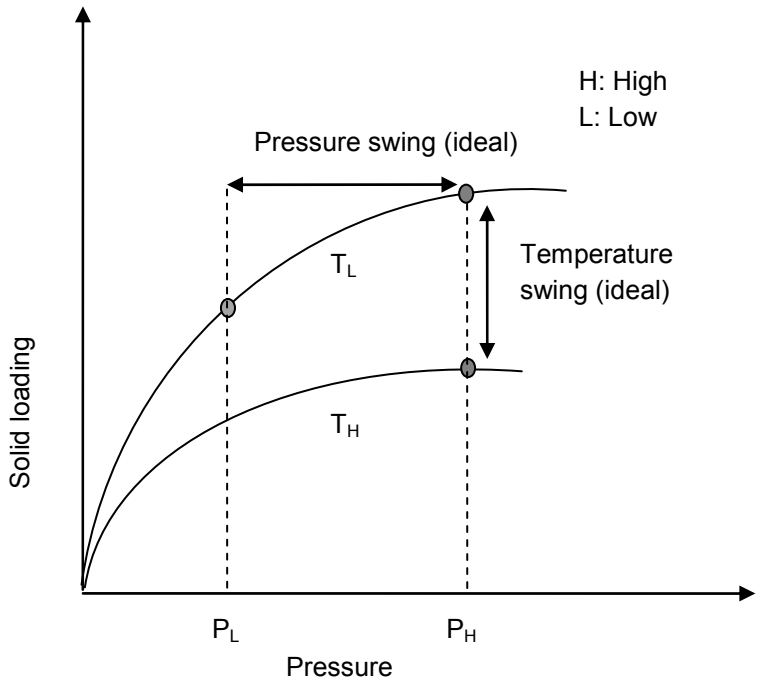

Figure 2.8: Comparison of pressure swing and temperature swing adsorption for adsorbent regeneration

2. Heating the bed for desorption of impurities

3. Cooling the bed back to the adsorption conditions

For heating and cooling operation both, direct means such as using purge/inert gas or indirect means involving heating jackets, coils or microwave can be employed [96, 97].

The key advantage of TSA over PSA is its ability to separate impurities having a tendency to form strong bonding with the adsorbent (chemisorption) [78], as a change of only few degrees in temperature can cause considerable change in the loading amount, leading to an effective separation. Consequently, TSA is usually preferred for purification purposes instead of bulk separation. On the other hand, a major challenge related to the use of TSA is the relative long duration of the processing steps necessary to change the bed temperature, as compared to a PSA system. It should be noted that bed pressure transients can be quickly realized in

a packed bed by changing the valve settings, while temperature changes requires heating the whole mass of adsorbent and metallic wall requiring hours or even days [23] to complete one cycle, adversely effecting the cycle productivity.

2.5.2 Membrane Based Separation

Gas separation employing membrane technology is also very widely used in the process industry. Here, the separation principle is based on the difference in the rate of permeation across the membrane material for different components in the feed mixture. In terms of ease of operability, membrane offers significant advantage over PSA, as its module is much simpler to operate as compared to the periodic operation requirement of PSA separation systems [3]. Furthermore, for the bulk separation applications, which are characterized by low to moderate selectivity requirements [81], membrane is an attractive operation.

For gas purification purposes, the requirement of high membrane selectivity translates into low permeation rate across the membrane material, making them suitable only for small scale applications. In order to perform gas purification at large scales [10, 18], re-compression equipment and extra membrane modules are necessary to obtain the desired purity in several stages, making it a highly energy intensive operation. In contrast, the selectivity in PSA is typically much higher than the membranes, and furthermore, since the product leaves the system as retentate, high production levels can be achieved.

2.5.3 Cryogenic Distillation

In general, for gas production at very large scale, cryogenic distillation is usually preferred in comparison to the adsorptive or membrane processes [1, 81]. Here, the distillation operation is performed at very low temperatures to maintain the gaseous components in their liquid state. The basic separation principle is to

exploit the difference in the relative volatility of various components in the given feed mixture. In contrast to the membrane separation method, cryogenic separations are quite capable of producing gases at very high purities, on a large scale (up to tons/day)[10].

On the other hand, the energy demand for cryogenic distillation of gaseous systems is quite high [137], as a large amount of refrigeration power is required to bring the gaseous system to liquid phase, and thus is a preferred choice if the final product also has to be delivered at high pressure.

Chapter 3

Mathematical Modeling of PSA Systems

3.1 Introduction

From a modeling perspective, a PSA model should be able to capture the exact dynamics of the entire system during these cyclic stages. In the past, significant contributions for capturing the PSA dynamic behavior by first principle based models have been made. Table 3.1 provides an overview of PSA dynamic modeling literature for a variety of applications and configurations. It clearly shows the emergence of more rigorous and detailed models with time as modeling tools like gPROMS [56] are also becoming increasingly powerful to handle such stiff and distributed system of equations. Nonetheless, the application of these models have been mainly towards the dynamic simulations of single bed PSA systems.

A key feature of this work is the development of a detailed, first principles based mathematical model of PSA system for its employment in design and control studies. The main features, and important assumptions related to this model are explained next.

Table 3.1: A brief overview of important literature studies on PSA dynamic modeling (Z = Zeolite, AC = Activated carbon)

Authors	Feed Mixture	PSA Cycle	Isotherm	Mass Transfer	Heat effects	Pressure Effects	Dispersion	Valve Modeling
[175]	H_2-CH_4, H_2 bulk separation	1 bed, 5 steps	AC, Langmuir-Freundlich	Pore diffusion	Non isothermal	No gradients	Ideal plug flow	No
[45]	Air, O_2 production	Skarstrom cycle	Z, Langmuir	LDF (Linear driving force model)	Isothermal	No gradients, stays constant during adsorption and purge	Axially dispersed flow	No
[136]				Various limiting cases of external and internal resistances	Non isothermal	Blake-Kozeny equation	Ideal plug flow	No
[83, 84]	H_2-CH_4, H_2 purification	4 beds, 9 steps	Langmuir	LDF	Non isothermal	Ergun's equation	Ideal plug flow	Yes
[167]	H_2 from coke gas	PSA in series, 8 steps	loading ratio correlation	LDF	Non isothermal	No gradients	Axially dispersed plug flow	No
[171]	H_2 purification from coke oven gas	2 bed, 7 steps	Layered adsorbent - Z and AC, Langmuir-Freundlich	LDF	Non isothermal	Ergun's equation	Axially dispersed plug flow	No
[58]	Propane-propylene separation	1 bed, 5 steps	Z, Multisite Langmuir	Both internal and external resistances considered	Non isothermal, separate equations for fluid, solid and column wall	Ergun's equation	Axially dispersed flow	No
[129]	H_2 purification from H_2, CH_4, CO, CO_2, N_2	1 and 4 beds, 5 steps	Layered adsorbent - Z and AC, Multisite Langmuir	Both internal and external resistances considered	Non isothermal, separate equations for fluid, solid and column wall	Ergun's equation	Axially dispersed flow	No

3.2 Adsorbent Bed Dynamic Modeling

One common assumption made in the modeling work shown here is applicability of Ideal gas law over the entire operating range of pressure and temperature, for the gaseous species mixture under investigation. The main reason of this assumption is the relatively low level of of operating pressure (varying from 1 atm - 7 bars) along with narrow range of temperature changes (with minimum level around 300 K) encountered in this work.

3.2.1 Adsorption Isotherm

An adsorption isotherm mathematically defines the relationship between the concentration of the molecules of a given species in the gas phase with its concentration in the adsorbed phase, under equilibrium conditions and constant temperature. A variety of isotherms have been studied and employed in past modeling studies (see Table 3.1) and can be classified in two main categories of single site or multi site adsorption isotherms, depending on whether a single adsorbate molecule occupies one or multiple adsorption sites [93, 9]. The actual choice of adsorption isotherm thus completely depends upon both the gas and solid system under consideration, as the equilibrium adsorbed phase concentration of a given component strongly depends upon several important factors such as partial pressure in gas phase of the given component, temperature, and the electrostatic interaction between the molecules with the adsorbent and the other species at the adsorption sites.

$$\begin{aligned} \frac{Q_i^*}{Q_i^{max}} &= a_i K_i C_i RT \left[1 - \sum_{i=1}^{N_{comp}} \left(\frac{Q_i^*}{Q_i^{max}}\right)\right]^{a_i} \\ K_i &= K_{\infty_i} e^{\frac{-\Delta H_i}{RT}} \end{aligned} \tag{3.1}$$

In this regard, popular choices such as Langmuir, Freundlich, loading ratio correlation, idealized adsorbed solution theory (IAST) represents the single site adsorption isotherms. On the other hand, the multi-site Langmuir adsorption isotherm from Nitta et al. [107], which is also employed in this work (Eq. 3.1) is suitable for capturing the adsorption dynamics of multi-component mixtures. It is important to note that multi site adsorption isotherms, even though computationally intensive from the modeling point of view, more closely capture the actual adsorption behavior for multi-component systems, under a wide range of dynamic pressure and temperature conditions [93, 58, 129, 85, 174, 137].

3.2.2 Mass Transfer Rates

Adsorption takes place at the adsorption site inside the adsorbent particle. The rate of mass transfer of the gaseous molecules of a multi-component mixture, from the bulk phase to the actual adsorption site, plays a significant role in the overall separation dynamics. The actual mass transfer rates not only depends upon the gaseous species affinity for the adsorbent material, but also on the adsorbent physical internal structure, which basically governs the physical path that gaseous molecules follow from the bulk phase to the actual adsorption site. The adsorbent internal physical structure is usually classified in two main categories. The first class is of the homogeneous adsorbents having similar pore structure throughout the body and are characterized by unimodal pore size distribution. The second class belongs to the composite adsorbents, where a single adsorbent particle is made by combining several micro-porous particles together, leading to a bi-modal pore distribution related to the macropores and micropores.

Depending upon the pore classification of adsorbents defined above, the major mass transfer resistances to the adsorbate uptake rate are of the following types.

- **External fluid film resistance**

This resistance is related to the species mass transfer from the bulk phase to the surface of adsorbent. Its contribution to the overall mass transfer resistance gains significance either when the gaseous phase is not well mixed (leading to appreciable concentration gradients inside the bulk phase itself), or if the boundary layer thickness around the adsorbent particle is quite appreciable (i.e. comparable to the size of particle itself). For gaseous flow in packed columns, this resistance only weakly contributes [137] to the overall mass transfer resistance.

- **Macropore diffusion**

  The diffusion inside the pores whose mean diameter is considerably higher than the mean free path of the adsorbate molecules is termed as macropore diffusion. For these large pores the bulk diffusion mechanism still prevails, tilting towards Knudsen diffusion if their sizes are just greater than the mean free path of the adsorbate molecules.

- **Micropore diffusion**

  Micropores are characterized by pore diameter comparable to the adsorbate molecules mean free diameter. Inside these pores, the adsorbate molecules experience a strong interaction from the solid walls, and for all practical purposes can be considered as adsorbed. Consequently, the mass transfer rates inside these pores are quite low, which makes micropore diffusion the most important and rate limiting step in kinetically controlled PSA separations.

In addition to this, some amount of surface diffusion at the solid wall surface both at the outside surface and the pore walls (macropore), can also add to the overall mass transfer flux.

On one hand, incorporating system of equations to capture every mass transfer resistance mentioned above is expected to yield a rigorous model, while on the other hand, computation solution of such a formulation for multi-bed, multi-step PSA assembly can be a challenging task. In past PSA modeling studies, as shown in Table 3.1, linear driving force (LDF) model, which approximates the actual intra-particle diffusion rates with a semi-empirical lumped expression (see Eq. 3.2) has been very widely used [148, 26, 178].

$$\frac{\partial \overline{Q}_i}{\partial t} = K_{LDF_i}(Q_i^* - \overline{Q}_i) \tag{3.2}$$

The underlying assumption [133, 66, 156] for the applicability of this model is that the PSA cycletime stays considerably higher than the diffusional time constant for the given gas-solid system. For the case of very fast PSA cycles such as RPSA, addition of corrective terms have been considered to maintain its validity.

3.2.3 Mass Balance

Mass balance formulation for each species in the gas phase, when applied on the packed bed system shown in Fig. 3.1 is given by the following Eq. (3.3).

$$(\epsilon_b + (1-\epsilon_b)\epsilon_p)\frac{\partial C_i}{\partial t} + \frac{\partial U C_i}{\partial z} + \rho_p(1-\epsilon_b)\frac{\partial \overline{Q_i}}{\partial t} = \epsilon_b D_z \frac{\partial^2 C_i}{\partial z^2} \tag{3.3}$$

Here, it is important to note that a given species is not only present in void space of the bed, but also in the void space of each pore in the *non adsorbed* state, inside the adsorbent. Furthermore, since this non adsorbed mass is completely inside the adsorbent pellet, it will only contribute to the accumulation term (first term of Eq. 3.3), and not towards other related terms.

Another important feature of the formulation is the consideration of the dispersion effects, which accounts for the effect of fluid-solid hydrodynamic interac-

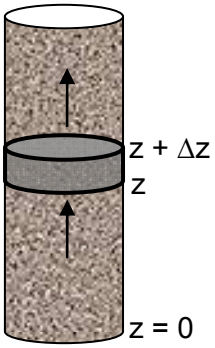

Figure 3.1: Packed bed system description for PSA modeling

tions (mixing patterns) on mass transfer inside the packed bed. In general, for a cylindrical geometry, dispersive effects are prevalent in both radial and axial direction. However, for column with appreciable length to diameter ratio, the radial flow generated due to fluid-solid mixing is negligible as compared to the changes in the axial direction. Consequently, only axial dispersion is taken into account, where the axial dispersion coefficient is evaluated from the work by Wakao and Funazkri [162], as shown in Eq. 3.4. Here, Sc and Re are the non dimensional groups Schmidt number (Eq. 3.5) and Reynolds number (Eq. 3.6), respectively.

$$\frac{\epsilon_b D_z}{D_m} = 20 + 0.5 ScRe \tag{3.4}$$

$$Sc = \frac{\mu}{\rho_{gas} D_m} \tag{3.5}$$

$$Re = \frac{\rho_{gas} U d_p}{\mu} \tag{3.6}$$

3.2.4 Energy Balance

Table 3.1 highlights the extensive usage of isothermal operation assumption in the previous studies. From modeling point of view, this means that only the

effect of pressure dynamics (swings) on the adsorption behavior is taken into account. In fact, the primitive PSA design was labeled as a "heat less dryer" [137]. However, with PSA being employed for the bulk separation and purification operations handling multi-component mixtures, the heat of adsorption can be quite significant and neglecting heat effects inside the bed can seriously impact the model performance. Therefore, incorporating energy balance in the modeling framework, although amplifies the computational complexity for a given model, is of utmost importance, and is formulated in Eq. (3.7).

$$\begin{aligned}
&(\epsilon_b + (1-\epsilon_b)\epsilon_p) \sum_{i=1}^{N_{comp}} C_i (C_{p_i} - R) \frac{\partial T}{\partial t} + \rho_p (1-\epsilon_b) \sum_{i=1}^{N_{comp}} \overline{Q_i} (C_{p_i} - R) \frac{\partial T}{\partial t} \\
&+ U \sum_{i=1}^{N_{comp}} C_i C_{p_i} \frac{\partial T}{\partial z} - (\epsilon_b + (1-\epsilon_b)\epsilon_p)\, RT \sum_{i=1}^{N_{comp}} \frac{\partial C_i}{\partial t} + C_{p_s} \rho_p (1-\epsilon_b) \frac{\partial T}{\partial t} \\
&- \rho_p (1-\epsilon_b) \sum_{i=1}^{N_{comp}} \frac{\partial \overline{Q_i}}{\partial t} (-\Delta H_i) + \left(\left(1 + \frac{\Delta d_w}{D} \right)^2 - 1 \right) C_{p_w} \rho_w \frac{\partial T}{\partial t} \\
&= \lambda \frac{\partial^2 T}{\partial z^2}
\end{aligned} \tag{3.7}$$

The above formulation is a combined gas/solid energy balance and incorporates the contribution of solid phase, gas phase both in adsorbed and non adsorbed state, and the metal wall subsystems in a single expression and thus provides a single temperature value for the whole system (see also Appendix A). The main condition for the lumped energy balance to remain valid is the requirement of thermal equilibrium between the various subsystems, caused by fast rates of heat transfer among them. Furthermore, the beds are also assumed to be operating under adiabatic conditions. In the past, only few studies have considered applying separate energy balances for each sub system, however the results were found to be only marginally better than the results obtained from the lumped formulation [129].

Similar to the mass balance case, dispersion effects in the radial direction are neglected, while the axial heat dispersion coefficient is evaluated from the work of Wakao et al. [163], as shown in 3.8.

$$\alpha_z = 0.7\alpha_m + 0.5 d_p \epsilon_b U \tag{3.8}$$

$$\alpha_z = \frac{\lambda}{\rho_g C_{p_g}} \tag{3.9}$$

$$\alpha_m = \frac{k_g}{\rho_g C_{p_g}} \tag{3.10}$$

Here, α_z is the effective axial thermal diffusivity, and α_m is the molecular thermal diffusivity.

3.2.5 Momentum Balance

Pressure variations inside the bed plays an important role at every stage of a PSA cycle. Many previous studies have neglected the effect of pressure gradients for simplicity (see Table 3.1), and instead employed an overall mass balance formulation for predicting the axial velocity variations. Here, distinction should be made between the pressure transients, which are forced externally through the boundary conditions, and the axial pressure drop (also referred to as pressure gradient), which develops inside the bed. During the adsorption and purge step, as both ends of the column are open and the bed is in continuous flow mode, both pressure drop and pressure transients are negligible. On the other hand, depressurization and re-pressurization steps are characterized by sharp pressure transients gradients, as the pressure changes not only in time but also in the axial direction. Several studies dedicated on probing the role of pressure drop [61, 134, 173, 144], point out the profound role it plays in the accurate modeling

of PSA operation.

In principle, accurate capturing of momentum transfer inside the packed bed requires the incorporation of full scale Navier Stokes equations in the PSA model. Here, it is important to note that inside a PSA bed both laminar and turbulent conditions can be active at the same time. For example, in the semi-batch processing steps of the PSA cycle, the flow conditions near the closed end of the column are laminar, while at the other end where the fluid is leaving the bed at high velocities, turbulent conditions are prevalent. In such a scenario, the usage of first principles based Navier Stokes equation is even more profound as it can handle both flow regimes. On the other hand, the actual solution of Navier Stokes equation, especially for turbulent regime requires further modeling information such as Eddy diffusion modeling, making its real implementation and solution a tough problem [19].

As an alternative, the quasi steady state [144] Ergun equation, as shown in Eq. (3.11), is widely used to approximate the pressure variations inside the packed bed, and is the option employed here as well.

$$-\frac{\partial P}{\partial z} = \frac{150\mu(1-\epsilon_b)^2}{\epsilon_b^3 d_p^3}U + \frac{1.75(1-\epsilon_b)\sum_{i=1}^{N_{comp}} C_i MW_i}{\epsilon_b^3 d_p}|U|U \tag{3.11}$$

In the above equations (3.3)-(3.11), ϵ_b and ϵ_p are treated as constant parameters, assuming that they remain unchanged for all hydrodynamic conditions encountered throughout the PSA cycle. In particular, constant ϵ_b assumption is under test during the start of any PSA processing step which is of semi-continuous flow nature. For example, it is not uncommon to observe momentary flow spikes during the re-pressurization or blowdown step which can *slightly* re-adjust the packed bed configuration. Furthermore, thermodynamic and transport properties C_{p_i}, μ, ρ_p and C_{p_s} are assumed to be constant at their feed conditions.

3.2.6 Valve Flow/Pressure Behavior

The flow-pressure relation (velocity boundary condition) at the adsorber ends [33, 32, 104] is governed by the valve equation in Eq. (3.12).

$$\begin{aligned} U &= \frac{R}{\epsilon\pi D^2} CV \sqrt{1 - \left(\frac{P_{low}}{P_{high}}\right)^2} \quad if \left(\frac{P_{high}}{P_{low}}\right) < P_{critical} \\ &= \frac{R}{\epsilon\pi D^2} CV \sqrt{1 - \left(\frac{1}{P_{critical}}\right)^2} \quad otherwise \\ where \qquad & P_{critical} = \left(\frac{2}{1+\gamma}\right)^{\frac{\gamma}{1-\gamma}} \; \gamma = \frac{C_p}{C_p - R} \end{aligned} \tag{3.12}$$

Since C_{p_i} is assumed to be constant at feed conditions, $C_p \left(= \sum_{i=1}^{N_{comp}} C_{p_i} y_{feed_i} \right)$, making $P_{critical}$ a constant as well for valves related to different processing steps. This is in spite of the fact that the stream conditions during blowdown and purge operations at the feed end ($z = 0$), are quite different from the stream conditions during the rest of the steps. In order to account for such differences, C_p is evaluated at the same temperature (as feed conditions) but at the presumed off-gas composition, for these two valves.

3.3 Cyclic Steady State

Starting from a given initial condition, a PSA system takes a number of cycles to reach a state in time, called as cyclic steady state (CSS), where value of all system variables at the end of a cycle are same as at the start of the same cycle. In this regard, the following methods can be employed for mathematical evaluation of the CSS condition.

- **Method 1 - Full measurement**

  One common way for defining CSS is shown in Eq. 3.13, where all the

differential variables in the PSA model represented by **xp** are measured at the start and end of each cycle. Here, the system is said to have reached CSS when all elements of CSS error, represented by $\mathbf{e}_{CSS}$, are identically zero.

$$\mathbf{e}_{CSS}(t) = \mathbf{xp}(t) - \mathbf{xp}(t - t_{cycletime}) = 0 \tag{3.13}$$

From the modeling perspective, since the number of such cycles necessary to reach CSS is not known in advance, the simulations need to be carried out for a arbitrarily long time period, assuming that CSS will be satisfied within this time frame.

- **Method 2 - Relaxed method**

  Method 1, albeit quite rigorous, is time consuming in nature and difficult to implement for computationally intensive PSA system model. As an alternative, a relaxed version of Eq. 3.13 can also be followed, which is shown in Eq. 3.14, where the system is assumed to have reached CSS, when maximum magnitude of the CSS error, denoted by e_{CSS_max}, reaches below a small positive number ε.

$$\begin{aligned} \mathbf{e}_{CSS}(t) &= \mathbf{xp}(t) - \mathbf{xp}(t - t_{cycletime}) \\ e_{CSS\_max}(t) &= max\,|\mathbf{e}^{o}_{CSS}(t)| \leq \varepsilon \end{aligned} \tag{3.14}$$

- **Method 3 - Lumped variables measurement**

  In practice, it is difficult to track all PSA variables for the CSS condition, as required in Method 1 and 2. To tackle this, lumped variables can be defined, as shown in Eq. 3.15 and 3.16, which monitors the values of average bed

properties instead of the exact value of each system variable.

$$\mathbf{xp}_{avg} = \int_0^1 \mathbf{xp}(z^*)dz^*; \quad z^* = z/L \tag{3.15}$$

$$e_{CSS\_max}(t) = \left|\mathbf{xp}_{avg}(t) - \mathbf{xp}_{avg}(t - t_{cycletime})\right| \leq \varepsilon \tag{3.16}$$

- **Method 4 - PSA performance indicators measurement**

  An extension of above mentioned Method 3 is to measure just the most important variables related to the PSA system - performance indicators. As already mentioned in Chapter 1 of this thesis, the three key performance indicators of PSA operation are product recovery, product purity and adsorbent productivity, mathematically defined in Eq. 3.17, 3.18, and 3.19, respectively.

$$Recovery_i = \frac{\int_0^{t_{feed}} C_i U A_{bed}\Big|_{z=L} dt}{\int_0^{t_{feed}} C_i U A_{bed}\Big|_{z=0} dt} \tag{3.17}$$

$$Purity_i = \frac{\int_0^{t_{feed}} C_i U A_{bed}\Big|_{z=L} dt}{\sum_{i=1}^{N_{comp}} \int_0^{t_{feed}} C_i U A_{bed}\Big|_{z=L} dt} \tag{3.18}$$

$$\begin{aligned} Productivity_i &= \frac{\int_0^{t_{feed}} C_i U A_{bed}\Big|_{z=L} dt}{\tau_{cycletime} M_{adsorbent}} \\ &= \frac{\int_0^{t_{feed}} C_i U A_{bed}\Big|_{z=L} dt}{\tau_{cycletime} L A_{bed}(1-\epsilon_b)\rho_p} \end{aligned} \tag{3.19}$$

It should be noted that the above definitions of performance indicators are

defined on the per cycle basis and are applicable only during a case when no side streams are drawn from the product side during the feed step of the PSA cycle. For example, for the PSA cycle mentioned in Figure 2.5, a side stream from the product(coming out during the feed stage) is employed to pressurize an other column undergoing product re-pressurization. In such a scenario, the performance indicators definitions are based on the net product leaving the system.

Chapter 4

Explicit/Multi-Parametric MPC Control of PSA Systems

4.1 Preliminaries

4.1.1 Model Predictive Control

Model predictive control is an advanced control methodology, wherein each controller move is evaluated by solving an optimization problem, while taking into account operational constraints and system dynamic behavior through a predictive model [123, 124, 91, 125]. The optimal controller action provided by MPC is very different to a standard PID controller, where the control move is obtained by solving an empirical equation which incorporates the system dynamic information, indirectly through the tuning parameters such as proportional gain.

It is important to note that the optimization framework employed in the MPC formulation allows for great flexibility in terms of choosing the functional form of the objective function and the constraints, leading to different MPC variations. For example, the output-MPC formulation of Eq. 4.1, combines the contribution of control variable deviation from the set point with the overall manipulative variable effort (Δu term) towards the disturbance rejection, in a single objective function.

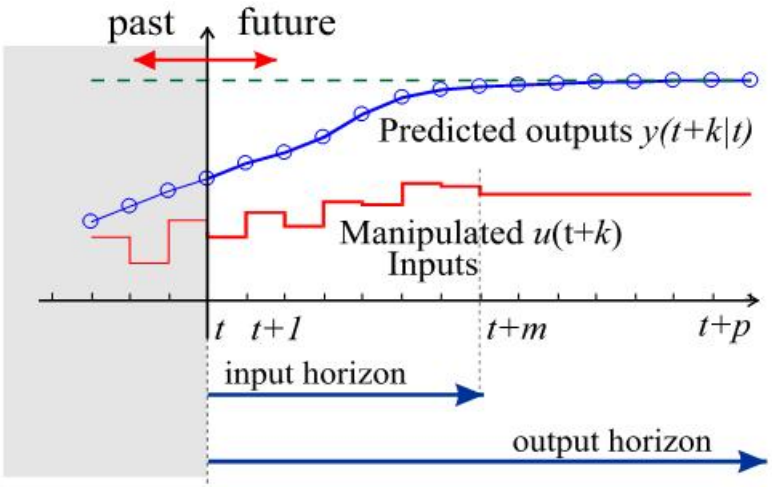

Figure 4.1: The receding horizon policy employed in the MPC implementation

$$
\begin{aligned}
\min_{u} \quad Z &= \sum_{t=1}^{H_p-1} (y(t)-y^r(t))'(y(t)-y^r(t)) + \sum_{t=0}^{H_u-1} \Delta u(t)' R \Delta u(t) \\
s.t. & \\
x(t+\Delta t) &= Ax(t)+bu(t) \\
y(t) &= cx(t) \\
u_{low} \leq \quad u(t) &\leq u_{high} \\
\Delta u_{low} \leq \quad \Delta u(t) &\leq \Delta u_{high} \\
y_{low} \leq \quad y(t) &\leq y_{high}
\end{aligned} \tag{4.1}
$$

The actual functioning of MPC is based on the receding horizon philosophy (see also Figure 4.1), where the current plant state and output variables, along with a suitable plant model, are utilized to calculate the future sequence of optimal input variables. The following main steps are involved in calculating the optimal control move.

Step 1 At time t, the plant output variables (y) are measured and are employed to obtain the latest estimate of the state variables (x).

Step 2 For the given values of prediction horizon and control horizon, a constrained quadratic optimization problem Eq. 4.2 is solved to obtain the future values of the plant input variable. Here, the plant predictive model, as shown in Eq. 4.3, is employed to express the future state predictions in the form of input variables (u), as expressed in Eq. 4.4.

$$\begin{aligned} D^*(x(t)) = \min_{U_c} \quad & \{\tfrac{1}{2}U_c' H U_c + x(t) F U_c + \tfrac{1}{2} x(t)' Y x(t)\} \\ s.t. \quad & GU \leq W + Ex(t) \end{aligned} \tag{4.2}$$

Here, U_c is the vector containing the control moves sequence, while H, F, and F are the MPC weight matrices.

$$\begin{aligned} x(t+\Delta t) &= Ax(t) + bu(t) \\ y(t) &= cx(t) \end{aligned} \tag{4.3}$$

$$x(t+k|t) = A^k x(t) + \sum_{j=0}^{k-1} A^j b u(t+k-1-j) \tag{4.4}$$

Note that sometimes, the control horizon for future control move prediction is kept smaller than the prediction horizon, resulting in an optimization formulation of smaller size, where only the control moves till $H_u - 1$ are determined from the optimization problem, keeping rest of them fixed at the value at $H_u - 1$.

Step 3 From the complete sequence of optimal input trajectory obtained in *Step 2*, the first control move is applied to the plant while the rest are ignored. The whole procedure is repeated from *step 1* as the next measurement from the plant is made available.

The above steps indicate that the MPC control law is implicit in nature and

requires repeated *online* solution of the optimization problem, as the state of the plant evolves in time. A further implication of online optimization is that MPC application to problems with fast dynamics, especially situations where the sampling interval duration is comparable to time required to solve the optimization problem, is rather quite limited.

4.1.2 Explicit/Multi-Parametric Model Predictive Control

Recent advances made in the field of multi-parametric programming now makes it possible to obtain the governing MPC control law beforehand, or *offline*. Pistikopoulos et al. [119], first demonstrated this by employing multi-parametric techniques to reformulate the original MPC problem into a multi-parametric optimization problem. In the last decade, there has been tremendous growth in the industrial applications of mp-MPC as outlined in Table 4.1.

In contrast to MPC controller, multi-parametric MPC comprises an offline step, where most of computational intensive calculations are performed, making its online implementation much simpler. The functioning of mp-MPC in the form of two main steps, offline and online, is explained here in detail.

Offline step

The main purpose of this step is to formulate and solve the multi-parametric control optimization problem. In order to achieve this, first the quadratic optimization problem in Eq. 4.2 is converted to a multi-parametric quadratic programming problem by performing the linear transformation shown in Eq. 4.5.

$$z_m \triangleq u + H^{-1}F'x_t \tag{4.5}$$

The resulting multi-parametric quadratic optimization formulation is given in

Table 4.1: A brief overview of explicit/multi-parametric MPC case studies

Authors	Explicit/multi-parametric MPC application
Borrelli et al. [24]	Vehicle traction control
Grancharova et al. [57]	Control of gas−liquid separation plant for the flue gas treatment
Krogstad et al. [82], Hegrenæs et al. [63, 64]	Satellite attitude control through magnetic torquers
Dua et al. [41]	Robust controller formulation for blood glucose level control in Type 1 diabetes scenario
Beccuti et al. [17]	Control scheme for boost dc-dc converters
Johansen et al. [70]	Optimal constrained control allocation in marine surface vessels with rudders
Georgiadis et al. [51]	Controller scheme for metal hydride based hydrogen storage system
Dua et al. [42]	Automatic control of blood glucose concentration for Type 1 diabetes
Panos et al. [111]	Robust formulation for hydrogen storage in metal-hydride bed reactor

Eq. 4.6:

$$\begin{aligned} V(x(t)) &= \min_{z_m} \quad \frac{1}{2} z_m' H z_m \\ &s.t. \\ G z_m &\leq W + S x(t) \end{aligned} \tag{4.6}$$

Here, z_m represents the new set of optimization variables, while S is defined in the Eq. 4.7:

$$S = E + G H^{-1} F' \tag{4.7}$$

In the new formulation, x_t which is now acting as a parameter of the optimization problem (Eq. 4.6), appears only in the constraint equations as compared to being involved both in the objective function and constraints in the original MPC problem formulation (Eq. 4.3).

Next, sensitivity analysis is performed on the Karush-Kuhn Tucker (KKT) conditions of the multi-parametric quadratic optimization problem, shown in Eq. 4.8, in order to obtain the optimal z_m as an affine function of parameter x_t, expressed in Eq. 4.9.

$$\begin{gathered} H z_m + G' \gamma = 0 \\ \gamma_i (G_i z_m - W_i - S_i x(t)) = 0, \quad i = 1, ...q \\ \gamma \geq 0 \end{gathered} \tag{4.8}$$

$$\begin{bmatrix} z_m(x) \\ \gamma(x) \end{bmatrix} = -(M_0)^{-1} N_0 (x - x_0) + \begin{bmatrix} z_m(x(0)) \\ \gamma(x(0)) \end{bmatrix} \tag{4.9}$$

Here, M_0 and N_0 are constant matrices, as shown in Eq. 4.10 and 4.11, i

represents the ith row the matrix while Y is null matrix.

$$M_0 = \begin{bmatrix} H & G_1^T & \dots & G_q^T \\ -\gamma_1 G_1 & -V_1 & & \\ \vdots & & \ddots & \\ -\gamma_q G_q & & & -V_q \end{bmatrix} \tag{4.10}$$

$$N_0 = \begin{bmatrix} Y, & \gamma_1 S_1, & \dots, & \gamma_p S_p \end{bmatrix}^T \tag{4.11}$$

The parameter space, or the set of x values for which the explicit relationship between $[z_m(x), \gamma(x)]$ and the parameter x, around the point $[z_m(x(0)), \gamma(x(0))]$, remains optimal is termed as a critical region. This special property is attributed to the fact that the parameter x, appears only in the constraints of the multi-parametric quadratic programming problem, Eq. 4.6, leading to a scenario, where for certain values of x, the current set of active constraints and lagrange positive condition remains valid. The mathematical definition of a critical region (CR) is given in Eq. 4.12.

$$CR^R = \{\check{G} z_m(x) \leq \check{W} + \check{S} x(t), \check{\gamma(x)} \geq 0\} \tag{4.12}$$

Following this approach, the critical regions and the corresponding explicit control laws for the whole parametric space range defined by the user are obtained in the offline step [121, 120], and stored for the online usage.

Online step

In the closed loop environment, the plant measurements are taken as usual and passed to the mp-MPC controller, which in turn first evaluates the critical region the particular state measurement set belong to and then retrieve the corresponding control law to be passed to the process system. Note that the online

work is now reduced to performing function evaluations, as compared to solving a full length optimization problem, to retrieve the control laws [116, 121, 120]. Furthermore, reduced online computational load directly translates to reduced computational hardware requirements, leading to economical benefits.

4.1.3 PSA Control

Pressure swing adsorption (PSA) is one of the many unit operations invented before the underlying theories behind it were fully understood. Since its commercial inception in late 1950s, PSA technology has evidenced substantial growth in terms of size, versatility and complexity [137, 174]. Modern PSA systems, used widely in the gas separation industry can vary from 2 adsorbent bed separating air, to 16 bed system producing pure hydrogen in excess of 100,000 Nm^3/hr [170]. PSA operation is not only highly nonlinear and dynamic but also poses extra challenges due to its periodic nature, directly attributed to the network of bed interconnecting valves whose active status keeps changing over time. The timing of these valves in turn controls the duration of process steps that each PSA bed undergoes in one cycle. In the past, only a few studies have appeared in the open literature on PSA control even though there is an increasing interest to improve their operability [161]. Bitzer [20] presented model-based feedforward-feedback purity control of a 4-step, 2-bed PSA system producing oxygen from air. Since the original model used to capture the PSA systems was not suitable for feedforward controller purposes, a reduced model was derived by approximating the species axial concentration profiles through empirical wave functions. However, the applicability of this key assumption for more complex and realistic PSA system has not been fully demonstrated. Torre et al. [157] proposed a model predictive control (MPC) for purity control of a 6-step, single-bed vacuum swing adsorption configuration, separating oxygen from air.

The main objective of this study is to perform detailed studies towards the design of a single-input/single-output (SISO) explicit/multi-parametric MPC controller for a complex PSA system, where the control variable product purity is manipulated by adsorption time. In the next section, the detailed description of a systematic framework [116] employed for rigorous design and validation of explicit/multi-parametric MPC (mp-MPC) controller is provided.

4.2 Explicit/Multi-parametric MPC Framework

Figure 4.2, depicts the explicit/multi-parametric programming framework employed to design the controller [116]. It comprises four main steps which are described as follows:

Step 1 High fidelity model of PSA system is developed to represent the real PSA system as closely as possible.

Step 2 Modern system identification techniques are explored to approximate the original high-level model developed in step 1 to low-level reduced models which are more suitable for controller purposes. Since the PSA system under study is too complex to be reduced to a simpler first-principles based model, and the fact that we are designing a controller for a SISO system, building linear (parametric) black box models seems to be a suitable approach. To better evaluate the effect of model reduction on the controller performance, a library of reduced models is generated, and their closed loop responses are compared while subjected to the same disturbance profile.

Step 3 Latest multi-parametric algorithms [122, 119, 121, 120] are employed to formulate the mp-MPC controller design problem, based on the reduced models identified in step 2.

Step 4 In-silico closed loop simulations are performed for validating the de-

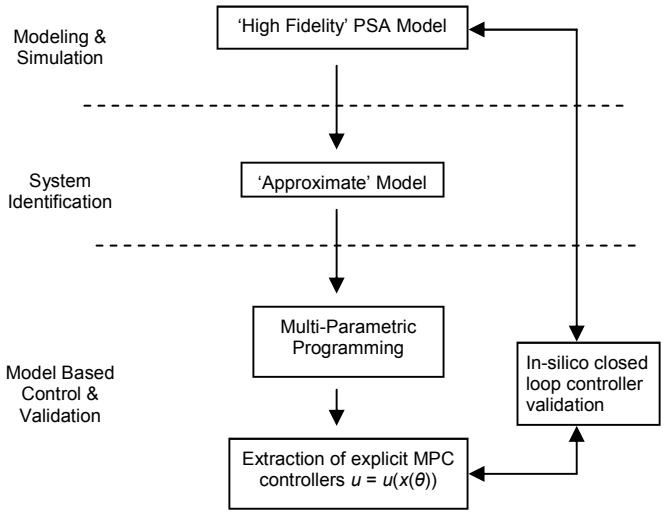

Figure 4.2: Framework for multi-parametric programming and explicit/multi-parametric MPC

rived controllers. The high fidelity model built in step 1 now acts as the virtual PSA plant. Closed loop responses of the controllers are obtained for various type of disturbances and mp-MPC tuning parameters. If the controller performance is not satisfactory, the whole process is repeated again, until desired performance is obtained.

4.3 PSA Mathematical Modeling and Simulation

4.3.1 PSA Dynamic Model

A detailed, first principle based mathematical model of the PSA system is developed for this study in gPROMS® (PSE, Ltd.). Figure 4.3 shows a graphical overview of the PSA system under consideration. Each of the four beds contains activated carbon as an adsorbent and undergoes a cyclic operation comprising nine process steps [83], separating a 70% H_2 and 30 % CH_4 mixture into high purity H_2. The main features of the dynamic model are shown here (and differs

slightly from the details mentioned in Chapter 3 of thesis). Furthermore, the velocity dependent terms in the axial heat and mass transfer dispersion coefficients [162, 163] have been neglected.

Mass balance

$$(\epsilon_b + (1-\epsilon_b)\epsilon_p)\frac{\partial C_i}{\partial t} + \frac{\partial U C_i}{\partial z} + \rho_p(1-\epsilon_b)\frac{\partial \overline{Q_i}}{\partial t} = \epsilon_b D_{zi}\frac{\partial^2 C_i}{\partial z^2} \tag{4.13}$$

Energy balance

$$\begin{aligned}&\frac{\partial\left(T\sum_{i=1}^{N_{comp}} C_i(C_{p_i}-R)\right)}{\partial t} + \frac{\partial\left(UT\sum_{i=1}^{N_{comp}} C_{p_i}C_i\right)}{\partial z}\\ &+\rho_p C_{p_s}\frac{1-\epsilon_b}{\epsilon_b}\frac{\partial T}{\partial t} + \rho_p\frac{1-\epsilon_b}{\epsilon_b}\sum_{i=1}^{N_{comp}}\frac{\partial \overline{Q}_i}{\partial t}\Delta H_i = \lambda\frac{\partial^2 T}{\partial z^2}\end{aligned} \tag{4.14}$$

Momentum balance

$$-\frac{\partial P}{\partial z} = \frac{150\mu(1-\epsilon_b)^2}{\epsilon_b^3 d_p^3}U + \frac{1.75(1-\epsilon_b)\sum_{i=1}^{N_{comp}} C_i MW_i}{\epsilon_b^3 d_p}|U|U \tag{4.15}$$

Intraparticle diffusion - LDF model

$$\frac{\partial \overline{Q}_i}{\partial t} = K_{LDF_i}(Q_i^* - \overline{Q}_i) \tag{4.16}$$

Adsorption isotherm

$$\begin{aligned}\frac{Q_i^*}{Q_i^{max}} &= a_i K_i C_i RT\left[1 - \sum_{i=1}^{N_{comp}}\left(\frac{Q_i^*}{Q_i^{max}}\right)\right]^{a_i}\\ K_i &= K_{\infty_i} e^{\frac{-\Delta H_i}{RT}}\end{aligned} \tag{4.17}$$

Valve characteristics

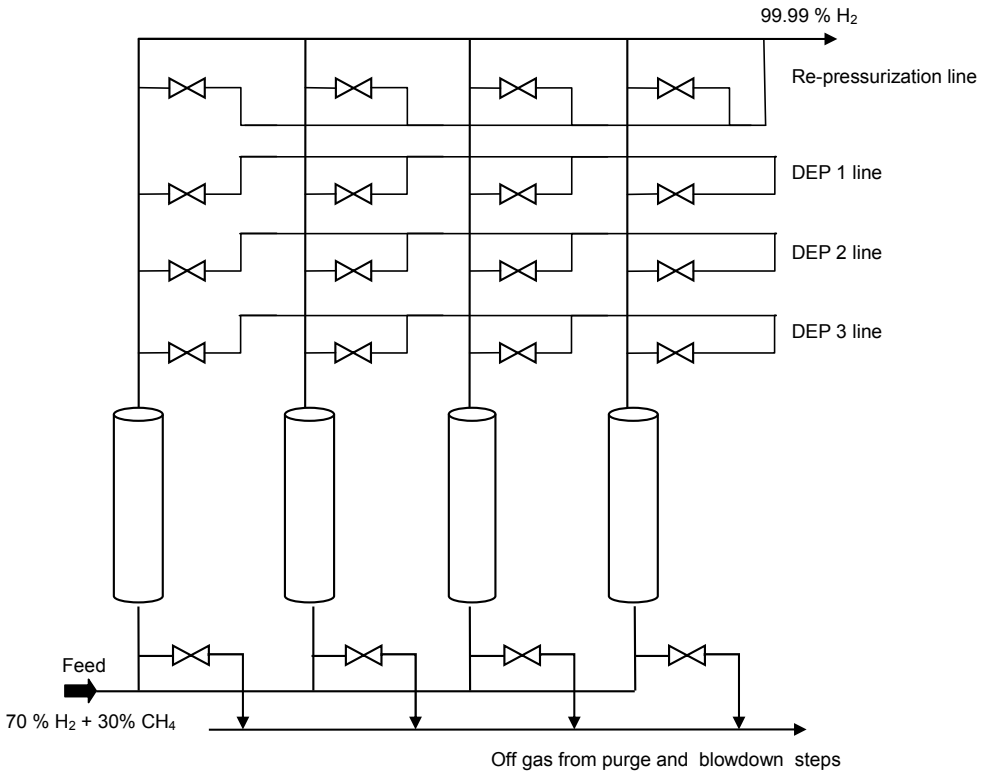

BED 1	FEED			DEP 1	DEP 2	DEP 3	Bd	Pu	PE 1	PE 2	REPRES
BED 2	PE 2	REPRES		FEED			DEP 1	DEP 2	DEP 3	Bd	Pu	PE 1
BED 3	Bd	Pu	PE 1	PE 2	REPRES		FEED			DEP 1	DEP 2	DEP 3
BED 4	DEP 1	DEP 2	DEP 3	Bd	Pu	PE 1	PE 2	REPRES		FEED		

Figure 4.3: Four bed, 9 step multi-valve PSA configuration employed for this study. FEED: production step; DEP1: first co-current depressurization; DEP2: second co-current depressurization; DEP3: third co-current depressurization; Bd: counter-current depressurization or blowdown; Pu: counter-current purge; PE 1: first co-current pressure equalization; PE 2: second co-current pressure equalization; REPRES: counter-current re-pressurization with product.

Table 4.2: Boundary conditions for the feed, first and second depressurization steps, for the nine step PSA cycle

$z = 0$	$z = L$
Feed	
$UA_{bed} = \dot{Q}_{feed}$	$P = P_{product}$
$C_i = \frac{Py_{i_{feed}}}{RT}$	$\frac{\partial C_i}{\partial Z} = 0$
$T = T_{feed}$	$\frac{\partial T}{\partial Z} = 0$
First co-current depressurization	
$U = 0$	$U = f_{valve}\left(P, P_{cope2}, CV_{codep1}\right)$
$\frac{\partial C_i}{\partial Z} = 0$	$\frac{\partial C_i}{\partial Z} = 0$
$\frac{\partial T}{\partial Z} = 0$	$\frac{\partial T}{\partial Z} = 0$
Second co-current depressurization	
$U = 0$	$U = f_{valve}\left(P, P_{purge}, CV_{codep2}\right)$
$\frac{\partial C_i}{\partial Z} = 0$	$\frac{\partial C_i}{\partial Z} = 0$
$\frac{\partial T}{\partial Z} = 0$	$\frac{\partial T}{\partial Z} = 0$

$$
\begin{aligned}
U &= f_{valve}\left(P_{high}, P_{low}, CV\right) \\
&= \frac{R}{\epsilon\pi D^2} CV \sqrt{1 - \left(\frac{P_{low}}{P_{high}}\right)^2} \quad if \left(\frac{P_{high}}{P_{low}}\right) < P_{critical} \\
&= \frac{R}{\epsilon\pi D^2} CV \sqrt{1 - \left(\frac{1}{P_{critical}}\right)^2} \quad otherwise \\
where \qquad & P_{critical} = \left(\frac{2}{1+\gamma}\right)^{\frac{\gamma}{1-\gamma}} \gamma = \frac{C_p}{C_p - R}
\end{aligned} \tag{4.18}
$$

Time varying boundary conditions corresponding to each process step of the PSA cycle at both ends of the column are shown in tables 4.2, 4.3, and 4.4, where $f_{valve}\left(P_{high}, P_{low}, CV\right)$ function corresponds to Eq. (4.18).

Table 4.3: Boundary conditions for the third depressurization, blowdown, and purge steps, for the nine step PSA cycle

$z = 0$	$z = L$
Third co-current depressurization	
$U = 0$	$U = f_{valve}\left(P, P_{cope1}, CV_{codep3}\right)$
$\frac{\partial C_i}{\partial Z} = 0$	$\frac{\partial C_i}{\partial Z} = 0$
$\frac{\partial T}{\partial Z} = 0$	$\frac{\partial T}{\partial Z} = 0$
Blowdown	
$U = f_{valve}\left(P, P_{blowdown}, CV_{blowdown}\right)$	$U = 0$
$\frac{\partial C_i}{\partial Z} = 0$	$\frac{\partial C_i}{\partial Z} = 0$
$\frac{\partial T}{\partial Z} = 0$	$\frac{\partial T}{\partial Z} = 0$
Counter-current Purge	
$U = f_{valve}\left(P, P_{purge}, CV_{purge}\right)$	$CU = -f_{valve}\left(P_{codep2}, P, CV_{codep2}\right) C_{codep2}$
$\frac{\partial C_i}{\partial Z} = 0$	$C_i = \frac{P}{RT}\frac{C_{i_{codep2}}}{C_{codep2}}$
$\frac{\partial T}{\partial Z} = 0$	$T = T_{codep2}$

Table 4.4: Boundary conditions for the first, second pressure equalization, and product repressurization steps, for the nine step PSA cycle

$z = 0$	$z = L$
First counter-current pressure equalization	
$U = 0$	$CU = -f_{valve}\left(P_{codep3}, P, CV_{codep3}\right) C_{codep3}$
$\frac{\partial C_i}{\partial Z} = 0$	$C_i = \frac{P}{RT}\frac{C_{i_{codep3}}}{C_{codep3}}$
$\frac{\partial T}{\partial Z} = 0$	$T = T_{codep3}$
Second counter-current pressure equalization	
$U = 0$	$CU = -f_{valve}\left(P_{codep1}, P, CV_{codep1}\right) C_{codep1}$
$\frac{\partial C_i}{\partial Z} = 0$	$C_i = \frac{P}{RT}\frac{C_{i_{codep1}}}{C_{codep1}}$
$\frac{\partial T}{\partial Z} = 0$	$T = T_{codep1}$
Counter-current repressurization with product	
$U = 0$	$CU = -f_{valve}\left(P_{product}, P, CV_{corepres}\right) C_{product}$
$\frac{\partial C_i}{\partial Z} = 0$	$C_i = \frac{P}{RT}\frac{C_{i_{product}}}{C_{product}}$
$\frac{\partial T}{\partial Z} = 0$	$T = T_{product}$

4.3.2 PSA Dynamic Simulations

To evaluate the performance of PSA system under consideration, dynamic simulation studies are conducted with the set of model and boundary conditions described in section 4.3.1. In these simulations, it is further assumed that all nine process steps have the time durations shown in equation (4.19).

$$\begin{aligned} t_{codep1} &= t_{codep2} = t_{codep3} \\ &= t_{blowdown} = t_{purge} = t_{pe1} \\ &= t_{pe2} = \tau \\ t_{repress} &= 2 \times \tau \\ t_{ads} &= 3 \times \tau \\ t_{cycle} &= 12 \times \tau \end{aligned} \tag{4.19}$$

In the rest of this chapter, τ will be referred to as the adsorption time (see also the notations section). The details of feed stream, PSA geometrical design parameters, and other modeling parameters are provided in tables 4.5 and 4.6. Initially, all beds are assumed to be saturated with 100 % pure H_2 ($\partial \overline{Q}_{H_2}/\partial t = 0$) at feed temperature and pressure of 7 bar, 2.5 bar, 2.5 bar, and 7 bar, respectively. As the dynamic simulations proceed, the PSA system evolves *cycle by cycle* to a state where all the differential and algebraic variables in the model have (practically) the same values at the start and the end of a cycle. Therefore, for all $\mathbf{x} = x(P, C_i, T, \overline{Q}_i, Q_i^*, U)$; $\mathbf{x}(t) = \mathbf{x}(t + t_{cycl})$. This is an important property of the PSA operation and is referred to as the cyclic steady state (CSS). Figure 4.4. shows the cycle-wise evolution to CSS of two key PSA performance indicators, the product purity and the product recovery, given by Equations (4.20) and (4.21).

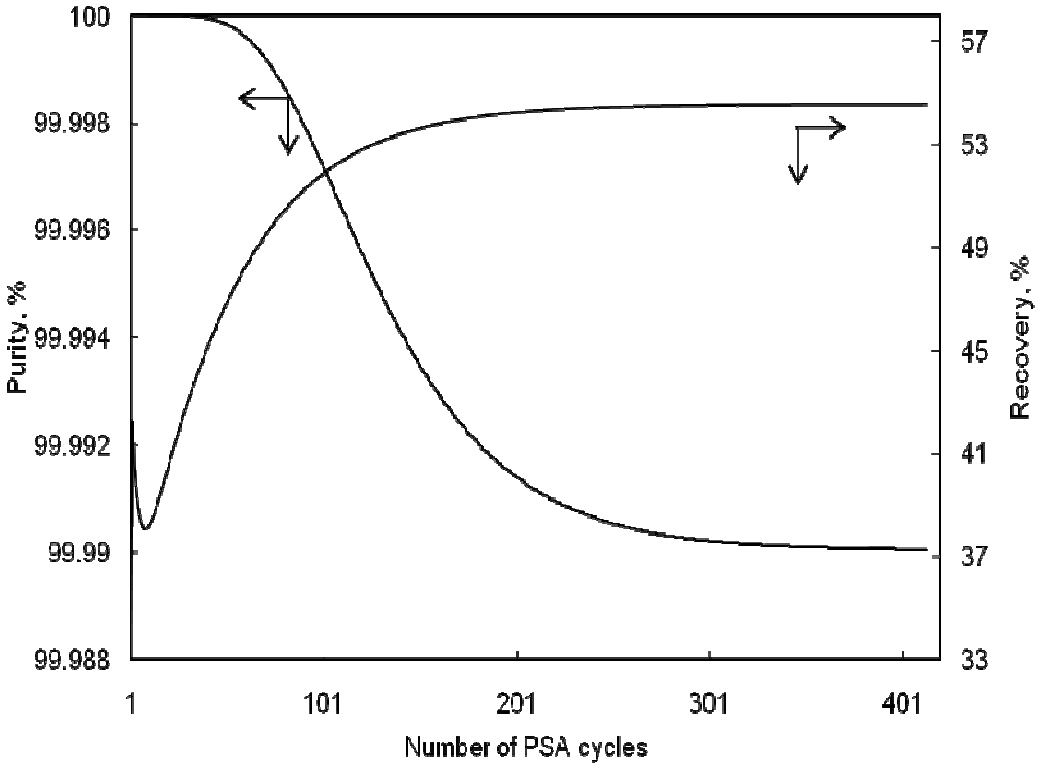

Figure 4.4: Variation of hydrogen purity and recovery with each PSA cycle for the base case PSA

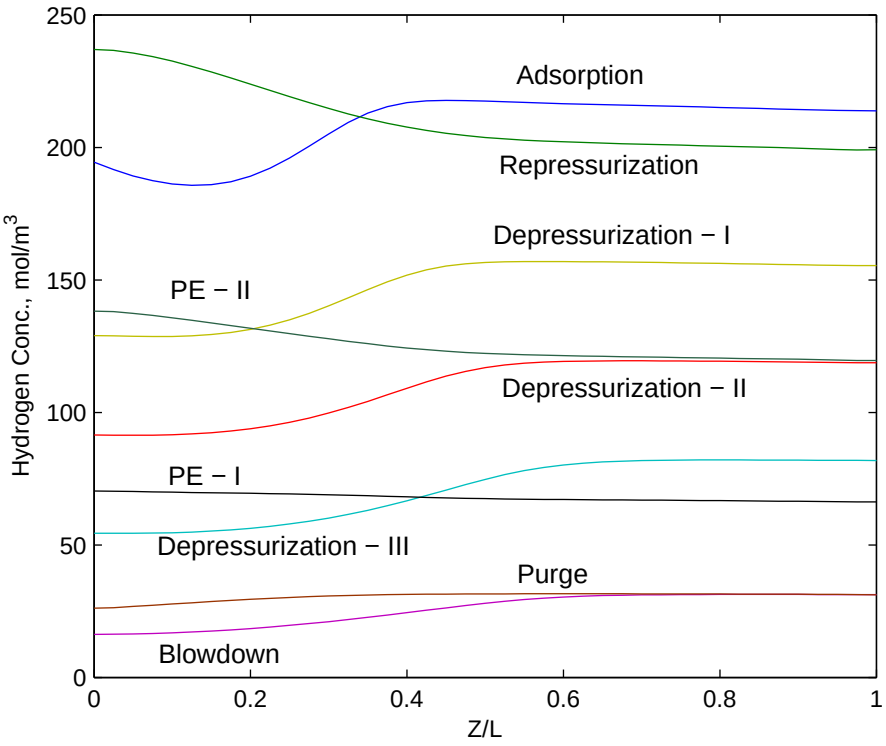

Figure 4.5: Hydrogen axial concentration profiles at CSS at end of each PSA process step

$$Purity = \frac{\int_0^{t_{ads}} C_{H_2} U A_{bed}\Big|_{z=L,BED1} dt - \int_{t_{codep1}}^{t_{ads}} C_{H_2} U A_{bed}\Big|_{z=L,BED2} dt}{\sum_{i=1}^{N_{comp}} \left[\int_0^{t_{ads}} C_i U A_{bed}\Big|_{z=L,BED1} dt - \int_{t_{codep1}}^{t_{ads}} C_i U A_{bed}\Big|_{z=L,BED2} dt\right]} \tag{4.20}$$

$$Recovery = \frac{\int_0^{t_{ads}} C_{H_2} U A_{bed}\Big|_{z=L,BED1} dt - \int_{t_{codep1}}^{t_{ads}} C_{H_2} U A_{bed}\Big|_{z=L,BED2} dt}{\int_0^{t_{ads}} C_{H_2} U A_{bed}\Big|_{z=0,BED1} dt} \tag{4.21}$$

Figure 4.5 and 4.6 shows the axial concentration profiles of H_2 and CH_4 at the end of each of the nine process steps, once CSS is achieved.

CH_4 profiles in particular, demonstrate how the impurity level inside the col-

Table 4.5: Modeling parameters for the base case PSA

Design parameters	Symbol	Value
Number of beds		4
Feed pressure	P_{feed}	7 bars
Feed temperature	T_{feed}	303.15 K
Feed flow rate	$\dot{Q}_{feed}$	8.0 SLPM
Blowdown pressure	$P_{blowdown}$	1 atm
Bed length	L	0.6 m
Bed diameter	D	0.12 m
Particle diameter	d_p	3 mm
Adsorption time	τ	85.2 s

Computational parameters	Value
Axial grid nodes	40
Axial discretization method	CFDM
Number of differential variables	811
Number of algebraic variables	939

Table 4.6: Modeling parameters for the gas-solid system

C_{pH_2}	=	28.698	C_{pCH_4}	=	36.894
C_{p_s}	=	709	ρ_p	=	842
D_{mH_2}	=	7.736105×10^{-6}	D_{mCH_4}	=	4.1233577×10^{-7}
K_{gH_2}	=	0.16835	K_{gCH_4}	=	0.03281
$K_{LDF_{H_2}}$	=	$15 \times 8.89 \times 10^{-2}$	$K_{LDF_{CH_4}}$	=	$15 \times 3.96 \times 10^{-3}$
MW_{H_2}	=	2.016×10^{-3}	MW_{CH_4}	=	16.04×10^{-3}
μ_{H_2}	=	8.76×10^{-6}	μ_{CH_4}	=	8.76×10^{-6}
ϵ_b	=	0.4	ϵ_p	=	0.566

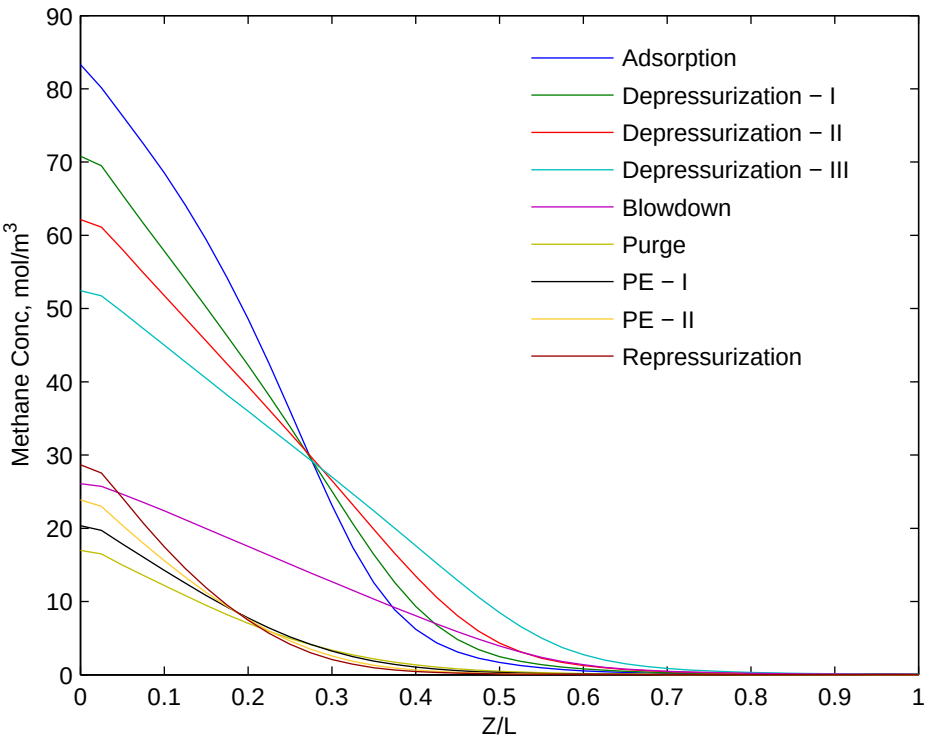

Figure 4.6: Methane axial concentration profiles at CSS at end of each PSA process step

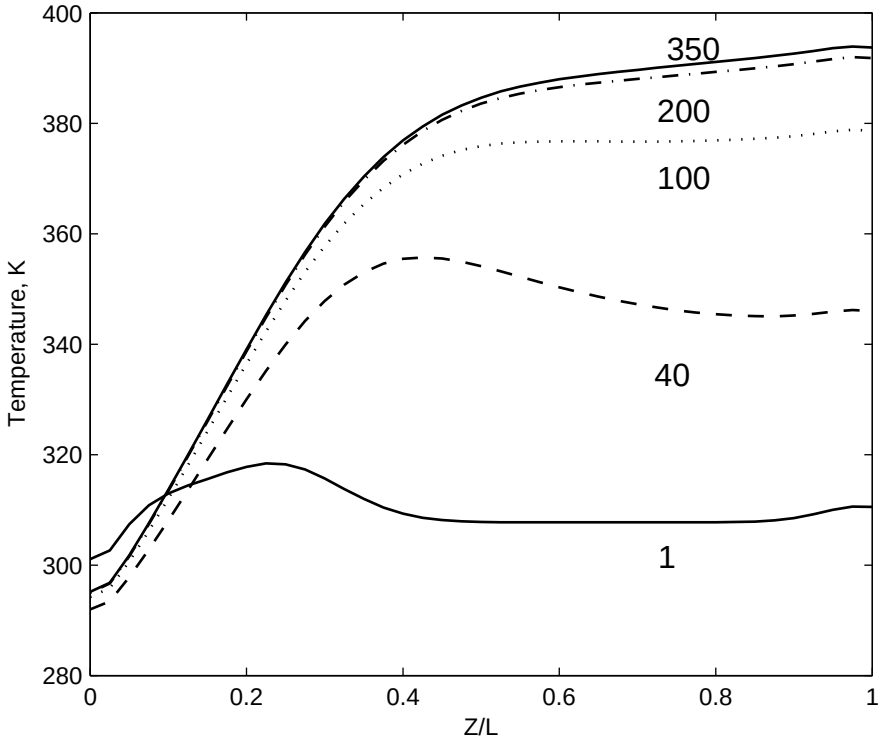

Figure 4.7: Evolution of axial temperature profiles with PSA cycles

umn evolves during a PSA cycle. Once the adsorption stage is over, the feed supply is closed and the product end is connected to other columns for the co-current depressurization steps - I, II, and III. This causes the impurity front to spread further towards the product end, leading to flatter concentration profiles. It can also be seen that during this time, the area under the curve remains almost constant as the bulk of impurities are still present inside the column. By the end of the purge stage, the impurity level reaches the minimum level. Thereafter, the impurities are further pushed towards the feed end (area under the curve remains almost the same as only small amount of impurities enter the column) during the counter-current pressure equalization (PE I and PE II) and re-pressurization stages.

The nonisothermal nature of gas-solid system under study is demonstrated in

Figure 4.7 which shows the axial temperature profile at the end of each cycle (repressurization step) as a function of the number of PSA cycles. The temperature at the end of cycle number 350 (which can be safely regarded as the CSS here) is quite different from the feed temperature of 303.15 K and the temperature profile after just one cycle. This justifies the inclusion of the energy balance equation in the overall model even though it increases the computational load.

4.4 System Identification

The system model developed in the last section essentially acts as a virtual PSA plant in the absence of a real PSA, and is crucial in assessing its dynamic performance under various operating conditions. However, such a large scale PDAE model is not directly suitable for model-based controller design. The essence of the system identification step is to identify a much simpler, preferably linear model relating the control variable, hydrogen purity with the manipulative variable, adsorption time, to reasonable accuracy. Bitzer [20], Bitzer and Zeitz [21, 22] derived a reduced PSA model by using simplifying assumptions for the original PDAE based model, and further using numerical inversion techniques for making it suitable for feedforward control purpose. Torre et al. [157] used an approximated, linear input-output (I/O) PSA model for their MPC controller, obtained by disturbing the PSA model with pseudo random binary signal (PRBS). Classical literature work on system identification [152, 89, 88, 182] provide further details on many possible techniques to identify reduced models for complex systems.

The identification procedure followed in this study starts by conducting dynamic simulations on the PDAE model, perturbed by various types of input (adsorption time) disturbances in the open loop environment. Even though step and impulse inputs are among the most commonly used disturbances in pro-

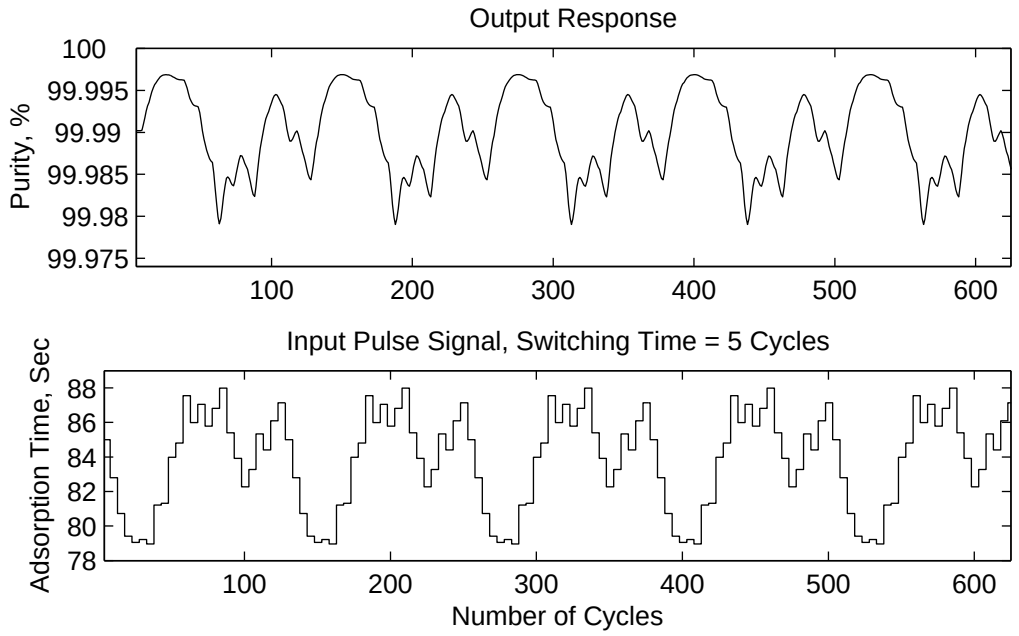

(a)

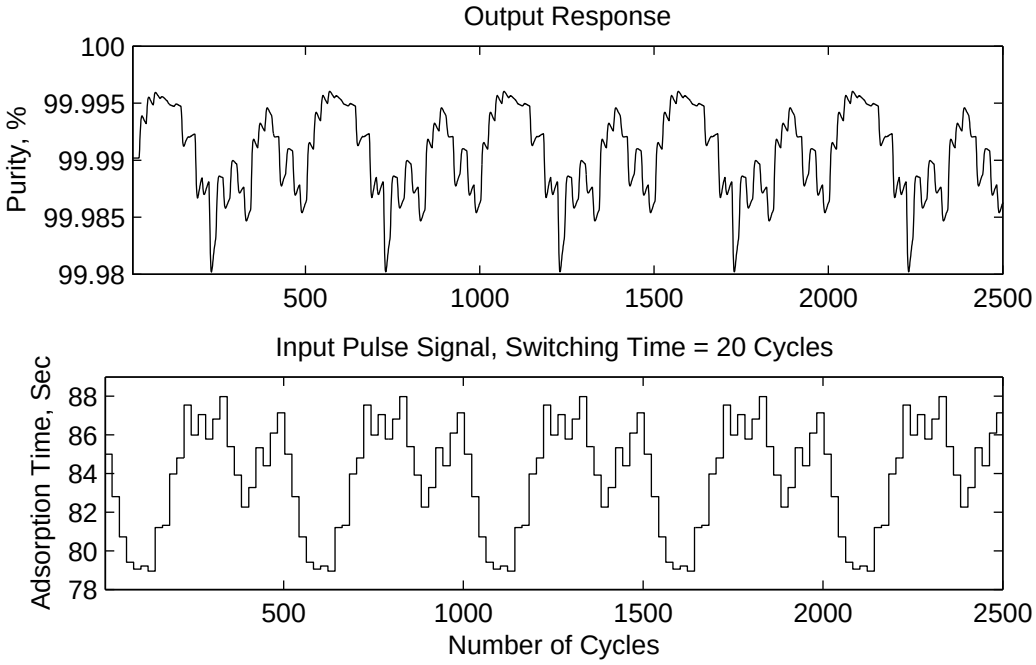

(b)

Figure 4.8: PSA purity response to adsorption time pulses with switching times of 5 and 20 cycles

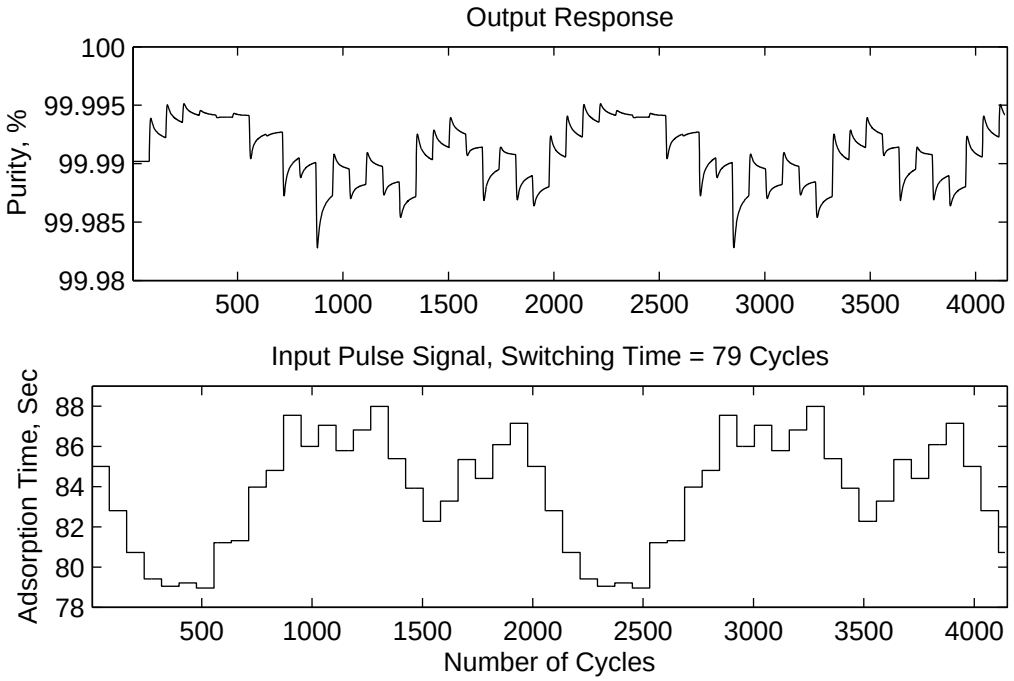

Figure 4.9: PSA purity response to adsorption time pulse with switching time of 79 cycles

cess industry due to their inherent simplicity, and ease of use in complex plant environment, even better reduced models can be obtained when the system is excited *persistently* [152, 88] over a large frequency band (of interest). Random pulsed inputs like filtered white noise, PRBS, and generalized binary noise (GBN) [152, 182] are ideal from this perspective, and have been used by industry and academia in the past. Keeping this in mind, the inbuilt random number generator *rand* in MATLAB® (2007b, The MathWorks) is employed to design random pulse signals, while taking additional considerations for the proper selection of two critical signal properties,

1. The maximum change to be allowed in signal amplitude from its previous value. A very large change can perturb the PSA system beyond the scope of fitting a single linear model. On the other hand, small changes do not disturb the system sufficiently to reveal its complete dynamic nature,

eventually leading to poor model identification.

2. The switching time for the pulse, t_{switch}, i.e. the time for which the signal stays constant before switching to the new (random) value. Very high values of switching time produces input-output behavior close to a step input change and thus does not offer any additional advantages. On the other hand, very low switching times do not allow PSA system to reveal its complete dynamic nature, apart from causing possible degradation of switch valve equipment.

In order to fix the first parameter, open loop experiments are performed with step signals of various step sizes, and a value of three seconds is finally selected. For t_{switch}, a well structured closed loop simulations based approach is employed wherein three random pulse signals are designed with the same magnitude (first parameter) but with different switching times. Figures 4.8a, 4.8b, and 4.9, shows the input-output response for input signals with t_{switch} of 5, 20, and 79, respectively. The best switching time is decided based on their closed loop performances which is discussed in section 4.5.1.

The fact that PSA operation is periodic and the manipulative variable is time itself, makes the choice of sampling frequency of measurements requiring additional attention. The sampling interval cannot be a fixed value for PSA operation, since all the process steps change and repeat after every cycle (time), whose duration in turn keeps changing (Eq. 4.19) in a closed loop setting. To overcome this challenge, purity-adsorption time measurements are recorded *every cycle* instead of fixed intervals. The measurements are made at product end ($z = L$) of the first bed, when the adsorption step of this bed is about to finish [83]. Multiple measurements, before the end of adsorption step and after it are also possible but are expected to increase the measurement cost, and the time

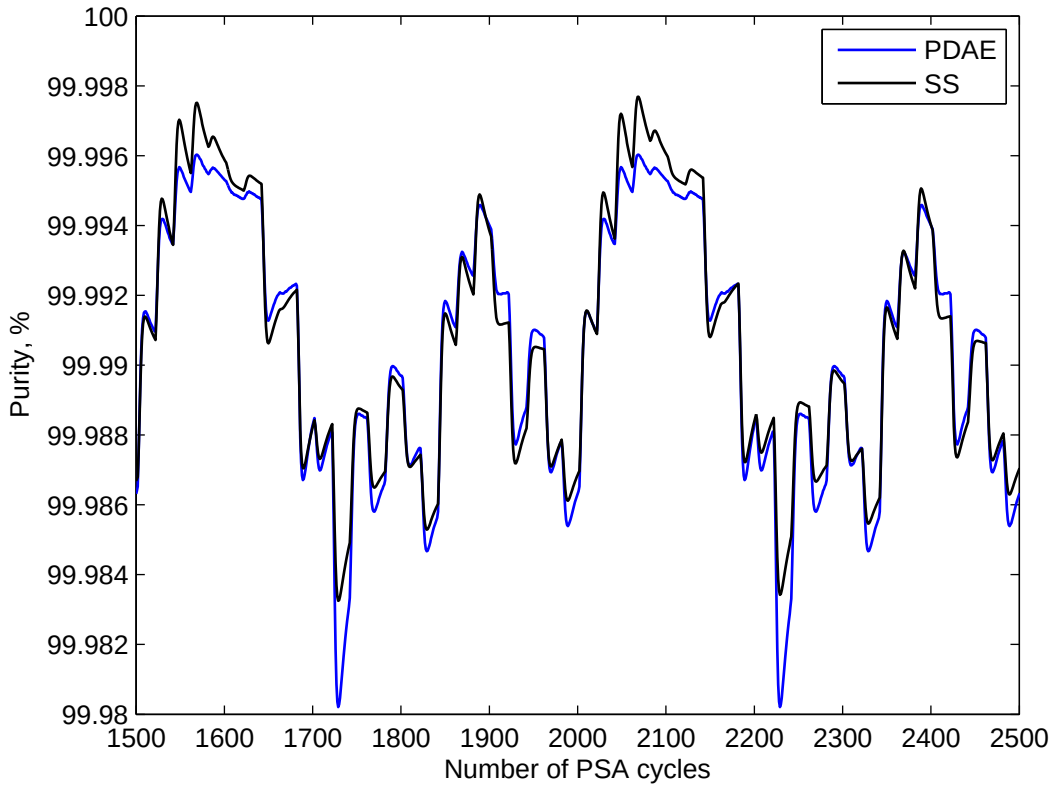

Figure 4.10: Comparison of simulated output data from the 8^{th} order state space model (Eq. 4.22 to 4.25) with the high fidelity PSA model

spent in analyzing the gas samples for purity, in reality. However, such a scenario cannot be ruled out and should be investigated in future studies.

$$\begin{aligned} x(k+1) &= Ax(k) + bu(k) \\ y(k) &= cx(k) \end{aligned} \tag{4.22}$$

$$A = \begin{bmatrix} 0.995200 & -0.094842 & -0.000503 & 0.000081 & 0.000952 & -0.000639 & 0.000471 & 0.000276 \\ 0.073930 & 0.901050 & 0.326910 & 0.067798 & 0.073069 & 0.002965 & -0.010204 & -0.003093 \\ -0.062509 & -0.328870 & 0.535580 & -0.289220 & -0.300420 & -0.085101 & 0.031899 & 0.089238 \\ 0.001968 & -0.023862 & 0.121230 & 0.763110 & -0.657910 & 0.207910 & 0.099469 & -0.037675 \\ 0.009228 & -0.029437 & 0.358270 & -0.240050 & 0.088491 & 0.399700 & -0.039895 & 0.010977 \\ 0.000416 & -0.004138 & 0.053762 & -0.013848 & -0.083413 & -0.793440 & -0.623400 & 0.289190 \\ -0.001794 & 0.001352 & -0.028014 & -0.051724 & -0.074588 & 0.455210 & -0.603850 & 0.667850 \\ -0.000856 & 0.000845 & 0.015982 & 0.048602 & 0.090379 & -0.190600 & -0.375270 & 0.051258 \end{bmatrix} \tag{4.23}$$

$$b = \begin{bmatrix} -0.00091 \\ 0.01446 \\ -0.02655 \\ 0.02073 \\ 0.04105 \\ 0.00955 \\ 0.02082 \\ 0.09066 \end{bmatrix} \tag{4.24}$$

$$c = \begin{bmatrix} 182.140 & -8.406 & -0.827 & -0.189 & -0.148 & -0.052 & 0.089 & 0.034 \end{bmatrix} \tag{4.25}$$

The resulting input-output response data is used within the MATLAB system identification toolbox to identify the best fit linear parametric model. For the output response obtained by input pulse of $t_{switch} = 5$ cycles, the best fit was achieved by a 4^{th} order state space model with a mismatch of 23 % from the

PDAE model response. Similarly, for the input pulse of $t_{switch} = 20$ cycles, a 8^{th} order SS model with a corresponding mismatch of 18 %, and for the input pulse of $t_{switch} = 79$ cycles, 16^{th} order SS model with mismatch of 14 %, were obtained. The 8^{th} order reduced SS model is presented in Eq. 4.22 to 4.25, while Figure 4.10 depicts performance comparison of the reduced model with the original PDAE model for the last 500 cycles.

4.5 Explicit/Multi-Parametric MPC for PSA

The control objective is defined as the fast tracking of hydrogen purity to set point of 99.99 %. Figures 4.11 and 4.12 show the long-term (CSS), and short-term time relationship of the product purity with the adsorption time (the manipulative variable) obtained by performing dynamic simulations on the base case system (tables 4.5 and 4.6). Figure 4.11, highlights the purity-recovery trade-off encountered during the PSA operations. Adsorption step time should not go to very low values to avoid uneconomical (low recovery) operation. Another very important reason to avoid very low values of adsorption time is to reduce the wear and tear of the switch valves interconnecting the adsorbent beds, as their active states change continuously depending upon the adsorption time.

Higher values of adsorption time should also be constrained, since a given amount of adsorbent can only accommodate a limited amount of the impurities. A large value of the adsorption time can over-saturate the bed (irreversible adsorption) making it unsuitable for future use. A much more direct method of avoiding over-saturation during the operation is to include it as a separate variable inside the optimization framework, and impose suitable hard constraints. However, measuring adsorbed amount of a species on solid surface in real time is rather impractical and instead the adsorption time as an indirect measurement,

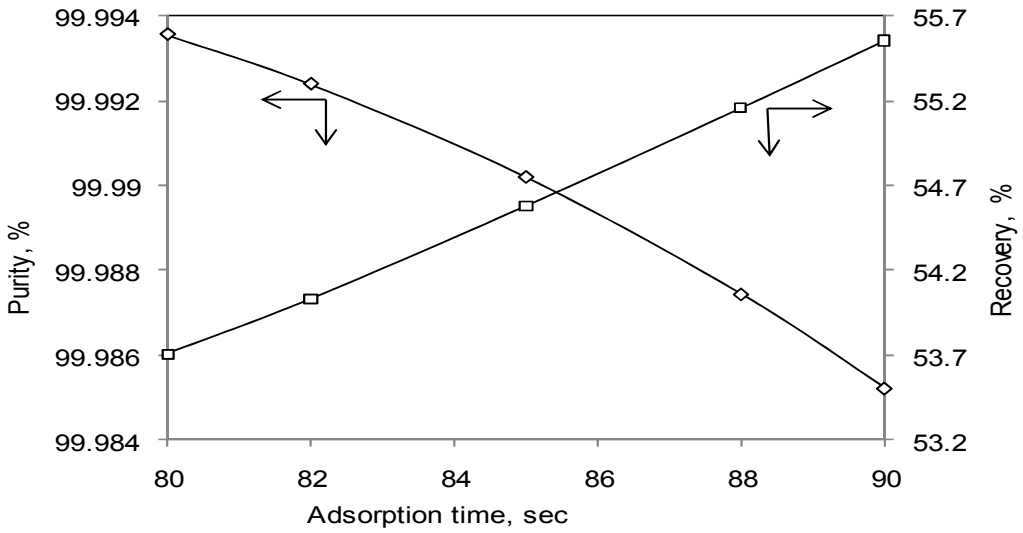

Figure 4.11: Variation of hydrogen purity and recovery with adsorption time at CSS for the base case PSA

Table 4.7: Parameters and critical regions for the reduced models derived in the system identification step

Switching time (PSA cycles)	Best fit SS model order	Number of parameters	No. of critical regions
5	4	7	22
20	8	11	22
79	16	19	22

can be used to overcome this challenge. Note that a large adsorption time not only changes the time duration of adsorption phase (during which the impurities enter the bed) but also increases the time duration of impurity removal blowdown and purge steps. However, once the adsorbent is damaged due to over-saturation, even long duration impurity removal steps would not be enough for regenerating the bed to desired state. Similarly, large changes in the adsorption time (Δu in Eq. (5.20)) should also be constrained to avoid over saturation ($+\Delta u$) or avoid sudden surge of inflow ($-\Delta u$).

A model based predictive controller (MPC) which incorporates the above men-

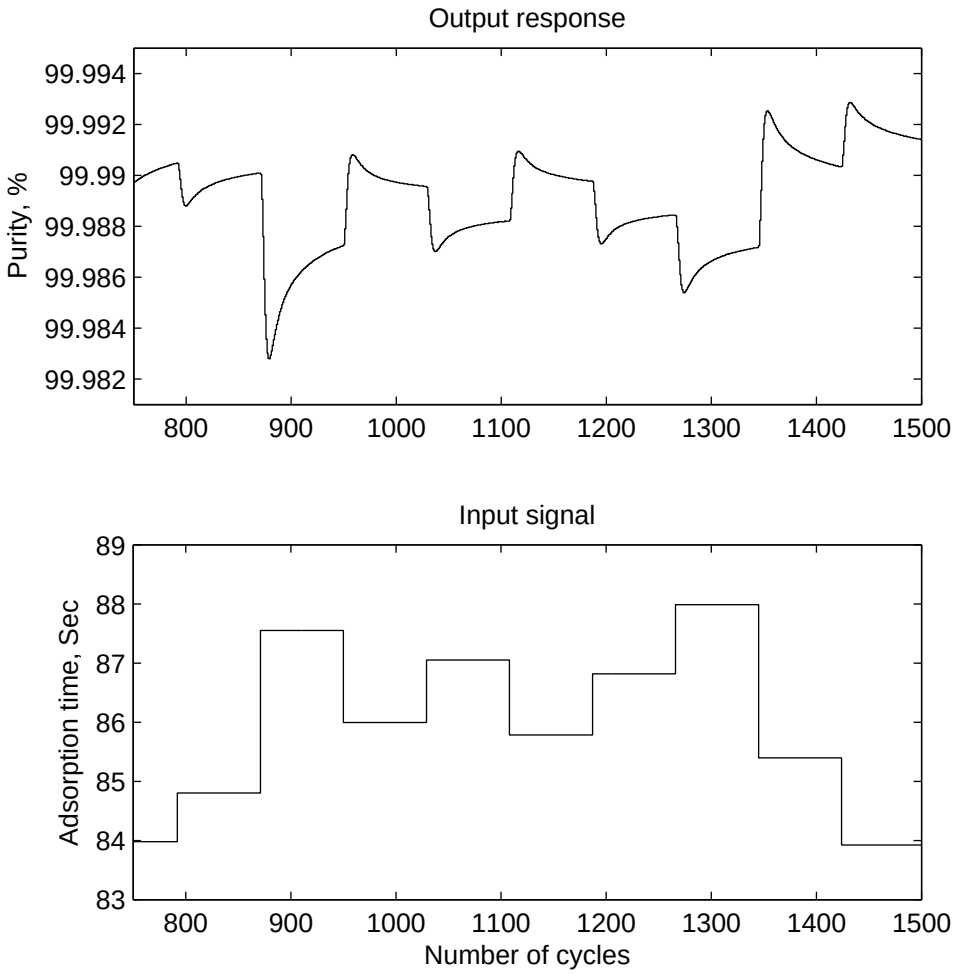

Figure 4.12: Cyclewise variation of hydrogen purity with adsorption time

tioned operational constraints in an optimization framework is formulated in Eq. (5.20). Here, y is the control variable, the hydrogen purity, y^r is the set point purity, and u is the manipulative variable, the adsorption time. Furthermore, y has been scaled as $y = (y_{original} - 0.9999) \times 10^5$, which also makes y^r as zero. The same scaling rule is employed while performing the system identification step to maintain consistency. The model mismatch error, $e(k)$ (= y_{plant} - y) is taken into consideration to ensure offset free tracking. N and M represents the prediction and control horizon, fixed to values 4 and 2, respectively. The sampling interval is taken as one complete PSA cycle, where k is the particular sampling instant.

$$
\begin{aligned}
\min_{u} \quad Z &= \sum_{k=1}^{N-1} (y(k) - y^r(k))^T (y(k) - y^r(k)) + \sum_{k=0}^{M-1} \Delta u(k)^T R \Delta u(k) \\
s.t. & \\
x(k+1) &= Ax(k) + bu(k) \\
y(k) &= cx(k) + e(k) \\
55 \leq \; u(k) &\leq 115 \\
y(k) &\leq 1
\end{aligned}
\tag{4.26}
$$

In order to obtain the explicit control laws for the MPC problem in Eq. (4.26) specified above, the POP toolbox [122, 117, 118] is employed. In the first step which is performed offline, the MPC problem is re-formulated as a multi-parametric quadratic programming problem [119, 120, 121]. Table 4.7 shows the number of parameters obtained for each of the reduced SS model derived in section 4.4. For example, the 8^{th} order SS model requires 11 parameters, including 8 parameters x_1, x_2, ..., x_8 for each state ranging from -100 to 100, one for u ranging from 55 to 115, one for y ranging from -100 to 10, and the remaining one for y^r ranging from -0.1 to 0.1. In the next step, the multi-parametric program-

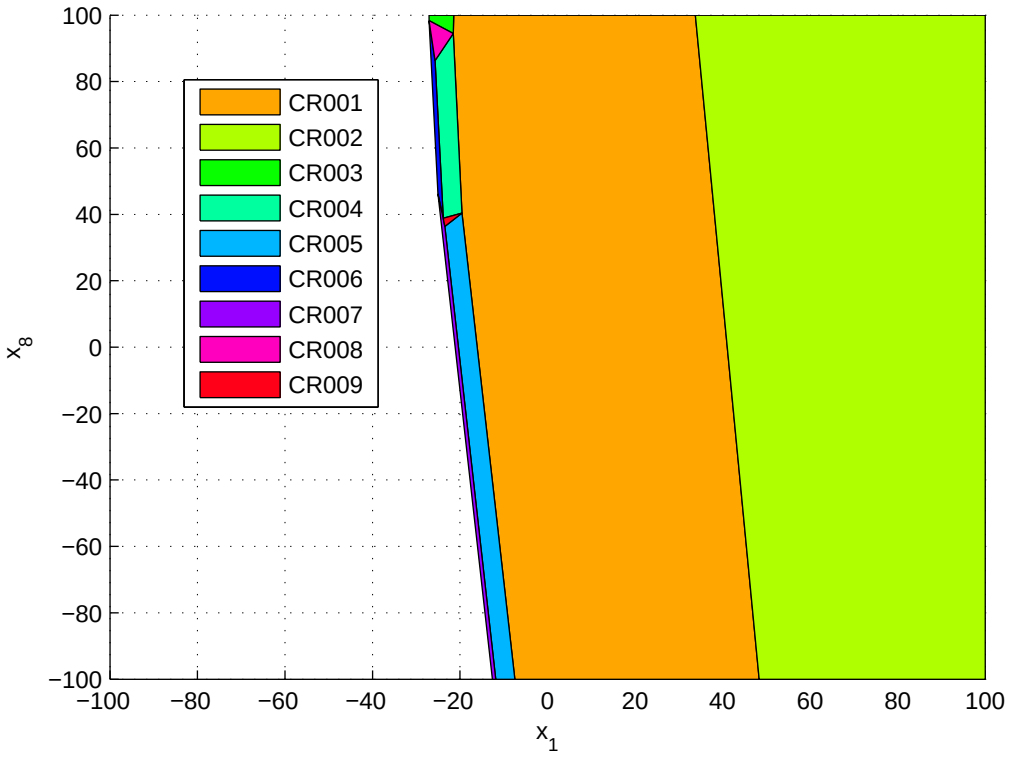

Figure 4.13: Two dimensional projection of the 22 critical region (CR) polyhedral, corresponding to the 8^{th} order reduced SS model (Eq. 4.22 to 4.25), [$x_2 = 0$, $x_2 = 0$, ..., $x_7 = 0$, $u = 85$, $y = 0$, $y^r = 0$], $N = 4$, $M = 2$ and $R = 30$

ming problem is solved, yielding a set of affine functions relating the control law explicitly to the parametric set. The corresponding critical regions over which these relationships hold are also derived and stored for later use (online). Table 4.7 shows the number of critical regions for each of the reduced SS model while Figure 4.13 depicts the critical region maps for state variables x_1 and x_8 of the 8th order SS model, with the regions in white color representing the infeasible region. The affine functions related to each critical region are shown in Table 4.8. Here, θ represents the particular parametric set (x_1, x_2, ...,u, y, y^r). The matrix inequalities, which each parametric set needs to satisfy for each critical region is not displayed here because of the large size of matrix A and vector b.[1]

[1]Provided upon request from the authors.

Table 4.8: Explicit control laws as affine function of parameters for the 8^{th} order SS model (Eq. 4.22 to 4.25)

$CR_1 : A_1\theta = b_1$

$$u = \begin{bmatrix} -0.353 & -2.235 & -0.857 & -0.026 & 0.038 & 0.016 & -0.003 & -0.025 & 0.939 & 0.067 & -0.067 \\ -0.538 & -3.337 & -1.310 & -0.036 & 0.061 & 0.025 & -0.005 & -0.039 & 0.907 & 0.097 & -0.097 \end{bmatrix} \theta + \begin{bmatrix} 0 \\ 0 \end{bmatrix}$$

$CR_2 : A_2\theta = b_2$

$$u = \begin{bmatrix} -0.091 & -0.606 & -0.217 & -0.008 & 0.008 & 0.004 & 0 & -0.006 & 0.496 & 0.020 & -0.020 \\ 0.000 & 0.000 & 0.000 & 0.000 & 0.000 & 0.000 & 0 & 0.000 & 0.000 & 0.000 & 0.000 \end{bmatrix} \theta + \begin{bmatrix} 26.851 \\ 55 \end{bmatrix}$$

$CR_3 : A_3\theta = b_3$

$$u = \begin{bmatrix} -5.346 & -59.731 & -9.373 & -0.878 & 0.252 & -0.160 & 0.036 & 0.073 & 0 & 3.696 & 0.000 \\ -5.361 & -58.885 & -9.538 & -0.860 & 0.268 & -0.145 & 0.032 & 0.055 & 0 & 3.603 & -0.032 \end{bmatrix} \theta + \begin{bmatrix} -36.958 \\ -35.706 \end{bmatrix}$$

$CR_4 : A_4\theta = b_4$

$$u = \begin{bmatrix} -4.841 & -36.760 & -11.331 & -0.987 & -0.232 & 0.170 & 0.100 & -0.187 & 0.128 & 1.237 & 0 \\ -6.693 & -50.694 & -15.677 & -1.354 & -0.310 & 0.237 & 0.136 & -0.262 & -0.206 & 1.702 & 0 \end{bmatrix} \theta + \begin{bmatrix} -12.387 \\ -16.991 \end{bmatrix}$$

$CR_5 : A_5\theta = b_5$

$$u = \begin{bmatrix} -4.328 & -24.562 & -10.749 & -0.111 & 0.696 & 0.228 & -0.081 & -0.368 & 0.259 & 0.623 & 0 \\ -6.885 & -38.997 & -17.108 & -0.172 & 1.113 & 0.364 & -0.130 & -0.588 & -0.179 & 0.985 & 0 \end{bmatrix} \theta + \begin{bmatrix} -6.185 \\ -9.878 \end{bmatrix}$$

$CR_6 : A_6\theta = b_6$

$$u = \begin{bmatrix} -8.993 & -68.209 & -21.057 & -1.827 & -0.425 & 0.317 & 0.184 & -0.349 & 0 & 2.293 & 0 \\ 0.000 & 0.000 & 0.000 & 0.000 & 0.000 & 0.000 & 0.000 & 0.000 & 0 & 0.000 & 0 \end{bmatrix} \theta + \begin{bmatrix} -94.272 \\ 115.000 \end{bmatrix}$$

$CR_7 : A_7\theta = b_7$

$$u = \begin{bmatrix} -14.294 & -81.014 & -35.515 & -0.360 & 2.307 & 0.755 & -0.268 & -1.219 & 0 & 2.048 & 0 \\ 0.000 & 0.000 & 0.000 & 0.000 & 0.000 & 0.000 & 0.000 & 0.000 & 0 & 0.000 & 0 \end{bmatrix} \theta + \begin{bmatrix} -186.96 \\ 115.00 \end{bmatrix}$$

$CR_8 : A_8\theta = b_8$

$$u = \begin{bmatrix} -5.346 & -59.731 & -9.373 & -0.878 & 0.252 & -0.160 & 0.036 & 0.073 & 0 & 3.696 & 0 \\ -5.879 & -13.666 & -18.833 & -1.528 & -1.090 & 0.769 & 0.239 & -0.680 & 0 & -2.262 & 0 \end{bmatrix} \theta + \begin{bmatrix} -36.958 \\ 22.616 \end{bmatrix}$$

$CR_9 : A_9\theta = b_9$

$$u = \begin{bmatrix} -5.017 & -58.607 & -10.214 & -2.927 & -2.473 & -0.011 & 0.524 & 0.303 & 0 & 2.476 & 0 \\ -6.408 & -15.479 & -17.478 & 1.773 & 3.302 & 0.530 & -0.547 & -1.051 & 0 & -0.296 & 0 \end{bmatrix} \theta + \begin{bmatrix} -24.762 \\ 2.956 \end{bmatrix}$$

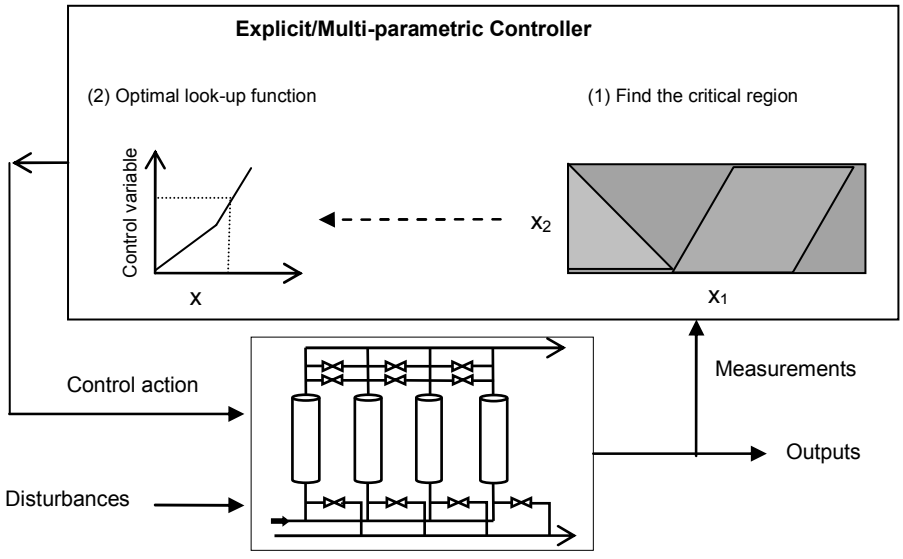

Figure 4.14: Online implementation of the explicit/multi-parametric controller for PSA

During the online operation (second step), as shown in Figure 4.14, as soon as the plant measurements are provided, the explicit/multi-parametric controller searches for the particular critical region corresponding to the measurement set, out of the 22 such regions, and extracts the corresponding control law.

4.5.1 Closed Loop Validation

To evaluate the performance of the designed controllers, a step increase of the PSA feed flow rate by 10 % from its design value is carried out and closed loop simulations are conducted with tuning factor R in Eq. (4.26) varying from 5 to 100. Here, the high fidelity PDAE model acts as the virtual plant. Figure 4.15 compares the closed loop performance of the derived mp-MPC controller configurations, with each curve corresponding to the reduced models designed in the system identification step. The closed loop simulation results are presented in terms of two PSA controller performance indicators; the controller response time, defined as the minimum number of PSA cycles required to permanently raise the hydrogen purity levels above the set point of 99.99 %, and the mean control effort (Δu) performed by the controller during the response time. The maximum change in manipulative variable (maximum Δu) during the response time is also calculated - large value highlights any violation of operational constraints on adsorption time changes, as mentioned in section 4.5.

From the plots in Figure 4.15, it is evident that increasing R slows down the controller response time (first performance indicator) while the mean control effort (second performance indicator) decreases. This behavior can be attributed to the particular type of objective function used in Eq. (4.26). It is also interesting to observe that even though the reduced models with $t_{switching}$ at 20 and 79 are different in terms of the input signal switching time, purity response and model fits, they have similar closed loop performance. This is in sharp contrast to the

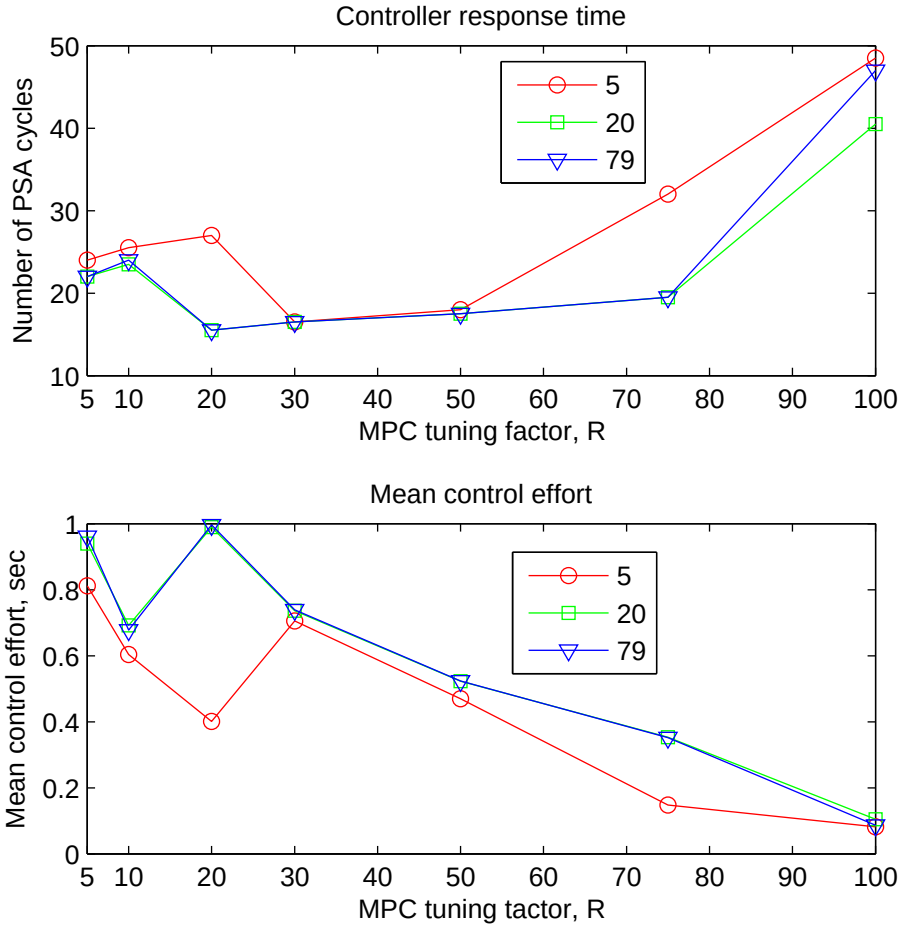

Figure 4.15: Comparison of reduced models with different $t_{switching}$, against two PSA controller performance indicators for the step disturbance case study

performance of the controller derived from a reduced model with $t_{switching}$ at 5 cycles. These results clearly demonstrates the potential benefits of rigorous system identification procedures for PSA.

Note that the controller configuration designed from the reduced model with a switching time of 20 cycles provides the best performance, as it gives the least value of the first performance indicator for a wide range of R while maintaining lower values of the second performance indicator. Furthermore, the best R value for this controller seems to be 30 as it provides the least value of the first per-

formance indicator. Henceforth, this is the controller setting used for comparing explicit/multi-parametric MPC with conventional PID controller.

4.5.2 Comparison With A PID Controller

PID controllers are also designed for comparison purposes. The systematic design procedure described in Seborg et al. [142] is followed here, comprising the following steps. First, the auto tuning method of Åström and Hägglund is used to evaluate the ultimate gain and ultimate period of the purity-adsorption time loop. In the next step, these values are used to derive the initial guess for the PID tuning parameters namely, the proportional gain, integral time and derivative time using the Ziegler-Nichols tuning relations. Finally, closed loop simulations are performed to further refine these tuning parameters, while the best results in terms of two performance indicators are obtained. The step disturbance procedure described in section 4.5.1 is employed for this purpose.

Table 4.9 provides a summary of closed loop performance comparison studies conducted on the PID and mp-MPC controller, for three types of disturbance scenarios:

10 % step increase in PSA feedrate For this scenario, mp-MPC controller shows controller response time of 13 cycles. This is twice as fast as the PID controller, which takes 25 cycles to performs the same task. Furthermore, the mp-MPC controller achieves this task while maintaining the control effort at lower values.

35 % impulse increase in PSA feedrate The disturbance this time is very fast as the open loop response settles down in nine PSA cycles. As a result, the closed loop performance of the PID and mp-MPC controller in terms of controller response time is almost same. However, the mean control effort for the PID controller comes out to be much larger than that for mp-MPC controller. PID

Table 4.9: Closed loop performance comparison of explicit/multi-parametric MPC with PID controller

10 % Step increase in PSA feedrate			
Controller	Response time (Cycles)	Average Δu (Sec)	Maximum Δu (Sec)
mp-MPC	13	0.74	1.8
PID	25	0.84	5.09
Open loop	∞		
35 % Impulse increase in PSA feedrate			
mp-MPC	7	0.75	1.60
PID	5	4.72	12.12
Open loop	9		
54 % Impulse increase in PSA feedrate			
mp-MPC	7	1.77	4.18
PID1	4	17.11	32.29
PID2	5	9.44	21.16
Open loop	10		

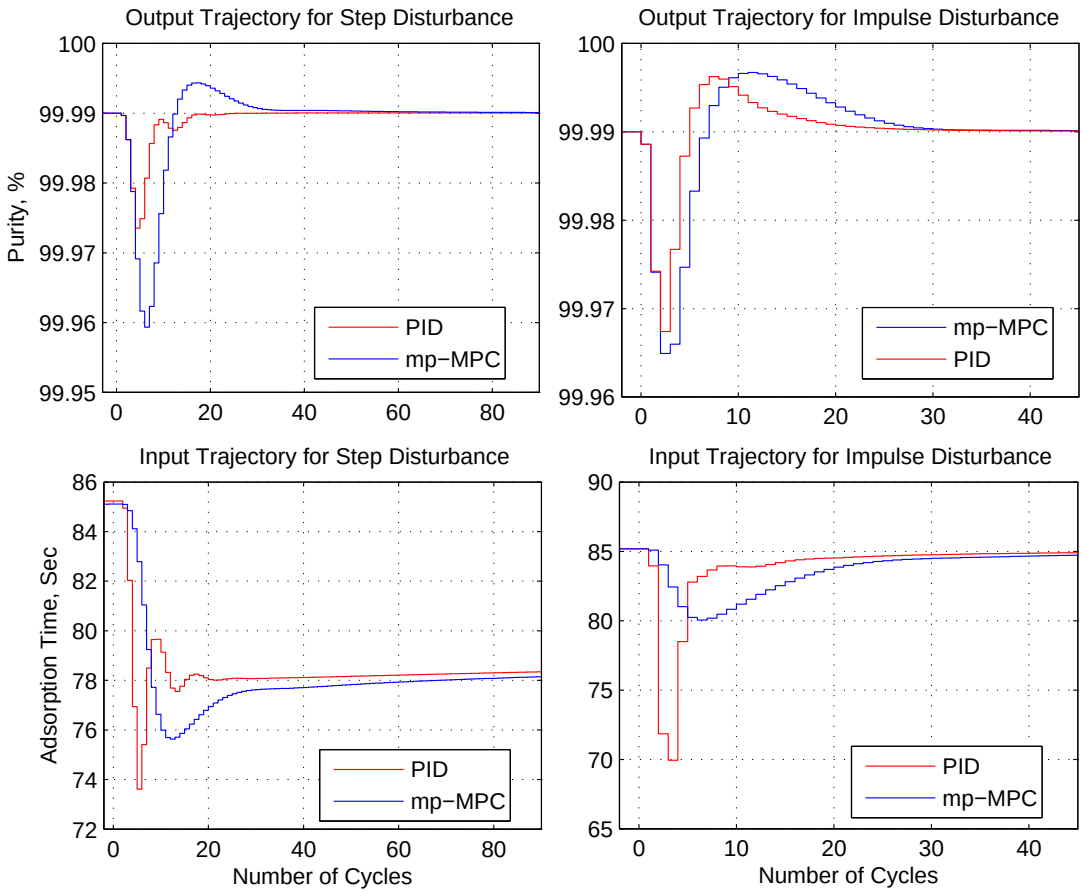

Figure 4.16: Closed loop performance comparison of mp-MPC and PID controllers for the 10% step and 35 % impulse disturbance scenarios

results shows that during the response time, maximum Δu is around 12 seconds. This is a large number and such a big change in adsorption time, as discussed earlier, can cause damage to the solid adsorbent and should be avoided. On the other hand, the mp-MPC controller provides a much better and safer response to the disturbance as exhibited in Figure 4.16.

54 % impulse increase in PSA feedrate In this scenario, open loop response settles down in 10 PSA cycles, as shown in Table 4.9. PID1 controller results corresponds to the case, when the tuning parameters are still left unchanged. This PID controller configuration takes least time to control the disturbance however, it also violates hard constraints on the adsorption time, as shown in Figure

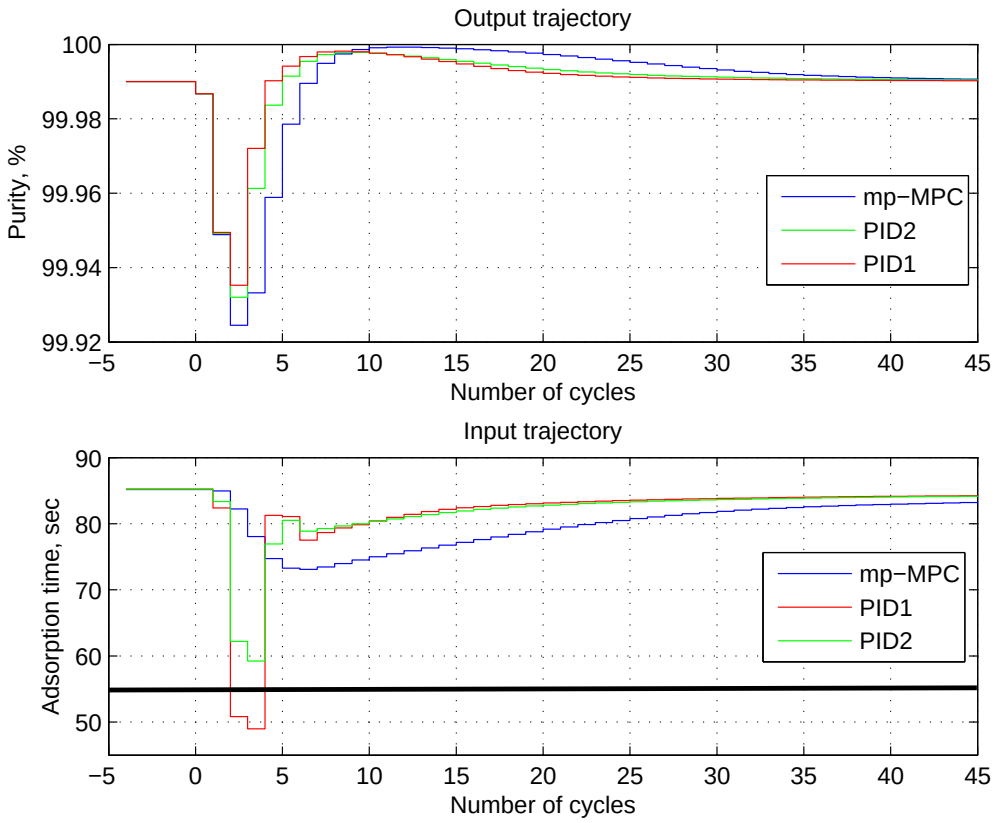

Figure 4.17: Closed loop comparison of mp-MPC and two different PID controllers for the 54 % impulse disturbance scenario

4.17. A further re-tuning of PID1 controller, represented by PID2 controller keeps the adsorption time above the 55 seconds limit. However, the mp-MPC controller provides much superior performance as it achieves almost the same controller response time at much lower values of mean control effort. Figure 4.17 further shows that the adsorption time trajectory during the response time is far away from the defined constraints, without requiring any re-tuning efforts.

4.6 Conclusions

This work presents a detailed study on an important but relatively unexplored area of PSA control, following a rigorous and comprehensive mp-MPC frame-

work. This integrated framework based approach, appears to be a better option for the controller design and validation of complex systems like PSA with strong nonlinearities coupled with interconnected column dynamics. Furthermore, multiple reduced models are built during the system identification step to probe the role of model mismatch during the closed loop validation step. The results shows that the model identified with pulse switching time of 20 cycles gives the best performance, although the model with switching time of 79 cycles both performs better than the 5 cycles case.

Multiple disturbance scenarios in the PSA feed rate are created for comparing the performance of mp-MPC with the standard PID controllers. For the step disturbance study, mp-MPC controller is twice as fast as the PID controller, while the control efforts for both controllers are comparable. On the other hand, for impulse disturbance studies, the speed of response of both controller modes is quite similar, while the controller effort for mp-MPC is considerably smaller than the PID controller. When the impulse disturbance is increased to 54 % change in feed rate, the PID controller violates the lower bound on the input variable, requiring re-tuning, while the mp-MPC handles this disturbance without any constraint violation.

Chapter 5

Simultaneous Design and Control Optimization of PSA Systems Under Uncertainty

5.1 Literature Review for PSA Optimization

5.1.1 Introduction

The traditional approach for design and operation of process systems usually employs a two step, sequential based approach. In the first step, a typical process synthesis problem is formulated to design a process which maximizes an economical objective while satisfying pre-defined steady state values of operating requirements [143, 141, 40]. Subsequently, to overcome the effect of uncertainty or unforeseen scenarios in design operating conditions, the system is over-designed by employing empirical or semi-empirical techniques [164, 158, 114] such as margin of safety etc. In the second step, to mitigate the effect of operating disturbances on plant performance, a suitable controller is designed [108, 87]. This sequen-

tial approach is the most widely used ones by the process design community [143, 114, 52].

Nonetheless, in the last few decades, the importance of incorporating real-time operability aspects during the design stage itself has been greatly emphasized. Some of the early contributions in this field [86, 100], albeit focussing on simplified linear systems, suggested various analytical tools and indices [150, 110] while providing meaningful insights into ways of integrating design and control formulations. A detailed survey of important contributions in this field is shown in Table 5.1, while Table 5.2 presents some more recent work in this area. An important trend which has emerged from the past studies is the wide acceptance of optimization based method [113, 98, 12, 15, 99] and their applications to various systems such as distillation columns [14, 13, 138], CSTRs [59] and systems represented by reduced models [131, 130].

5.1.2 PSA Optimization

A rigorous and detailed model, on one hand is extremely important for mimicking the real operation with accuracy, while on the other hand it can also be computationally challenging to solve for for modeling and optimization purposes. Further challenges are posed by the fact that the PSA operation is periodic in nature and never attains a true steady state, requiring computationally expensive simulations to be carried out for hundreds of cycles until cyclic steady state is established.

Table 5.3 outlines some of the key contributions in the PSA optimization field, highlighting the trade-offs between the model reduction approaches to reduce system complexity, and methodologies to directly evaluate the CSS conditions with detailed models. Note that most of these studies focusses on the acceleration of cyclic steady state (CSS) to minimize the computational load related to the

Table 5.1: Key contributions in the field of integrated design and control

Authors	Features
Nishida and Ichikawa [105]	Optimization for design of dynamic system with piecewise control
Nishida et al. [106]	A min-max formulation for design of dynamic system under parametric uncertainty
Lenhoff and Morari [86]	Multi-objective formulation; Simultaneously incorporation of steady state economics and dynamic performance indexes
Palazoglu and Arkun [110]	Optimization based approach with steady state economics as objective, and dynamic performance robustness indices ε constrained
Luyben and Floudas [90]	MINLP formulation with steady state economics as objective, and controllability index ε constrained
Mohideen et al. [98]	An iterative decomposition algorithm for simultaneous design and control under uncertainty
Bansal et al. [12]	Mixed integer dynamic optimization (MIDO) based iterative decomposition algorithm for simultaneous design and control optimization under uncertainty
Sakizlis et al. [138]	Extended the decomposition algorithm from [98] and [12] for the explicit/multi-parametric MPC controller mode

Table 5.2: A brief overview of some recent work in the field of integrated design and control

Authors	IDC formulation	Case study	Modeling details	Controller details
Asteasuain et al. [5]	Mixed integer dynamic optimization (MIDO) formulation at nominal conditions, controller performance indicators not included	Styrene bulk polymerization reactor	DAE	Superstructure based MIMO formulation of feedforward-feedback controller
Chawankul et al. [29]	Lumped the capital and operating cost at steady state along with the controller performance cost into a single objective function	Multi-component distillation column separation	DAE	Robust formulation of SISO control
Asteasuain et al. [6]	Decomposition algorithm [113, 98] with outer approximation approach for integer variables and over estimator to simply the process dynamic feasibility test	Design and control for grade transition of styrene polymerization process	DAE	Superstructure based MIMO formulation for feedforward-feedback configuration
Flores-Tlacuahuac and Biegler [49]	ISE treated as objective function, MIDO problem transformed to MINLP by employing finite element method on the state and control variables	CSTR	DAE	Superstructure based approach for process and control alternatives
Chawankul et al. [30]	Lumped the capital and operating cost at steady state along with the controller performance cost into a single objective function. Furthermore, The steady state model and dynamic models represented by simplified empirical correlations. Model mismatch treated as process uncertainty	Top and bottom purity control for depropanizer column	Empirical correlations deduced from RADFRAC (Aspen PLUS)	Robust formulation for MIMO based MPC controller
Malcolm et al. [92]	Decomposition algorithm [113, 98] with an extra step of steady state flexibility analysis before the dynamic one to reduce the search space of critical uncertain parameters scenarios. Furthermore, the optimal design and control problem are decoupled with the optimal control problem solved for fixed design. The solution of optimal control subproblem only effects the master optimal design problem if the operation fails in the flexibility tests	Polymerization reactor design and control, and binary column separation	DAE	Fixed controller structure with MIMO formulation
Ricardez-Sandoval et al. [130]	Algorithm based on employing finite impulse response model of the original system at nominal conditions to evaluate the worst case disturbance and critical parametric uncertainty simultaneously. The resulting design is validated by performing closed loop simulation on the original model	Tennessee Eastman process	DAE, lumped objective function containing steady state capital and operating cost with real-time process output variability cost	Fixed controller structure of PI loops
Hamid et al. [59]	Four stage decomposition algorithm with multi-objective formulation incorporating design and control objectives; used thermodynamics insights to narrow down the feasible region	Ethylene glycol production (CSTR) and separation (distillation column)	DAE	Controller structure based on analysis of control variable sensitivities to process disturbances and manipulative variables

Table 5.3: A brief overview of important literature studies on PSA optimization

Authors	PSA system	Modeling details	CSS acceleration	Optimization formulation	Objective function
Smith and Westerberg [151]	H_2-CH_4, H_2 bulk separation	Very simplified model, comprising time averaged mass and energy balances	Not required	MINLP	Capital and operating costs
Nilchan and Pantelides [104]	Single bed RPSA for air separation and two bed, six step PSA for N_2 purification from air	General framework for periodic adsorption processes	Complete discretization of spatial and temporal derivatives,	NLP	Average power
Ko et al. [79]	1 bed, 4 step CO_2 sequestration from CO_2-N_2	Constant superficial velocity	CSS evaluated by expressing spatial profile of differential variables in empirical expressions	NLP	Maximize CO_2 and N_2 purity
Jiang et al. [68]	1 bed, 3 step and 6 step air separation	Nonisothermal operation, steady state momentum balance	Direct determination approach augmented with a hybrid trust region method for Newton step improvement	NLP	O_2 recovery and specific work
Jiang et al. [69]	5 bed, 11 step for H2 purification from H_2, CH_4, CO, CO_2, NH_2	Nonisothermal and steady state momentum balance, bed dispersion neglected	Direct determination approach [68]	NLP	H_2 recovery
Cruz et al. [36]	O_2 production from air; three possible equalization configurations	Non isothermal operation, model formulated in the dimensionless form to reduce number of variables, employed empirical pressure profile for pressurization/depressurization stages	Not considered	NLP	Recovery and power consumption
Nikolić et al. [103]	H2 purification from H_2, C_4, CO, CO_2	Detailed and generic modeling framework [102]	Unibed approach	NLP, repeated optimization for optimal number of beds for pre defined PSA cycles	Recovery
Agarwal et al. [2]	2 bed, 4 step PSA, H_2 purification from H_2 and CH_4	Detailed model linear superficial velocity profiles	Performed model reduction employing proper orthogonal collocation	NLP	Recovery

optimization procedures. In this regard, three key methodologies, the complete discretization approach proposed by Nilchan and Pantelides [104], the unibed formulation from Kumar et al. [84], and the CSS direct determination approach [39] employed in the work of Jiang et al. [68], are discussed here in detail.

5.1.2.1 Direct Determination Approach

This approach employs numerical procedures to directly obtain the CSS, instead of solving the full scale PSA model, cycle by cycle. It starts by posing CSS as a two point boundary condition, as shown in Eq. 5.1, requiring the final state of the system to be exactly the same as the state after one complete PSA cycle.

$$\mathbf{e}_j = \begin{bmatrix} \mathbf{yp}(t_{cycletime})_j - \mathbf{yp}_j^0 \\ \mathbf{g}_j \end{bmatrix} = 0 \tag{5.1}$$

Here, j is the iteration counter, $\mathbf{yp}^0$ is the initial state of the PSA system, while $\mathbf{g}_j$ represents the PSA operational constraints which must be satisfied at the CSS such as the purity constraint. In general, $\mathbf{yp}$ is composed of n PSA variables, such as temperature, species concentration distributed over m grid points across the bed, as shown in Eq. 5.2.

$$\mathbf{yp} = \begin{bmatrix} yp_{11} & yp_{12} & \cdots & yp_{1n} \\ yp_{21} & yp_{22} & \cdots & yp_{2n} \\ yp_{31} & \cdots & \cdots & yp_{3n} \\ \vdots & & \ddots & \\ yp_{m1} & \cdots & \cdots & yp_{mn} \end{bmatrix} \tag{5.2}$$

Next, Newton method is applied on the Eq. 5.1, yielding a working formula for the evaluation of new estimate of the PSA CSS, as mentioned in Eq. 5.3. It is important to note that this method converges quadratically to the CSS, given

that the estimated CSS state is in the vicinity of the actual one.

$$\mathbf{yp}^0_{j+1} = \mathbf{yp}^0_j - \mathbf{J}_j^{-1}\mathbf{e}_j \tag{5.3}$$

A challenging task in the employment of the direct determination approach is the evaluation of the large Jacobian matrix $\mathbf{J}$, for each iteration, which contains the CSS sensitivity information with respect to all PSA system variables.

$$\mathbf{J}_j = \left.\frac{\partial \mathbf{e}}{\partial[\mathbf{yp}, \mathbf{d}]}\right|_{[\mathbf{yp}^0_j, \mathbf{d_j}]} \tag{5.4}$$

Towards this, Ding and LeVan [39] used hybrid Newton-Broyden method to directly update $\mathbf{J}^{-1}$, while employing an iterative secant method to estimate its initial value (for the first iteration). Jiang et al. [68], also used direct determination approach for PSA optimization and incorporated CSS condition as an constraint in the overall optimization formulation, as shown in Eq. 5.5. Consequently, the decision variables and the PSA state variables simultaneous converges to their final optimal values and CSS, respectively.

$$\begin{aligned}
\max_{d_P, yp^0} \quad & \phi(yp, yp^0, d_P) \\
s.t. \quad & \\
h1(\dot{yp}, yp, d_P, t) &= 0 \\
g1(\dot{yp}, yp, yp^0, d_P, t) &\leq 0 \\
e_{CSS} = yp - yp^0 &= 0 \\
LB \leq [yp^0, d_P] &\leq 0
\end{aligned} \tag{5.5}$$

Furthermore, Ayoub et al. [7] used direct determination approach to perform PSA modelling simulations by posing CSS evaluation as an optimization problem

with CSS error (Eq. 5.1) as the objective function to be minimized, and initial conditions as decision variables, while also studying the effect of various types of sensitivity evaluation methods.

5.1.2.2 Unibed Approach

The unibed framework, first mentioned in the work of Kumar et al. [84], attempts to reduce the PSA system size by employing only one bed for simulation purposes. The three key facts related to PSA operation which are exploited in the formulation are the following.

1. All adsorption columns of a PSA system for a fixed PSA cycle undergoes same sequence of processing steps but with a fixed time lag.

2. The duration of a particular processing step for any adsorption column is exactly the same.

3. During the process steps where two columns are interconnected to each other, any column will only require the process conditions information of the bed end (connecting end) of the other bed while interacting.

Consequently, the temporal profiles of the effluent streams for the bed-interconnecting steps are stored separately, and utilized later in the cycle, thereby eliminating the need for extra beds to perform the full operation. For example, for a four column PSA system only a single column is actually simulated and during the processing steps such as co-current depressurization step where the bed is connected to an other bed undergoing counter-current pressure equalization, the effluent temporal profiles of pressure, temperature, species gaseous concentration etc. are stored to be later used as influent temporal profiles during the corresponding pressure-equalization step. One key assumption here is the independence of the

final CSS conditions to the initial bed conditions and the transient behavior of the processing steps, as a result of bed interconnections.

Furthermore, the time instants at which the different effluent variables are stored can be different from the time instants at which the temporal information is required during the influent seeking process step. To resolve this, the interpolation schemes are employed [84, 69].

5.1.2.3 Complete Discretization Approach

In complete discretization approach proposed by Nilchan and Pantelides [104], the underlined PDAE based model is completely discretized in spatial as well as time domain resulting in a large system of nonlinear algebraic system of equations, which can be solved by a suitable NLP solver. To enforce the CSS conditions, its equation (Eq. 5.1) is included in the overall model formulation itself. Similar to the unibed formulation defined in section 5.1.2.2, only a single bed is modeled. Consequently, and since each processing step can have different duration, the equations are written in the time offsets form instead of usual time formulations. Similar to the direct determination approach, this method also requires a good initial guess to the non linear system of equations. However, in contrast to the direction determination approach it also require initial guess for the temporal profiles of the variables, which can be a challenging issue. This is usually generated by a single cycle simulation.

It is important to note that all of the CSS acceleration approaches to optimize PSA mainly focuses on predicting the final CSS correctly [68, 69]. The intermediate states towards the CSS evolution, are either not evaluated or are fictitious in nature, which for the case of control studies are of importance. In this work, the traditional dynamic optimization approach was considered as more suitable for control studies and is employed, where the model is integrated in time towards a

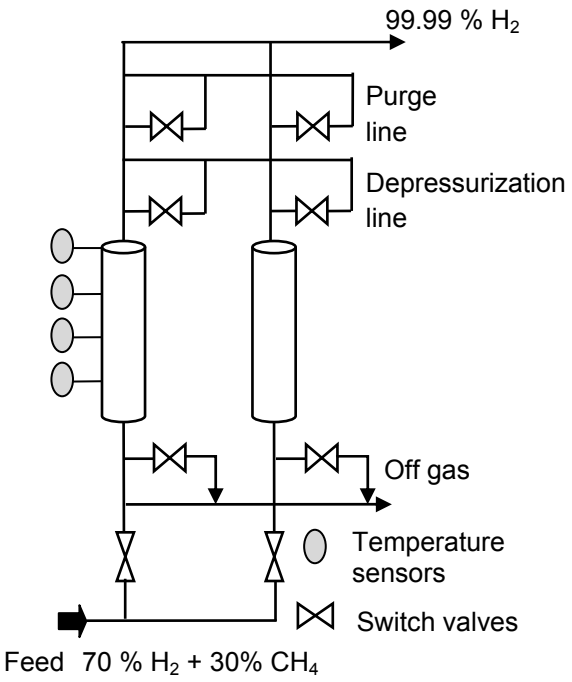

BED1	DEP	BLDN	PURGE	PE	REPRES	FEED
BED 2	PE	REPRES	FEED	DEP	BLDN	PURGE

Figure 5.1: Two-bed, 6-step, multi-valve PSA configuration employed for this study. FEED: production step; DEP: co-current depressurization; BLDN: counter-current depressurization or blowdown; PURGE: counter-current purge with product; PE: co-current pressure equalization; REPRES: co-current re-pressurization with feed

slow but true evolution to the CSS.

5.2 PSA Details and Problem Description

5.2.1 Modeling Details

Figure 5.1 depicts a graphical overview of the two-bed PSA system under consideration. Each bed is undergoing a cyclic operation comprising six processing steps and contains activated carbon as the adsorbent. Furthermore, it is also assumed that the structure of PSA cycle and sequence of processing steps remains fixed

for the purpose of optimization studies. The details of the first principles based dynamic model of PSA employed in this work are already mentioned in chapter 3 of this thesis, while the boundary conditions are listed in Tables 5.4 and 5.5. Furthermore, the velocity dependent terms in the axial heat and mass transfer dispersion coefficients [162, 163] have been neglected.

5.2.2 Objective Function

A commonly used objective function for PSA optimization is product recovery (see also Table 5.3). The main reason towards this trend is its direct relation to the plant operating cost [36], under the assumption that the PSA feed is already available at high pressure and does not require considerable compression work. In some cases, especially in air separation for O_2 and N_2 production, where the feed (air) is available only at atmospheric pressure, recovery alone is not a true indicator of PSA operating performance, and PSA overall compression work can also play a significant role. On the other hand, the key controller objective is to fast track the closed loop product purity to its desired set point in the event of process disturbances [21, 20, 72, 73]. In a PSA operation, since recovery and purity vary in opposite direction [73] with respect to important decision variables, a simultaneous optimization and control strategy appears to be an ideal platform to take account of the impact of these two conflicting objectives on the real-time PSA performance. In this study, an optimal PSA operational policy and controller configuration is desired which provides the maximum value of closed loop hydrogen recovery (Eq. 5.6) while obeying all operational constraints, for the separation of 70 % H_2 and 30 % CH_4 feed mixture to a product stream of hydrogen purity (Eq. 5.7) greater than 99.99 %, in the presence of the following disturbances and uncertainty.

Table 5.4: Boundary conditions for the feed, co-current depressurization and counter-current blowdown steps for the six step PSA cycle

$Z = 0$	$Z = L$
Feed	
$UA_{bed} = \dot{Q}_{feed}$	$P = P_{prod}$
$C_i = \frac{Py_{i_{feed}}}{RT}$	$\frac{\partial C_i}{\partial Z} = 0$
$T = T_{feed}$	$\frac{\partial T}{\partial Z} = 0$
Co-current depressurization	
$U = 0$	$U = f_{valve}\left(P, P_{dep}, CV_{dep}\right)$
$\frac{\partial C_i}{\partial Z} = 0$	$\frac{\partial C_i}{\partial Z} = 0$
$\frac{\partial T}{\partial Z} = 0$	$\frac{\partial T}{\partial Z} = 0$
Blowdown	
$U = f_{valve}\left(P, P_{bldn}, CV_{bldn}\right)$	$U = 0$
$\frac{\partial C_i}{\partial Z} = 0$	$\frac{\partial C_i}{\partial Z} = 0$
$\frac{\partial T}{\partial Z} = 0$	$\frac{\partial T}{\partial Z} = 0$

Table 5.5: Boundary conditions for the counter-current purge, counter-current pressure equalization and co-current product repressurization steps for the six step PSA cycle

$z = 0$	$z = L$
Counter-current Purge	
$U = f_{valve}\left(P, P_{purge}, CV_{bldn}\right)$	$CU = -f_{valve}\left(P_{prod}, P, CV_{purge}\right) C_{prod}$
$\frac{\partial C_i}{\partial Z} = 0$	$C_i = \frac{P}{RT}\frac{C_{i_{prod}}}{C_{prod}}$
$\frac{\partial T}{\partial Z} = 0$	$T = T_{prod}$
Counter-current pressure equalization	
$U = 0$	$CU = -f_{valve}\left(P_{dep}, P, CV_{dep}\right) C_{dep}$
$\frac{\partial C_i}{\partial Z} = 0$	$C_i = \frac{P}{RT}\frac{C_{i_{dep}}}{C_{dep}}$
$\frac{\partial T}{\partial Z} = 0$	$T = T_{dep}$
Co-current repressurization with product	
$U = f_{valve}\left(P_{feed}, P, CV_{repres}\right)$	$U = 0$
$C_i = \frac{P y_{i_{feed}}}{RT}$	$\frac{\partial C_i}{\partial Z} = 0$
$T = T_{feed}$	$\frac{\partial T}{\partial Z} = 0$

1. Feed temperature variations in a sinusoidal fashion with decaying amplitude as defined in Eq. 5.8

2. Step increase in PSA feedrate by 0.35 Nm^3/hr, as defined in Eq. 5.9

3. Bounded uncertainty in the hydrogen feed molar fraction, varying from 68 % to 73 %.

$$Recovery_{H_2} = \frac{\int_{t_{pres}}^{t_{feed}} C_{H_2} U A_{bed}\Big|_{z=L,BED1} dt - \int_{t_{bldn}}^{t_{purge}} C_{H_2} U A_{bed}\Big|_{z=L,BED2} dt}{\int_{0}^{t_{pres}} C_{H_2} U A_{bed}\Big|_{z=0,BED1} dt + \int_{t_{pres}}^{t_{feed}} C_{H_2} U A_{bed}\Big|_{z=0,BED1} dt} \times 100 \tag{5.6}$$

$$Purity_{H_2} = \frac{\int_{t_{pres}}^{t_{feed}} C_{H_2} U A_{bed}\Big|_{z=L,BED1} dt - \int_{t_{bldn}}^{t_{purge}} C_{H_2} U A_{bed}\Big|_{z=L,BED2} dt}{\sum_{i=1}^{N_{comp}} \left[\int_{t_{pres}}^{t_{feed}} C_i U A_{bed}\Big|_{z=L} dt - \int_{t_{bldn}}^{t_{purge}} C_{H_2} U A_{bed}\Big|_{z=L,BED2} dt\right]} \times 100 \tag{5.7}$$

$$T_{feed}(t) = T^0_{feed} + 15 sin\left(\frac{2\pi t}{10}\right) e^{-t/5} \tag{5.8}$$

$$\begin{aligned} \dot{Q}_{feed}(t) &= \dot{Q}^0_{feed} \qquad if \quad t \leq 0 \\ &= \dot{Q}^0_{feed} + 0.35 \quad otherwise \end{aligned} \tag{5.9}$$

For providing the controller action, a SISO PI controller (Eq. 5.10) is assumed, where purity is the control variable and feed step duration is considered as the manipulative variable [73]. Furthermore, integral square error (ISE) [142]

Table 5.6: Modeling parameters for the gas-solid system

Parameter	Value	Parameter	Value
$K_{LDF_{H_2}}$	$15 \times 8.89 \times 10^{-2}$	$K_{LDF_{CH_4}}$	$15 \times 3.96 \times 10^{-3}$
ϵ_b	0.4	ϵ_p	0.566
P_{prod}	7×10^5	P_{bldn}	101325
C_{p_w}	480	ρ_w	7900
d_p	3	T^0_{feed}	303.15

of purity, defined in Eq. 5.11, is treated as the controller performance indicator.

$$\begin{aligned} t_{feed}(k) &= t_{feed}(k-1) + K_c(e(k) - e(k-1)) + \frac{Kc\Delta t_s}{\tau_I}e(k) \\ e(k) &= (Purity_{H_2}(k) - 99.99) \times 10^5 \\ t_l &\leq t_{feed}(k) \leq t_h \\ \Delta t_l &\leq \Delta t_{feed}(k) \leq \Delta t_h \end{aligned} \tag{5.10}$$

$$ISE(t) = 10^5 \int_0^t (Purity_{H_2}(t) - 99.99)^2 dt \tag{5.11}$$

5.2.3 CSS Definition And Time Horizon of Dynamic Optimization Problem

In an ideal situation, the time horizon should be set to a large value to allow the PSA system to attain a CSS, which is defined as a state in time where all PSA variables take the same value at the start and the end of a cycle. On the other hand, it is well known that most significant changes in process variables usually occur in the few initial cycles. The number of such cycles however, depends upon the PSA design configuration, its operational policy and the gas-solid system.

Table 5.7: Operating parameters for the PSA CSS estimation study

Parameter	Value	Parameter	Value
CV_{bldn}	0.06504	CV_{dep}	0.00947
CV_{pres}	0.006	CV_{purge}	5×10^{-4}
D	0.157	L/D	6
$\dot{Q}_{feed}$	1.68	t_{feed}	95.1
t_{dep}	400	t_{pres}	30.1

In order to investigate this for the system under consideration (see Tables 5.6 and 5.7), a number of numerical experiments are conducted, employing a relaxed definition of CSS as shown in Eq. 5.12, where ε_{CSS} is a small positive number, which plays a critical role in the evaluation of the number of cycles required in settling key PSA variables, defined in a lumped fashion, as shown in Eq. 5.13.

$$\mathbf{e}_{CSS}(t) = \mathbf{yp}_{avg}(t) - \mathbf{yp}_{avg}(t - t_{cycletime}) \leq \varepsilon_{CSS} \tag{5.12}$$

$$\mathbf{yp}_{avg} = \int_0^1 \mathbf{yp}(z^*)dz^*; \quad z^* = z/L \tag{5.13}$$

The results, summarized in Table 5.8, show that lower values of ε_{CSS} require higher number of PSA cycles for all CSS indicators considered. Furthermore, the hydrogen gas phase molar concentration and bed temperature are the slowest to settle down for a given value of ε_{CSS}. In addition, observing PSA performance indicators, purity and recovery alone may not be adequate to define CSS, as in this case bed temperature is the slowest to settle down. Based on the above analysis, a value of 50 cycles is selected as the time horizon for PSA dynamic

Table 5.8: Number of PSA cycles to achieve specific CSS tolerances

	CSS tolerance				
PSA Variable	10^{-5}	10^{-4}	10^{-3}	10^{-2}	10^{-1}
Purity	282	24	1	1	1
Recovery	377	270	166	2	1
$C_{avg}(H_2)$	569	332	233	127	8
$C_{avg}(CH_4)$	339	234	126	25	7
$\overline{Q}_{avg}(H_2)$	179	23	3	1	1
$\overline{Q}_{avg}(CH_4)$	112	66	13	4	1
$Q^*_{avg}(H_2)$	180	23	3	1	1
$Q^*_{avg}(CH_4)$	112	67	13	4	1
T_{avg}	586	343	234	128	4

optimization studies.

5.2.4 Decision Variables

A number of decision variables related to PSA process design, cycle scheduling and controller design should be selected carefully in order to obtain an optimal performance. The key process design variables considered are the column length, column diameter and switch valve CVs (ON-OFF operation), while the nominal feed rate ($\dot{Q}^0_{feed}$) is included as an operational decision variable. The key PSA schedule variables considered are the time durations of the processing steps of the underlying PSA cycle, as they directly control the extent of related governing physical phenomena, determining the PSA key performance indicators such as recovery, purity and other operational constraints. Figure 5.1 shows that out of the time duration variables of the six processing steps, only three can be varied independently in order to maintain a synchronized PSA operational cycle. It is important to note that the optimal tuning of switch valves(achieved by incorporating their CVs as decision variable) is crucial to maintain suitable pressure-temporal profiles at the bed ends for varying bed dimensions and step durations. For the controller synthesis problem, manipulative variable bias value, controller gain and integral time are considered as decision variables.

5.2.5 Operational Constraints

In past studies on PSA optimization (Table 5.3), incorporating hydrogen purity constraint has been considered sufficeint for the design of an optimal PSA operation. However, only providing purity violation information to the NLP solver can often lead to solutions where other important state variables may take values indicating unrealistic physical behavior during the time horizon of operation. One

such consideration is the high value of fluid superficial velocity, especially during the flow reversal processing steps including blowdown and repressurization with feed, which may result in fluidization of the bed. Another important consideration is the sharp rise of bed temperature during the first few PSA cycles in the adsorption stage. Bed temperatures above a certain limit can be detrimental to the adsorbent activity and should be avoided. Consequently, such operational constraints are also incorporated in the overall optimization formulation. In this regard, to ensure that the hydrodynamic regime of the PSA is always under packed bed conditions, superficial fluid velocity at bed ends is constrained to be always less than the minimum fluidization velocity [168]. Similarly, the temperatures at bed locations of $z/L = 0.25, 0.5, 0.75, 1$ (cf. sensors shown in Figure 5.1) is constrained.

It is important to note the class of constraints discussed with respect to time. Purity acts as an end point constraint, while velocity and temperature violations, on the other hand should be measured through the complete time horizon of operation. The treatment of path constraints for dynamic optimization problem has been a subject of serious attention, specially for the control vector parameterizations (CVP) [159] approach. The complete discretization approach proposed by Cuthrell and Biegler [37] does not suffer from this drawback as the discretized path constraints becomes part of the overall NLP problem. Towards the CVP approach, Feehery and Barton [47] proposed an elegant technique which involves consuming one DOF from the overall list of available DOFs to satisfy a given path constraint. However, the selection criteria to choose this DOF are not unique and rely completely upon the user. For this particular study, we consider an approach where path constraints are converted into end point constraints by defining violation variables for each path constraint [160, 16], as shown below.

if $violation = true$ **then**

$\frac{\partial vio\_v}{\partial t} = violation^2$

else

$\frac{\partial vio\_v}{\partial t} = 0$

end if

From a real-time control perspective, it is important to constrain both high and low values of adsorption time (Eq. 5.10) to achieve a safe and economical operation. Very low values of feed step duration translate to shorter PSA cycles performing loading and unloading of the adsorbent with the impurities at a quicker rate, while significantly enhancing its degradation in the form of wear and tear [154]. Furthermore, this also demands a faster ON and OFF operation of the switch valves, reducing their lifetime, which is directly related to number of switches per unit time. On other hand, long feed steps can oversaturate the bed since the adsorbent has only a limited capacity for the impurities. In addition to this, large changes in the adsorption time (Δt_{feed}) should also be constrained to avoid oversaturation (Δt_h) or avoid sudden surge of inflow (Δt_l) [73]. It is important to note that in general practice, the controller constraints mentioned in Eq. 5.10 can be treated as constraints in the original NLP problem itself. In this work, the explicit nature of the PI control law is exploited, and an IF-ELSE logic is built to incorporate these equations along with the general PDAE model of PSA. This approach, enhances the convergence rates of the dynamic optimization problem without compromising its rigor.

5.3 A Framework For Simultaneous Design and Control Optimization of PSA Systems Under Uncertainty

In general, a system designed only under nominal conditions is liable to fail for small changes of uncertain conditions, in terms of constraint violations and performance degradation. To obtain an optimal PSA design which is operable under the full range of uncertain parameters, and known time varying disturbances, a rigorous and systematic approach [98, 12] is employed. The framework in Figure 5.2 depicts the employed methodology comprising three main steps.

Step 1 In this step, the uncertainty parameter (hydrogen feed composition) is discretized into a finite number of critical scenarios. Since the hydrogen feed composition can vary from 68 % to 73 %, three critical scenarios are chosen for discretization purposes (i.e. $Ns = 3$ in Eq. 5.14). The first scenario corresponds to 73 % feed composition with probability of 15 %, the second scenario correspond to 68 % hydrogen feed composition with 15 % probability, while the third represents the nominal case of 70 % hydrogen feed composition with 70 % probability. The resulting simultaneous design and control optimization formulation is depicted in Eq. 5.14, where h_{d1} and h_{c1} are the equality constraints representing

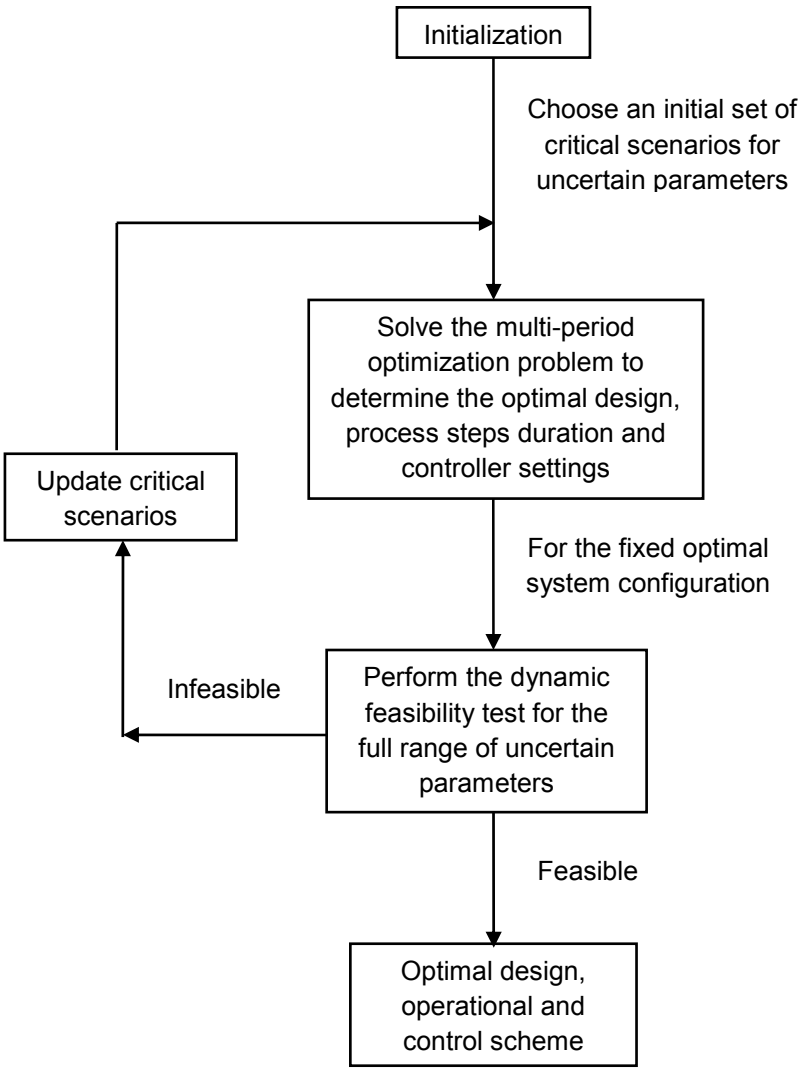

Figure 5.2: A framework for simultaneous design, operational and control optimization under uncertainty

the PSA model and controller description, respectively.

$$
\begin{aligned}
\max_{d_P, d_c, v, t \in [0, t_f = 50 cyles]} \quad & obj = \sum_{m=1}^{Ns} w_{\theta_m} Recovery_{H_2}(\theta_m)\Big|_{t_f} \\
s.t. \quad & \\
h_{d1}(\dot{xd}, xa, d_P, v, \theta_m, t)_m &= 0 \quad m = 1, 2 \ldots Ns \\
h_{c1}(\dot{xd}, xa, d_c, v, \theta_m, t)_m &= 0 \quad m = 1, 2 \ldots Ns \\
99.99 \leq Purity_{H_2}(\theta_m, t_f)_m &\leq 100 \quad m = 1, 2 \ldots Ns \\
0 \leq ISE(\theta_m, t_f)_m &\leq \varepsilon_c \quad m = 1, 2 \ldots Ns \\
0 \leq U^i_{vio}(\theta_m, t_f)_m &\leq \varepsilon_d \quad i = 1, 2 \quad m = 1, 2 \ldots Ns \\
0 \leq T^j_{vio}(\theta_m, t_f)_m &\leq \varepsilon_d \quad j = 1, 2, 3, 4 \quad m = 1, 2 \ldots Ns
\end{aligned} \tag{5.14}
$$

It should also be noted that ISE is treated as a constraint [90] (instead of being considered as a separate objective function), which makes ε_c a tuning parameter which can be changed to obtain a stable and fast controller response. Here, the value of ε_c and ε_d are fixed at 2 and 10^{-5}, respectively. Furthermore, h_{d1} represents the PSA design constraints, while h_{c1} represents the PSA controller constraints.

Step 2 In this step, the multi-period dynamic optimization problem formulated in the last step is solved [56]. The resulting optimal decision variables and PSA performance indicators are shown in the Table 5.9. The maximum expected closed loop hydrogen recovery in this case comes out to be around 61 % WITH an expected value of ISE at 1.42.

Step 3 In this step, the dynamic feasibility test [38] is performed to check whether the optimal design and control system obtained in the last step is feasible for the complete range of uncertain parameter. The dynamic feasibility test problem is formulated, as shown in Eq. 5.15 below. Here, g_l are the set of PSA

Table 5.9: Optimal decision variables, their upper and lower bounds and optimal performance variables for PSA optimization under uncertainty study

Decision variable	LB	UB	Value
Process design			
CV_{bldn}	0.065	1	0.0652
CV_{dep}	0.01	1	0.010
CV_{repres}	0.06	1	0.06
CV_{purge}	7.7×10^{-5}	5×10^{-4}	5×10^{-4}
D	0.05	0.5	0.1598
L/D	2	6	6
Operational			
$\dot{Q}^0_{feed}$	0.5	1.7	1.699
t_{dep}	15	150	93.432
t_{repres}	30	150	37.83
Controller design			
$t_{feed}(t_0)$	60	400	336.211
Kc	0.001	100	0.1842
τ_I	0.001	10^5	4.049
Performance variables for multi-period design			
θ	$Recovery_{H_2}$	$Purity_{H_2}$	ISE
68 %	60.86 %	99.99 %	1.571
70 %	60.933 %	99.99 %	1.41
73 %	61.01 %	99.99 %	1.3
$E(Recovery_{H_2})$	60.933	$E(ISE)$	1.418

Table 5.10: Solver and convergence statistics for the PSA multi-period optimization solution

Parameter	Value
Number of axial discretization nodes	40
Discretization scheme	CFDM
Number of differential variables	1249
Number of algebraic variables	1233
DAE solver absolute and relative convergence tolerance	10^{-6}
Number of NLP iterations	8
Number of NLP line searches	14
NLP solver convergence tolerance	6.4×10^{-4}
CPU time	32897 s
Fraction of CPU time spent on sensitivity integration	58 %
Computer processor	Intel Xeon E5450 @ 3.00 GHz

inequality constraints. If ψ is negative, then the design is feasible for the operating range of uncertain parameter. If it is positive, then the design is infeasible and the critical scenario obtained from the complete solution of Eq. 5.15 is augmented with the list of critical scenarios described in ***Step 1***, and the whole procedure is repeated till feasibility is achieved.

$$\psi = \max_{l=1,..Ncr} \left[g_l(\theta^*) = \max_{\theta \in [68\%,73\%], t \in [0, t_f = 50 cycles]} g_l(\theta, t_f) \right] \tag{5.15}$$

It is important to note that formulation in Eq. 5.15 assumes that there are no time variant decision variables in the optimization problem. The value of ψ (Eq. 5.15), for the current design and control configuration comes out to be -7.5 $\times$ 10^{-5}, with the purity lower bound as the limiting constraint. Since this is a negative value, the optimal PSA design obtained here is feasible and the algorithm terminates.

5.4 Computational Results and Discussions

For the PSA system shown in Figure 5.1, the resulting design and control configuration obtained by the employment of the methodology mentioned in previous section is shown in Table 5.9, while the corresponding computational statistics are outlined in Table 5.10. Note that for the two-bed PSA system under consideration, the total CPU time to solve the full optimization problem is around 9.2 hours. Table 5.9 also depicts the optimal values of key degrees of freedom related to process design, operation and controller design of the PSA system. In particular, the following remarks can be made:

1. The duration of feed step is the largest as compared to other two steps. For the 2-bed, 6-step PSA cycle under consideration, where feed is provided

in only one step (per bed) and then discontinued, this result seems quite logical, and can be attributed to the fact that it is during the feed step that actual recovery of product happens, which the optimizer attempts to maximize

2. The system spends least amount of time in the pressurization/blowdown stage. This is because for the given PSA cycle, the system aims to quickly repressurize the column (from feed) in an attempt to minimize the impurity intake during this time, as well quickly depressurize (blowdown) the column to minimize the product losses in the off gas

To further assess the design performance, dynamic simulations are performed [56] with the optimal PSA system listed in Table 5.9, and feed composition parameter fixed at 70 % value. In the following, this design configuration will be referred to as the nominal PSA design.

The spatial variation of gas phase concentration of impurity component at the end of each processing step at CSS is shown in Figure 5.3. Figures 5.3 and 5.4, in particular illustrate the impurity adsorption and desorption dynamics for each PSA process step. During the feed mode, 20 % of bed (towards the feed end) is almost saturated with methane. By the end of depressurization step, the impurity front moves slightly forward as the product end is now open in order to pressurize the other column undergoing pressure equalization. This behavior also emphasizes the importance of each processing step duration. For example, a little extra long depressurization step can lead to impurity leaving the product end to the clean product end of the other column. On the other hand, a shorter duration step will not completely utilize the high purity product available at high pressure, some of which will be lost with the off gas in the next step (blowdown). Blowdown step marks the start of the adsorbent regeneration stage,

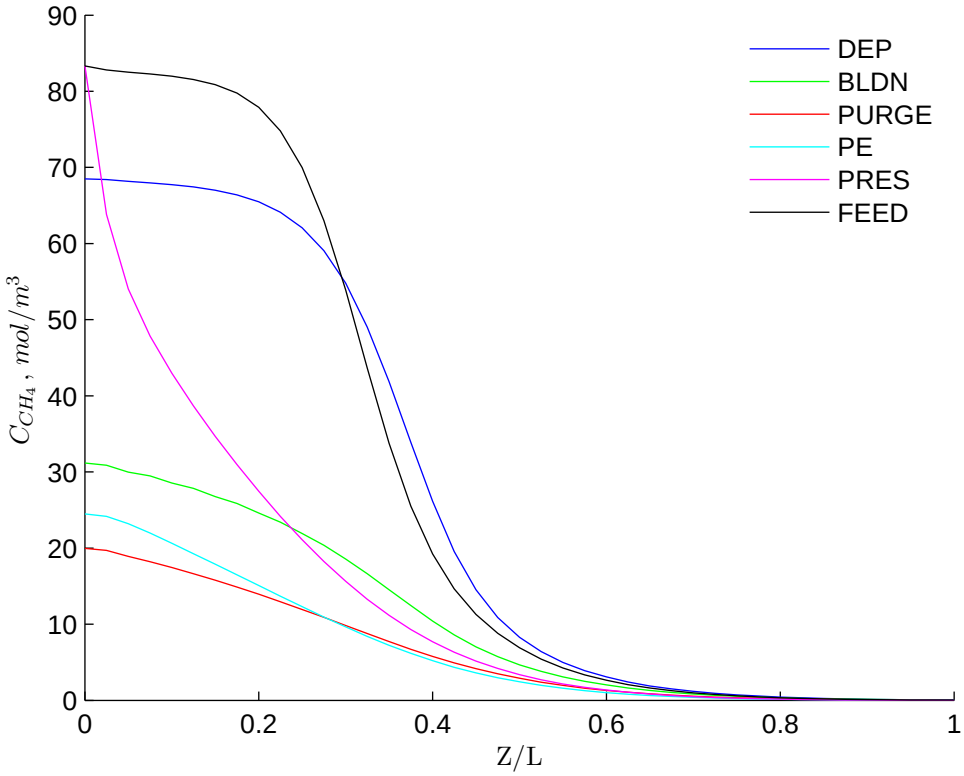

Figure 5.3: Axial distribution of gas phase methane concentration at CSS

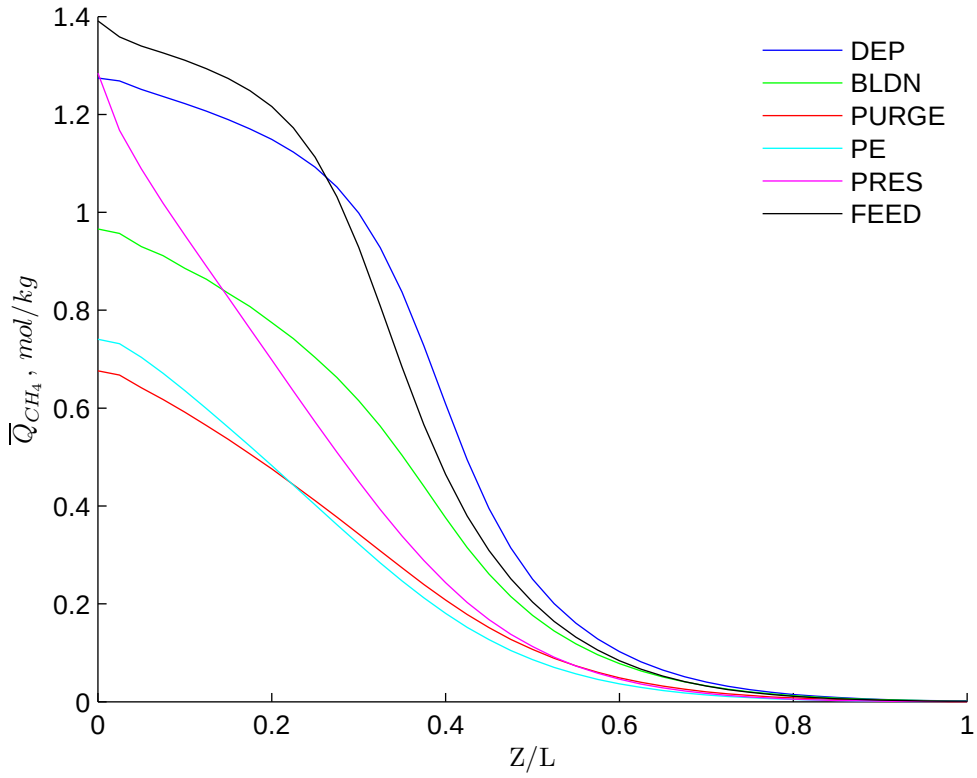

Figure 5.4: Axial distribution of $\overline{Q}_{CH_4}$ at CSS

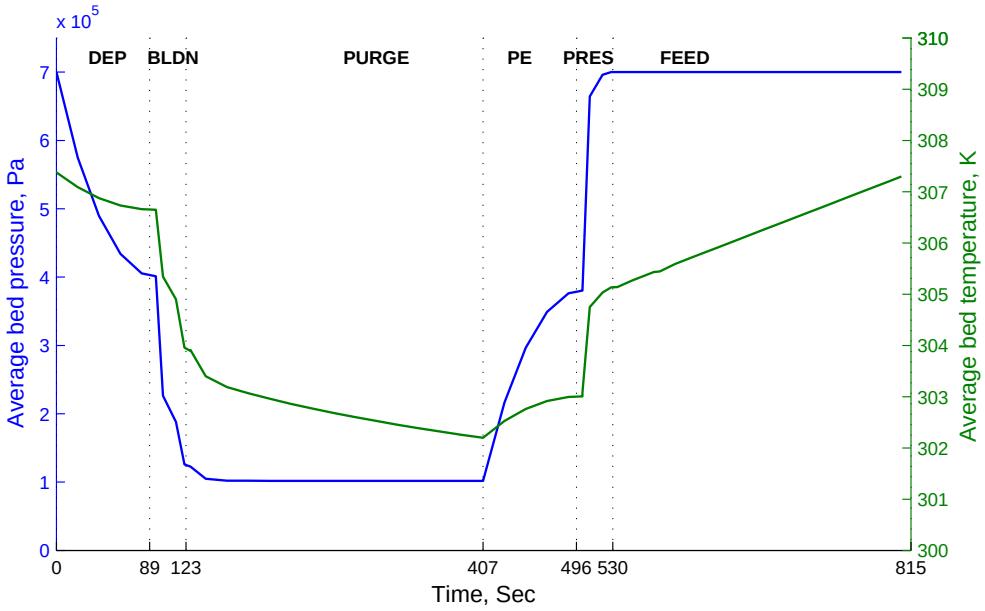

Figure 5.5: Time evolution of pressure swing and the associated temperature swing over a PSA cycle at the optimal conditions

as the methane concentration falls sharply. By the end of purge step, the impurity level in the bed has reached its minimum level. During the pressure equalization by product and pressurization by feed step, the column is pressurized back to the feed pressure. It is important to note that substantial adsorption in the bed can happen during the re-pressurization with feed step. This demands a fast re-pressurization step, where the gas phase concentration increases much faster than the solid phase concentration. A closer comparison of Figures 5.3 and 5.4 confirms this behavior where it can be seen that the area under the curve rises much sharply for C_{CH_4} than $\overline{Q}_{CH_4}$, while moving from PE step to PRES step. In fact detailed calculations performed shows that the $C_{CH_4 avg}$ (Eq. 5.13) increases twice as fast as $\overline{Q}_{CH_4 avg}$.

Figure 5.5 depicts the complex interactions between the pressure swings, and the corresponding temperature swings for one complete PSA cycle for the first bed. From this plot, it can been deduced that the temperature swing cycle is much

slower to settle down as compared to pressure swing and also has an unfavorable effect on the PSA performance due to the temperature rise during the adsorption stages and drop during the desorption stages. Furthermore, it also reveals that the repressurization at CSS is much faster than the blowdown, as the bed pressure at the end of blowdown stage has not reached the lowest pressure possible.

5.5 Comparisons With A Sequential Strategy

Table 5.11 compares the optimal PSA operational configurations obtained from the application of sequential and the simultaneous approaches while assuming perfect certainty in feed composition at $y_{H_2} = 70$ %.

The results shows that if the ISE is kept around the same value obtained from the sequential approach, the simultaneous approach provides better closed loop recovery. In this case, the actual recovery possible is 61.638 % which is almost 3 % higher (on relative basis) than the recovery obtained with the sequential approach. When comparing the results in different columns of Table 5.11, it should be noted that t_{feed} is the duration of the feed step for the sequential analysis, while it is the initial value (bias value) of PI control law for the simultaneous optimization studies. It is also evident from the results that the simultaneous approach lead to a design which is marginally bigger in size with respect to both diameter and length (as L/D ratio is unchanged). The largest change is observed in the step durations of the PSA cycle, as the simultaneous optimization based approach predicts higher time duration for all processing steps at optimal CSS conditions in comparison to the sequential approach. These observations suggests that the simultaneous approach results in a bigger and slower PSA system in an attempt to effectively handle specified disturbances, while also increasing the closed loop recovery at CSS conditions.

Table 5.11: Comparison of optimal PSA systems obtained from sequential and simultaneous approach

Decision variable	Sequential approach		Simultaneous approach	
	Process synthesis (Maximize $Recovery_{H_2}$)	PI controller design (Minimize ISE)	($\varepsilon_c = 2.5$)	($\varepsilon_c = 1$)
$CV_{blowdown}$	0.06502		0.06532	0.065
CV_{dep}	0.0102		0.01	0.01
CV_{repres}	0.06		0.06	0.06
CV_{purge}	5×10^{-4}		5×10^{-4}	5×10^{-4}
D	0.1574		0.16	0.15936
L/D	6		6	6
$\dot{Q}^0_{feed}$	1.698		1.7	1.7
t_{dep}	86.58		97.124	92.3317
t_{feed}	399.99		311.051	366.118
t_{repres}	30.15		38.273	31.358
Kc		0.55323	0.061	0.336
τ_I		7.64	1.06	7.45
Performance variables				
$Recovery_{H_2}$	62.98	59.88	61.638	60.82
$Purity_{H_2}$	99.99	99.99	99.99	99.99
ISE		2.2	2.45	0.99

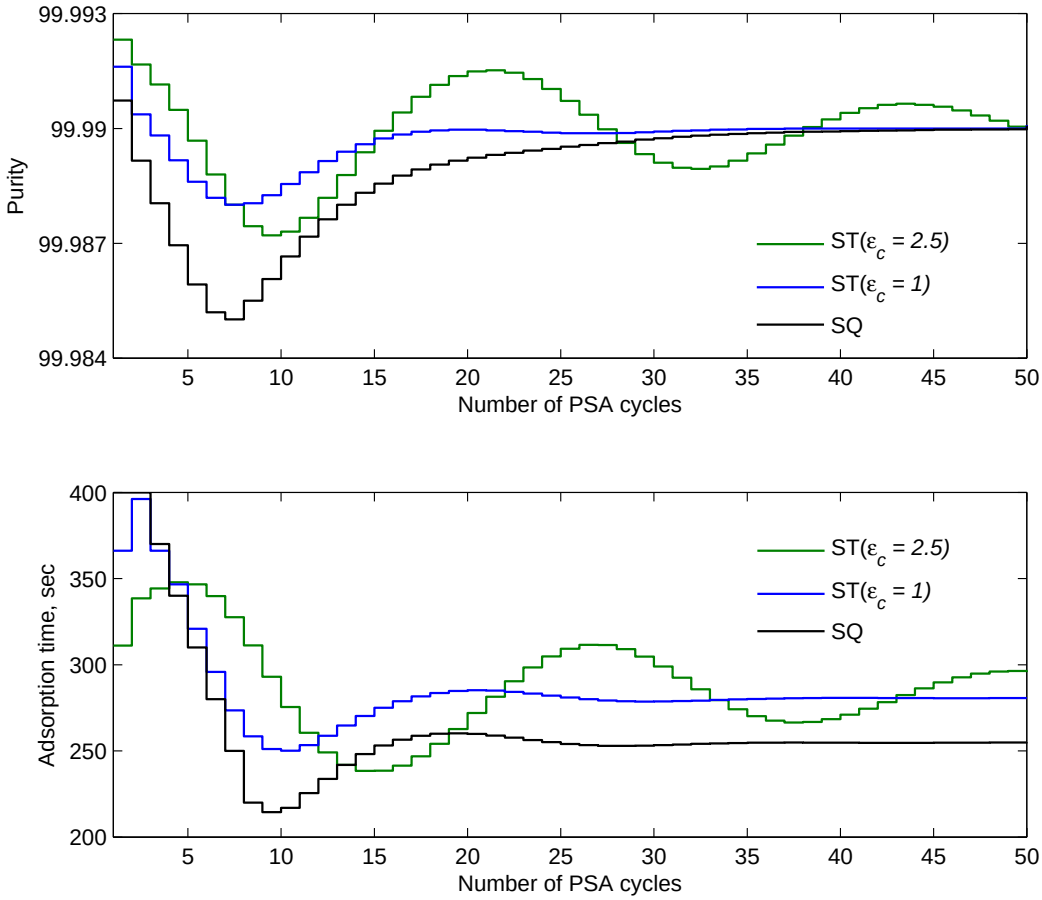

Figure 5.6: Comparison of closed loop controller performance for various optimal PSA systems and controller settings. ST: Simultaneous approach, SQ: Sequential approach

The resulting controller responses are compared in the Figure 5.6. It shows that with the sequential approach, the product purity drops to a relatively low value of 99.985 % in the first few cycles. In contrast to this, the simultaneous formulation provides significant improvements in purity response. For the case of ISE = 2.5, the purity response is somewhat oscillatory, although very tightly bounded to the set point. It can also be seen that lowering ε_c improves the purity response significantly in terms of reducing the oscillatory effect. However, this improvement is achieved at the price of slight reduction in product recovery, albeit the product recovery level is still higher than the SQDC case.

5.6 Explicit/Multi-Parametric MPC for PSA

At this point it appears worthwhile to investigate how a MPC controller would behave for the design and operational configuration obtained from the multi-period optimization. To further investigate this, an explicit/multi-parametric MPC controller is built for the nominal PSA design case (Table 5.9).

MPC in general, is an advanced control methodology specially suitable for highly complex, interconnected dynamic systems. In contrast to a standard PID based controller, MPC provides optimal control action by taking into account the system's dynamic behavior and operational constraints [123, 124, 91, 125]. It is based on receding horizon philosophy, where the current plant state and output variables, along with a suitable plant model are utilized to calculate the future sequence of optimal input variables, via solving an online optimization problem. Recent advances made in the field of multi-parametric programming now make it possible to obtain the governing MPC control law beforehand, or *offline* [119], leading to reduced online computations and other economic benefits [116, 121, 120].

Since the large-scale PSA model developed is not directly suitable for model based controller design, a system identification step [152, 89, 88, 182] is performed to identify a much simpler, preferably linear model relating the control variable with the manipulative variable to reasonable accuracy. The identification procedure followed in this study involves conducting dynamic simulations on the PDAE model, perturbed by a random pulse of input (feed step duration) disturbance, to ensure that the PSA system is excited *persistently* [152, 88] over a large frequency band (of interest), in the open loop environment. The resulting input-output response data (Figure 5.7) is used within the MATLAB system identification toolbox to identify the best fit linear parametric model. The best fit is achieved for a 5^{th} order state space model (Eq. 5.16 to 5.19) with a mismatch of less than 5 % from the PDAE model response.

$$\begin{aligned} x(k+1) &= Ax(k) + bu(k) \\ y(k) &= cx(k) \end{aligned} \tag{5.16}$$

$$A = \begin{bmatrix} 0.99880 & 0.10001 & 0.00169 & -0.00164 & -0.00034 \\ -0.03130 & 0.96193 & 0.03544 & -0.04382 & 0.03722 \\ 0.13610 & -0.18581 & 0.75535 & 0.13967 & 0.13908 \\ 0.04925 & -0.01173 & -0.36065 & 0.79947 & 0.49361 \\ 0.06341 & -0.08066 & -0.29210 & -0.36313 & 0.02829 \end{bmatrix} \tag{5.17}$$

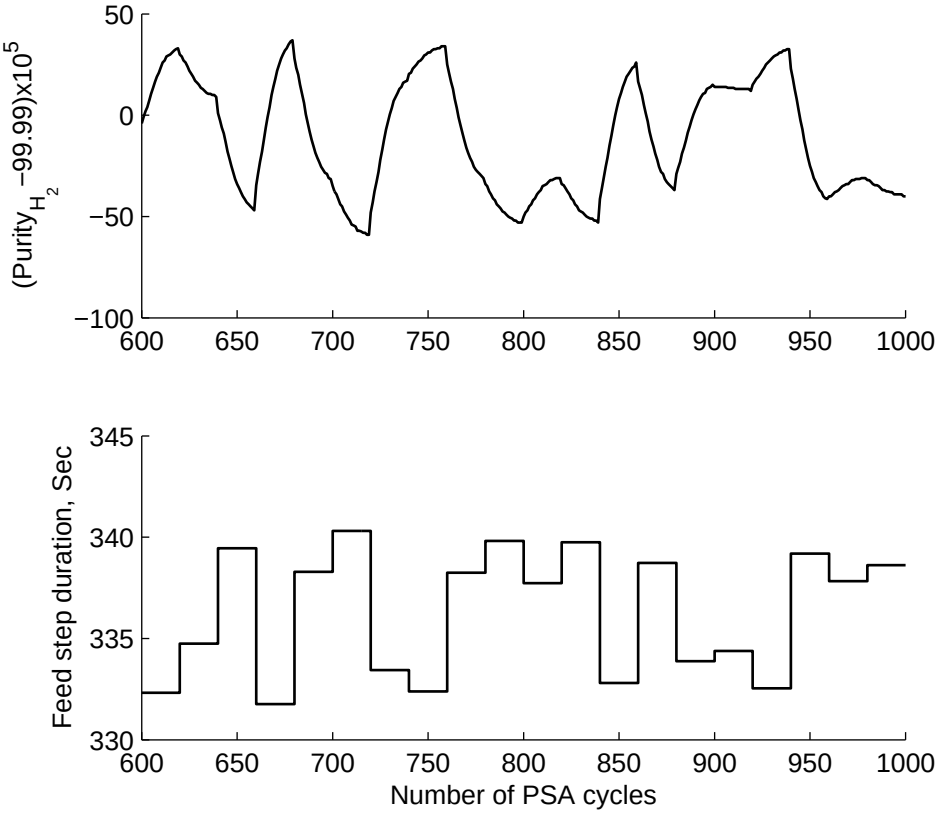

Figure 5.7: Purity response corresponding to the random variations in the manipulative variable

$$b = \begin{bmatrix} 0.00523 \\ -0.03004 \\ -0.01797 \\ -0.27463 \\ 0.15461 \end{bmatrix} \tag{5.18}$$

$$c = \begin{bmatrix} -503.883 & -27.586 & -0.528 & 1.038 & -0.307 \end{bmatrix} \tag{5.19}$$

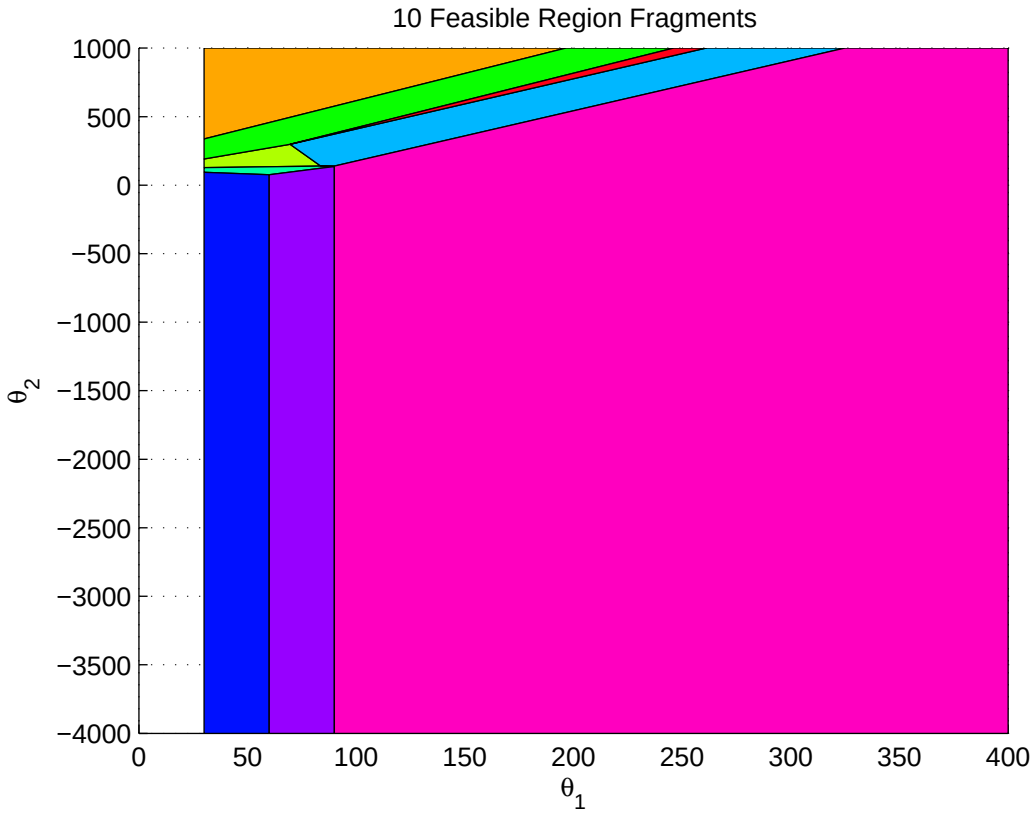

Figure 5.8: Two-dimensional projection of 101 critical region polyhedra corresponding to the reduced state space model, $[x_1, ...x_5 = 0, t_{feed}(k) = u = \theta_1, (Purity_{H_2} - 99.99) \times 10^5 = y = \theta_2, y_{set} = 0]$

$$
\begin{aligned}
\min_{u} \quad Z &= \sum_{k=1}^{N-1} (y(k) - y^r(k))^T (y(k) - y^r(k)) + \sum_{k=0}^{M-1} \Delta u(k)^T R_U \Delta u(k) \\
s.t. & \\
x(k+1) &= Ax(k) + bu(k) \\
y(k) &= cx(k) + e(k) \\
u_l \leq \quad u(k) &\leq u_h \\
\Delta u_l \leq \quad \Delta u(k) &\leq \Delta u_h \\
y(k) &\leq 1
\end{aligned} \tag{5.20}
$$

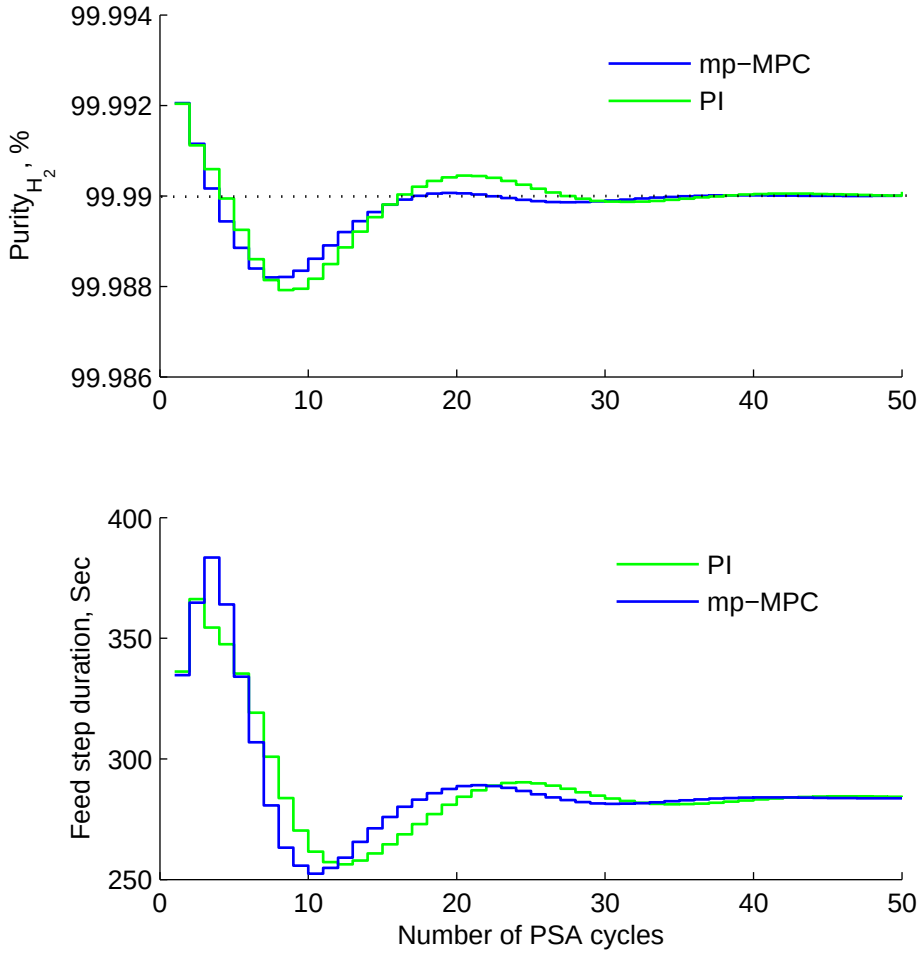

Figure 5.9: Comparison of closed loop performance for the PI and mp-MPC controller

A model based predictive controller (MPC), incorporating all controller constraints (Eq. 5.10) in an optimization framework is formulated in Eq. (5.20). The complete problem is set up in the POP toolbox environment [122] and involves 8 parameters. The best value for RU is obtained by perturbing the original rigorous PSA model with time varying disturbances (Eqs. 5.8 and 5.9) and performing closed loop simulations. This procedure yields a value of R_U (cf. Eq. 5.20) = 1 with 101 critical regions. Figure 5.8, shows a two dimensional projection of the multi-dimensional polyhedra, while the resulting closed loop performance is shown in the Figure 5.9 along with the PI control performance. The comparison shows that the mp-MPC controller provides much more robust response in terms of less oscillatory behavior in purity response. It is also important to note that the PI controller in this case is a special one as it considers all the system constraints, in a fashion similar to a mp-MPC controller. This appears to be main reason for the observation that the mp-MPC controller performance is not strikingly different from the PI case. The predictive power of the mp-MPC however, using the system dynamic model, seems to be the key feature for its slightly superior performance than the PI case.

5.7 Conclusions

This work presents a detailed study for the simultaneous design, operation and control of a PSA system following a rigorous and step by step built framework based optimization approach while utilizing a detailed mechanistic mathematical model. Important PSA operational challenges, constraints and objectives are discussed in detail and incorporated in the mathematical framework. The best closed loop recovery obtained for the PSA system under consideration is around 61 %, while the purity response to multiple disturbance scenarios is found to be

quite satisfactory. The benefits of PSA design based on this approach approach as compared to the traditional sequential approach are shown in terms of improvement in closed loop recovery by almost 3 %, and better purity response. It is also found that the improved design is slightly bigger in size with slower PSA cycles. Furthermore, a mp-MPC is also designed to observe any further benefits related to the model based controller. The results show improvement, albeit marginal, in the closed loop response with respect to the optimized PI controller considered in the study.

Chapter 6

Design and Environmental Impact Analysis of a Hybrid PSA-Membrane Separation System

6.1 Introduction

Due to the increasing demand of hydrogen for its role as an efficient energy carrier, a major emphasis has been placed on developing new and innovative technologies that produce highly pure hydrogen at a cheap cost. With tougher environmental regulations and emissions standard, any such technology however, should not only be economically feasible but also environmental friendly. Consequently, to meet the future regulations and standards, sustainable energy systems based on fossil fuels will require a significant reduction of emitted greenhouse gases and other pollutants.

Currently, the most energy efficient route for hydrogen production is the steam

reforming of natural gas, where PSA is usually employed in the final step to produce high-purity hydrogen. In the context of PSA processes, attaining highest possible product recovery values without sacrificing product purity is highly sought after, as it directly improves the operating costs. During the blowdown and purge steps of the PSA cyclic operation, a fair amount of hydrogen can escape the system along with the impurity components as the off gas. For example, a typical PSA waste gas stream consists of $CO_2 \sim 55\%$, $H_2 \sim 35\%$, CH_4 & $CO \sim 15\%$. This stream is not usually recycled since it would need to be re-compressed to the PSA feed pressure and is also considerably richer in impurities. Furthermore, it also cannot be used for CO_2 sequestration since it contains significant amounts of H_2 and CH_4. On the other hand, it is important to note that if CO_2 emissions are captured as a relatively pure gas, they can further be sequestered or stored appropriately, thus reducing at the source,its amount emitted to the atmosphere.

One common procedure to improve product recovery in PSA is to employ more depressurization steps, enabling the use of high pressure product to pressurize columns operating at lower pressures, thereby minimizing the need of external product stream. However, the maximum number of pressure equalization steps is strongly dependent on the total number of beds, limiting the scope of this method to large scale improvements. Another option is to integrate the PSA system with other separation devices such as membranes to reduce the hydrogen losses. A hybrid PSA-membrane process is expected to combine the high throughput and H_2 product purity of a PSA process with the lower operating costs of a membrane process.

In the past, only few studies have been reported in the literature towards this field. Sircar et al. [149] presented a PSA-membrane hybrid process strategy to achieve higher hydrogen recovery from the PSA purification section of

the steam-methane reforming process. In their proposed design, the membrane module is placed downstream of the PSA system, with the PSA off-gas acting as membrane feed. The selective surface flow membrane considered for the study had the least affinity for permeation of hydrogen gas as compared to other gas components in the feed. As a result, the low pressure permeate consists mostly of impurities, while the retentate is rich in hydrogen. The high pressure retentate is compressed further and mixed with the feed gas before it enters the PSA. This combined process increased the hydrogen recovery from 77.6 % to 84 % while maintaining same hydrogen purity. Their work clearly suggests that there is a definite advantage for combining PSA and membrane to improve hydrogen recovery. Feng et al. [48] investigated two possible membrane-PSA hybrid configurations. In the first proposed configuration (named as membrane-assisted feed gas pressurization) membrane module is placed upstream of a two bed PSA. The permeate from membrane which is rich in the weakly adsorbing species is sent to a second bed to repressurize it. The retentate side gas becomes the feed of the first bed as usual. The second proposed configuration (named as membrane-assisted co-current depressurization) also uses two bed PSA and comprises of four process steps in one cycle. Here, membrane module is actually placed between the two beds. The permeate side inlet is connected to the bed undergoing depressurization, while its permeate side outlet is connected to the other bed undergoing repressurization. As a result of additional separation achieved by the membrane module, gas stream entering the bed getting repressurized is more purer compared to standalone PSA. The retentate side stream is used for counter-current purge of depressurized bed. The authors found that for the same feed flow rate, and membrane-assisted co-current depressurization hybrid configuration, hydrogen product purity increases with a marginal drop in recovery as compared to stand alone PSA. Esteves and Mota [43] used an elaborative simulation-based

framework to study the potential benefits of hybrid system. In their work they took H_2/CH_4 stream for separation and assigned recoveries of both components as the performance indicator. For the selected hybrid configuration, simulation results showed that both hydrogen recovery and CH_4 purity are better for the hybrid system as compared to the standalone PSA system [44]. All of the above findings justify the integration of membrane module with a PSA plant in order to improve the gas separation performance.

The main motivation of this work is to conduct a detailed study towards design and performance assessment of hybrid PSA-membrane system, while probing the role of various decision variables, design tradeoffs and settings. The separation task is to obtain fuel-cell ready hydrogen with purity in excess of 99.99% from a multi-component gas stream containing H_2, CO, CO_2, CH_4 and N_2 at the minimum operating cost or maximum hydrogen recovery. Finally, life cycle analysis (LCA) method is utilized to analyze the environmental impact of the optimum hybrid system and compare it with a optimum stand alone PSA system.

6.2 Stand Alone Membrane Simulation Studies

The main objective of performing simulation studies on a stand alone membrane module is to evaluate and compare its performance at various operating conditions related to the point of integration with the PSA system. Towards this purpose, two such possible locations have been considered in this study. In the first configuration "upstream", the membrane module is placed upstream of the PSA, which means that the feed stream from PSA upstream unit will now enter the membrane module instead of going straight to the PSA unit. Since the membrane material (DDR) used for this is CO_2 selective, a hydrogen-rich retentate (leaner in CO_2) is expected to come out from the tube side, which is then fed to

Table 6.1: Simulation parameters for the stand alone membrane studies

Parameter	Upstream configuration	Downstream configuration
Feed Pressure (tube side), bar	7	1
Feed Flow rate, SLPM	8.5	2 and 5
Membrane thickness, m	0.000025	0.000025
Feed Temperature, K	293.15	293.15
Feed composition (molar basis), %	H_2 = 73.3, CO = 2.9, CH_4 = 3.5, CO_2 = 16.6, N_2 = 3.7	H_2 = 39.7 , CO = 6.6, CH_4 = 7.8, CO_2 = 37.6 , N_2 = 8.3

the PSA system. Furthermore, as pressure drop along the membrane module is not significant, the retentate entering the PSA unit is expected to be at roughly the same pressure as the untreated feed gas, which further reduces the requirement of any external pressure generating device. On the shell side, the CO_2 rich permeate stream leaves the system as off gas.

In the second configuration "downstream", the off gas coming out of the PSA system during blowdown and purge operations at low pressure is passed through the membrane with the same material properties as employed in the upstream study. In contrast to the upstream configuration, the hydrogen rich tube side retentate from membrane needs extra pressure boost and cooling to match its conditions to the feed level from the operating conditions corresponding to the blowdown and purge steps.

The simulation parameters for the upstream and the downstream configuration studies are presented in Table 6.1. Note that the membrane model is supplied from the EU project Hy2SEPS consortium partners (D23, Membrane separation

system optimization and design, Hy2SEPS, EU Contract no: 019887).

6.2.1 Upstream Membrane Configuration

For performing the parametric study, membrane area and shell side pressure are considered as design parameters, where membrane area is varied from 0.001 m^2 to 10 m^2 in multiples of 10, while the shell side pressure is kept at values of 100000 Pa (blowdown pressure), and 100 Pa. For all of the simulations results reported here, CO_2 recovery is defined as the ratio of molar flow rate of CO_2 in the shell side permeate to the CO_2 molar flow rate in the tube side feed. Similarly, CO_2 purity is defined as the ratio of CO_2 molar rate obtained in permeate side to the total permeate molar flow coming out. Figure 6.1, shows the resulting CO_2 purity and recovery as a function of membrane area. It can be clearly seen that increasing membrane area increases the CO_2 recovery and decreases. Furthermore, decreasing the shell pressure to low values increases both recovery and purity of carbon dioxide, but the change is not large. For the shell side pressure of 100000 Pa, the maximum recovery obtained is around 48 %, and when the shell pressure is decreased to a value of 100 Pa, the maximum recovery obtainable increases to around 61 %. As far as the purity is concerned, maximum value obtained for the shell side pressure of 100000 Pa is around 54 %, and this value increases to 66.7 % for shell side pressure of 100 Pa. It can also be seen that at very high area values, CO_2 purity is same as feed indicating that there is no separation at all and the feed simply passes to shell side.

6.2.2 Downstream Membrane Configuration

For the downstream configuration three parameters are considered for simulation purposes. Firstly, the membrane area which is varied from 0.001 m^2 to 10 m^2 in

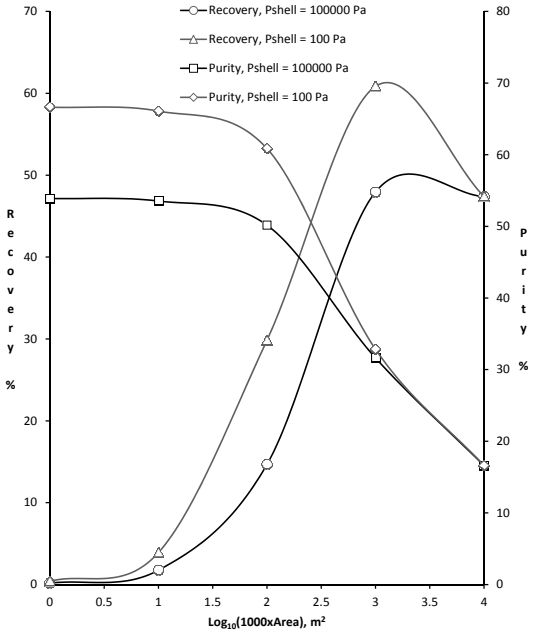

Figure 6.1: Variation of CO_2 purity and recovery with membrane area for the upstream configuration

the multiples of 10. The second parameter considered in the study is the shell side pressure for which two values of 1000 Pa and 100 Pa are chosen. Note that the pressure values selected here are significantly lower than the values selected for the upstream configuration study, to account for to the low operating pressure of the blowdown and purge processing steps of the PSA cycle. The third parameter selected is the input feed flow rate, for which values of 2 and 5 standard liters per minute (SLPM) are selected. Figure 6.2, shows the results obtained for CO_2 recovery and purity as a variation of these parameters.

It is clear from the plot that high values of both CO_2 recovery and purity are achievable for the same value of membrane area values considered in the upstream configuration. For example, the highest value of recovery and purity in this case is more than 90 %. The comparative study presented here clearly indicates that downstream configuration is much more attractive than the upstream, and is the configuration selected for integration with PSA.

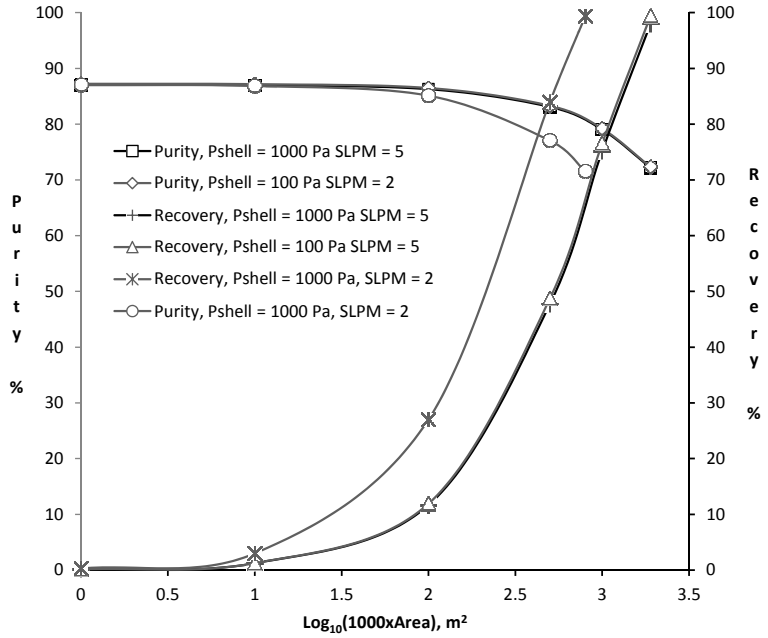

Figure 6.2: Variation of CO_2 purity and recovery with membrane area for the downstream configuration

6.3 Stand-Alone PSA Simulation Studies

A similar parametric study is done for the stand alone PSA separation system to estimate the best value of cycletime for the process, with H_2 recovery and purity teated as the main performance variables. The dynamic simulations were performed in the gPROMS modeling environment by solving simultaneously the set of boundary conditions and the modeling equations, defined in previous sections for the four beds. Here, at the initial time, all the beds are assumed to be containing pure hydrogen saturated with the adsorbent material at feed temperature and initial bed pressure. Initial pressure inside the beds are 7 bar, 2.5 bar, 2.5 bar, 7 bar, respectively. Table 6.2 outlines some of the important simulation parameters related to the study. The dynamic model is integrated in time and the simulation continues till the system reaches a cyclic steady state (CSS). In general, at CSS, system variables (both differential and algebraic) hold the same

value at the end and start of a cycle. In the present study, the following variables defined in Eq. 6.1 and 6.2 are used to determine CSS.

$$C_{avg_i} = \int_0^1 C_i(z^*)dz^*; \quad z^* = z/L; \quad i = 1, 2..NCOMP \tag{6.1}$$

$$T_{avg} = \int_0^1 T(z^*)dz^*; \quad z^* = z/L \tag{6.2}$$

Since, there are five components in the system, there are six such indicators for detecting CSS. The simulation stops when the maximum of the difference between the indicators at the start and end of a cycle becomes less than 10^{-4}.

From the simulations it is found that increasing cycletime also increases the hydrogen recovery but reduces the hydrogen purity. The best operating point corresponds to the cycletime for which the system achieves the maximum recovery with hydrogen purity being more than 99.99 %. For the present system, this comes at the value of 480 seconds, with hydrogen recovery at 56.7 %, and hydrogen product purity at 99.995 % .

6.4 Hybrid PSA-Membrane Simulation Study

The best method to design PSA membrane hybrid is by performing a full-scale dynamic optimization, with the objective of maximizing the PSA hydrogen product recovery. The key decision variables such as PSA cycletime, PSA bed length, number of beds, bed diameter and membrane area can then be estimated, with PSA hydrogen product purity and membrane CO_2 purity acting as constraint for the optimization problem. However, such a detailed dynamic optimization problem involving both PSA and membrane is quite time consuming since it involves repeated CSS evaluation for each new iteration, as different decision variables

Table 6.2: Modeling parameters for the base case PSA

Design parameters	Symbol	Value
Number of beds		4
Feed pressure	P_{feed}	7 bar
Feed temperature	T_{feed}	303.15 K
Feed flow rate	$\dot{Q}_{feed}$	8.5 SLPM
Blowdown pressure	$P_{blowdown}$	1 atm
Bed length	L	0.445 m
Bed diameter	D	0.072 m
Bed porosity	ϵ_b	40 %
Particle diameter	d_p	3 mm
Solid specific heat	C_{p_s}	1000 J/kg K
Adsorbent		Activated carbon (AC) and zeolite
AC portion		70 %
AC density	ρ_s	552 kg/m^3
Zeolite density	ρ_s	695 kg/m^3

variables are estimated. As an alternative to this, the optimization procedure followed here involves performing dynamic simulations on the hybrid system (see Table 6.3) to evaluate the effect of few important decision variables on the hybrid performance indicators. Furthermore, some of the important assumptions related to the PSA membrane integration are listed below:

1. From the off gases coming out of the blowdown and purge steps of PSA operation, only 2 SLPM of the total amount is employed as a feed to the membrane module.

2. It is further assumed that a suitable controller is in place for the off gas tank to maintain this rate at a constant value during the blowdown and purge steps of the PSA cycle.

3. This stream enters the membrane module at a temperature of 20 ^{0}C as DDR membrane operates better at low temperature and PSA off gas temperature is also near to this value.

4. The pressure of this stream entering the membrane has been assumed to be 1.5 bars which represents the average pressure of off gases during the blowdown and purge pressure. It is important to note that pressure at the bed outlet remains quite steady during the purge step of the PSA cycle however, during the blowdown step the pressure changes significantly from the higher depressurization pressure levels to atmospheric blowdown pressure. Consequently, the assumption of average pressure 1.5 bar during this operation seems quite reasonable.

5. The average composition of PSA off gas entering the membrane is calculated by assuming that off gas streams from four beds enters a well mixed tank at their actual (varying) pressure and temperature.

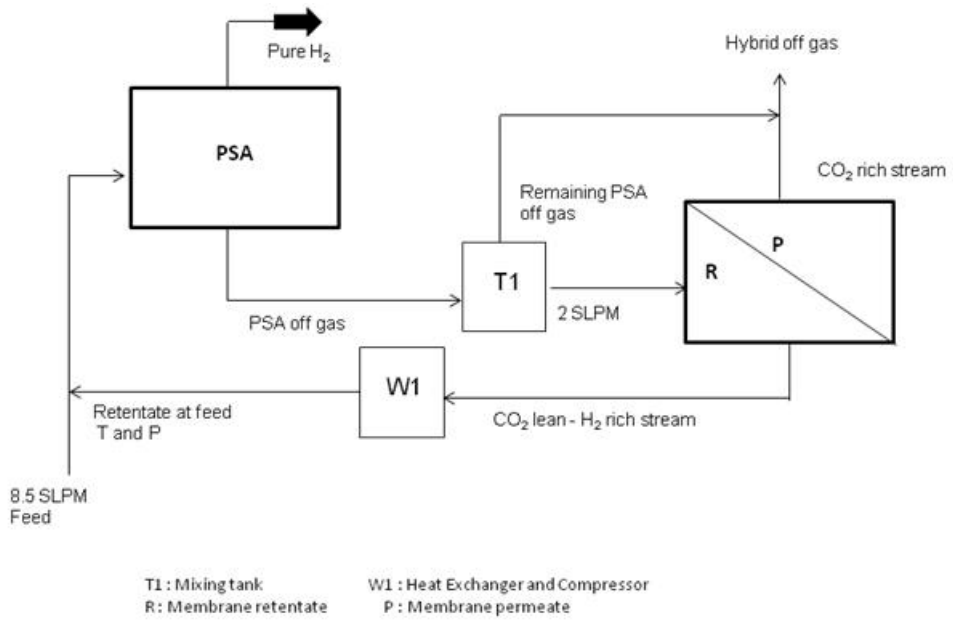

Figure 6.3: The hybrid PSA-membrane flow sheet chosen for the optimization studies

6. It is also assumed that tube side retentate is mixed with the usual PSA feed at PSA feed pressure and temperature. In practice, this requires a compressor and heat exchanger system. In the current simulation study, the model ignores calculating the heat and work load for these equipments.

7. The shell side permeate coming out of the membrane and the remaining off gases (as 2 SLPM is removed constantly) forms the off gas from the hybrid.

Figure 6.3, depicts the graphical overview of the proposed hybrid PSA-membrane configuration considered in this study.

6.4.1 Parameter Selection and Performance Indicators

Two important parameters are chosen for assessing the performance of the hybrid PSA-membrane separation system. First in the list is the area of membrane, as this plays an important role in achieving a desired CO_2 purity and recovery from

Table 6.3: Computational parameters for the hybrid PSA-membrane simulation study

Computational parameters	Value
Axial grid nodes	40
Axial discretization method	CFDM
Number of differential variables	1780
Number of algebraic variables	1652

the membrane module. This parameter is varied from 0.1 to 1.5 m^2 since the parametric studies conducted on the stand alone membrane where it showed that the best membrane performance can be achieved in this area range. The second parameter chosen for the parametric study is the PSA cycletime as its variation leads to considerable change in hydrogen product recovery and purity in the PSA process. However, the range of this parameter cannot be fixed a priori, as it needs to be varied until the PSA hydrogen purity of 99.99 % or excess is achieved for the given value of membrane area. The key performance indicators for the hybrid system remain the same as for the membrane and PSA stand-alone studies. Therefore, from the membrane perspective CO_2 purity and recovery has been taken as the key performance indicators. From the PSA perspective, hydrogen product recovery, and the PSA adsorbent productivity has been selected for the performance measurement, while H_2 product purity is treated as a constraint.

6.4.2 Computational Results

Tables 6.4 to 6.7 show the hybrid performance indicators as function of membrane area and PSA cycletime. It has been found that that for a given value of area,

Table 6.4: Hybrid performance indicators vs. PSA cycletime for membrane area of 0.1 m^2

$t_{cycletime}$	Pur_{H_2}	Rec_{H_2}	$Prod_{H_2}$	Pur_{CO_2}	Rec_{CO_2}
400	100	44.098	37.55858	64.152	27.497
432	99.996	64.333	54.79314	77.496	33.47
440	**99.993**	**65.493**	**55.78157**	**78.173**	**33.796**
448	99.989	66.606	56.72901	78.817	34.108
456	99.982	67.64	57.60938	79.411	34.397
480	99.94	70.436	59.99128	81.012	35.187

increasing PSA cycletime decreases H_2 product purity and increases H_2 product recovery, adsorbent productivity, CO_2 purity, and CO_2 recovery.

The highlighted row in each table represents the maximum time for which the H_2 purity constraints are met and thus represents the optimum point for the particular value of membrane area. H_2 product recovery for these cycletime values is compared against the membrane area in the Figure 6.4. On the abscissa is the membrane area in m^2, where a value of zero indicates the corresponding point for the standalone PSA. The plot also shows that as the area increases, the recovery goes through a maximum, and compared with the stand alone PSA case, increase in overall hydrogen recovery of more than 10 % has been achieved. Therefore, if maximizing the PSA hydrogen product recovery is the only criterion for hybrid design, then membrane area of 0.1 m^2 seems to give the best performance.

Table 6.5: Hybrid performance indicators vs. PSA cycletime for membrane area of 0.5 m^2

$t_{cycletime}$	Pur_{H_2}	Rec_{H_2}	$Prod_{H_2}$	Pur_{CO_2}	Rec_{CO_2}
448	99.997	61.152	52.08	62.923	82.49
464	**99.992**	**63.201**	**53.83**	**64.274**	**84.438**
480	99.981	65.071	55.42	65.497	86.221
560	99.683	72.13	61.43	70.072	93.033

Table 6.6: Hybrid performance indicators vs. PSA cycletime for membrane area of 1 m^2

$t_{cycletime}$	Pur_{H_2}	Rec_{H_2}	$Prod_{H_2}$	Pur_{CO_2}	Rec_{CO_2}
448	99.998	57.226	52.08	49.865	87.565
464	**99.995**	**60.258**	**53.83**	**51.915**	**91.22**
480	99.989	62.135	55.42	53.175	93.483

Table 6.7: Hybrid performance indicators vs. PSA cycletime for membrane area of 1.5 m^2

$t_{cycletime}$	Pur_{H_2}	Rec_{H_2}	$Prod_{H_2}$	Pur_{CO_2}	Rec_{CO_2}
448	99.996	58.5	52.08	44.195	88.675
464	99.991	60.374	53.83	45.451	91.116
480	**99.981**	**62.104**	**55.42**	**46.618**	**93.388**
560	99.947	64.399	61.43	48.202	96.473

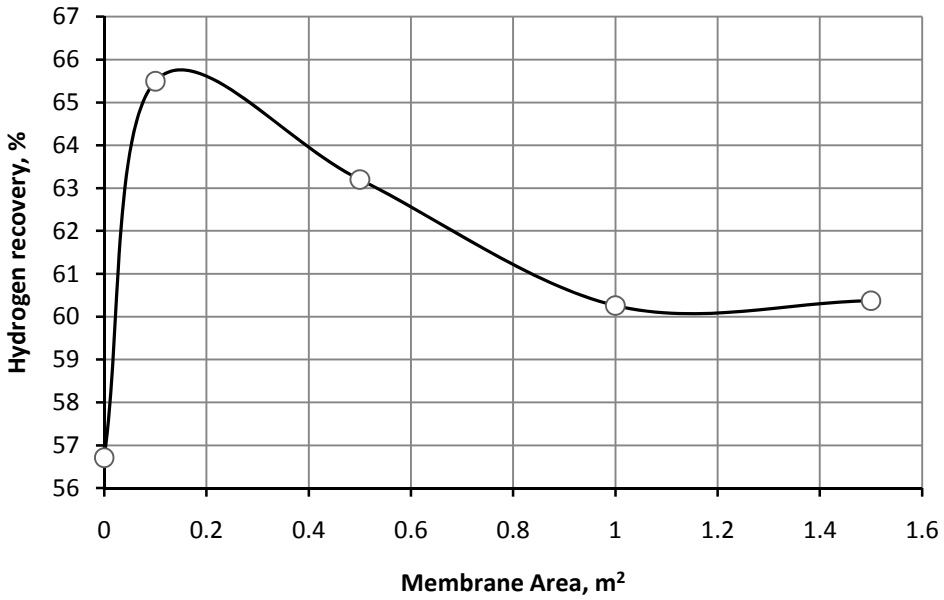

Figure 6.4: Variation of hydrogen recovery with membrane area for the cycle time optimized hybrid PSA-membrane configuration

6.5 Environmental Impact Analysis of The Hybrid PSA-Membrane Separation System

The hybrid separation system, in addition of providing pure hydrogen for commercial use, also emits carbon monoxide, methane, carbon dioxide continuously to the environment. These gases are widely known for their serious impact on our environment in the form of global warming. The main objective of the environmental impact analysis study performed here is to evaluate this impact and compare it with the stand-alone PSA separation system, by employing the life cycle analysis (LCA) methodology.

LCA is a quantitative methodology [153, 135, 80, 8, 71] of assessing the product or process related activities on its environment. It is a"cradle to grave" approach, where all processes or steps in whole supply chain of the generated product are analysed for their effect on the environment. The complete life cycle includes the extraction of raw materials from their respective sources, the pro-

duction of intermediate materials used for making the main product, the main production step, and finally the ultimate disposal, storage or emission of the materials involved in environment in any form (solid, liquid or gas). Other relevant aspects such as transportation of the raw materials, products or materials related to production process, retail, recycling are also included. Therefore, the basic idea is to incorporate detailed information of the main and side process to fully evaluate their effect on the environment. For any LCA study, raw materials, energy carriers (utilities like steam, and cooling water), electricity etc are considered as inputs, whereas emissions or disposal of any material to air, water or land are taken as outputs.

6.5.1 Goal Definition

The main goal of performing the LCA study is to evaluate the environmental impact of the hydrogen purification process from a hybrid of PSA-membrane process system and compare it with the hydrogen purification from the standalone PSA separation system. Since, in principle, multiple hybrid and stand alone configurations are possible, only the best or optimum are considered in this work for the LCA studies, where best is defined as the operating point corresponding to the PSA operation which yields the maximum hydrogen recovery while achieving hydrogen purity in excess of 99.99 %, as shown in the section 6.4.2. Furthermore, the first principles based model developed for the PSA and membrane in previous sections is assumed as the real system in operation.

6.5.2 System Description - Functional Unit

The system under study here is the purification section whose purpose is to purify pure hydrogen of purity more than 99.99 % from a multi-component gaseous mix-

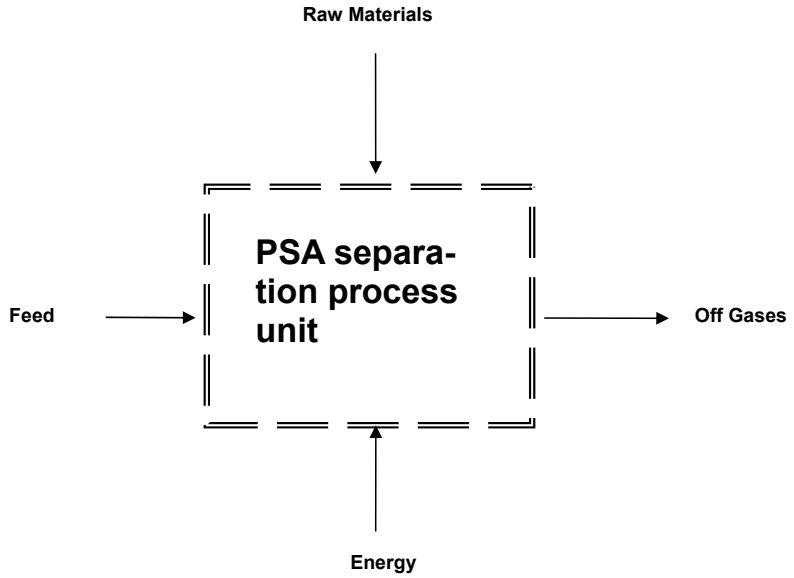

Figure 6.5: LCA system description for the stand alone PSA separation system

ture containing other components as carbon monoxide, methane, carbon dioxide, and nitrogen. In general practice, the off gases collected during the purge and blowdown stage of the operation are sent to heat recovery unit and emitted to environment or to a further CO_2 sequestration unit. In the current study, it is assumed that the off gas stream from the stand alone PSA process leaves the system boundary, whereas for the hybrid case a part of this stream is sent to a membrane module. The retentate from the membrane is recycled back to the system and mixed with the PSA feed, while the tube side permeate leaves the system boundary.

Figures 6.5 and 6.6 show the system specifications for the stand alone and hybrid PSA separation systems, respectively. In the current study, 1 kg of hydrogen product is taken as the functional unit.

6.5.3 Assessment criteria

In the present hybrid system all the five components H_2, CO, CH_4, CO_2, and N_2 emitted to environment are in gaseous state and will remain so throughout

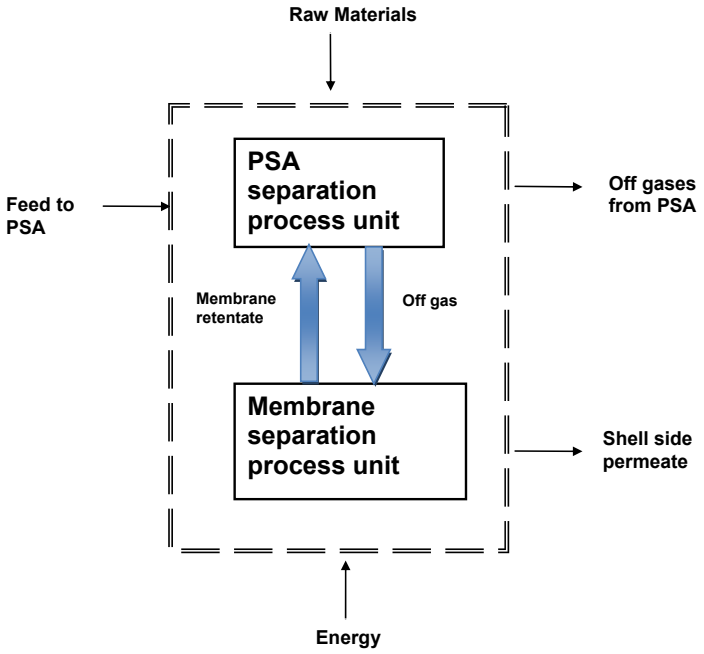

Figure 6.6: LCA system description for the hybrid PSA-membrane separation system

the operation. Out of these, methane and carbon dioxide are widely known for causing global warming which raises the earth surface temperature. Therefore, for these gases as environmental loads, global warming potential (GWP) [67, 95] is selected as environment assessment criteria. In this regard, the IPCC working group 4^{th} annual report [50] provides the definition and values of GWP for a list of chemicals, which contributes towards the global warming phenomena.

6.5.4 Life Cycle Inventory Analysis

Figures 6.5 and 6.6 also displays the three major inputs for the separation system under consideration for the LCA analysis. These three inputs are the feed gas from the reformer section, the raw materials such as membranes and PSA adsorbent, and all other energy inputs including utilities like steam and cooling water as energy carriers. Since the main purpose of this LCA is to compare the environmental impact of the hybrid PSA-membrane system with the standalone

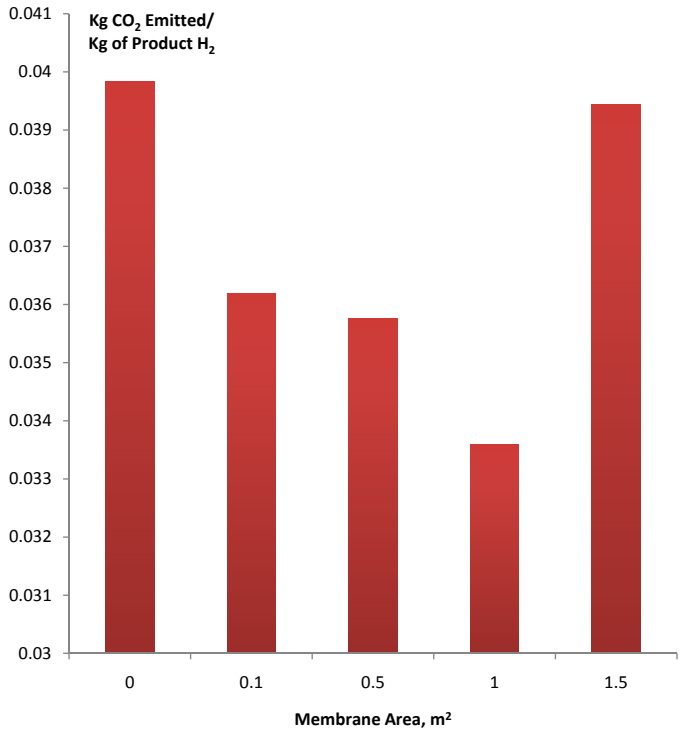

Figure 6.7: Variation of CO_2 emissions with the membrane area of the hybrid PSA-membrane separation system

PSA, the role of these inputs can be ignored. For example, the feed gas will have a contribution to total inventory for a single LCA study but it will clearly cancel out during a comparative study as its value is kept at the same value for the hybrid and PSA separation system. Also, manufacturing of intermediate products like the membranes and PSA adsorbent is a onetime process in product life cycle and thus its contribution as compared to actual every day off gas emissions can also be assumed negligible. The system output stream comprises of off gas containing H_2, CO, CH_4, CO_2 and N_2. Figures 6.7 and 6.8 shows the amount (kg) of each component leaving the system boundary per kg of product H_2. These figures draw a comparison of emission of each component as function of membrane area, where zero area means the corresponding results for standalone PSA process.

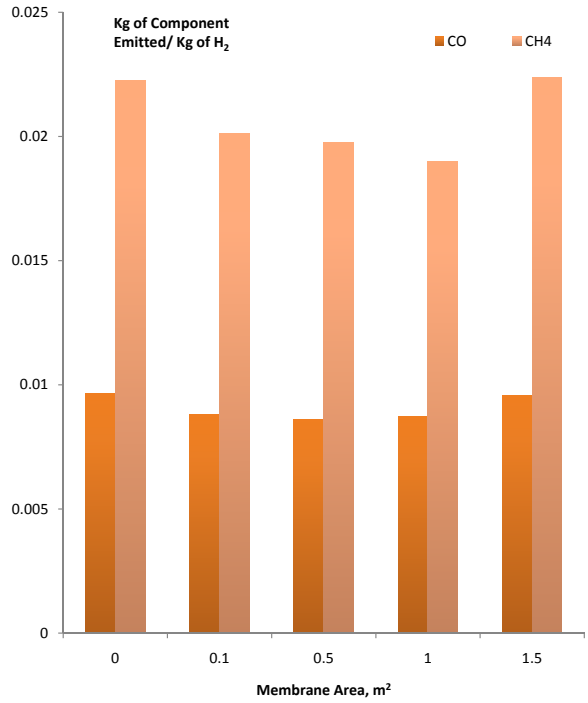

Figure 6.8: Variation of CO and CH_4 emissions with the membrane area of the hybrid PSA-membrane separation system

6.5.5 Life Cycle Impact Assessment and Interpretation

The life cycle impact analysis is done by calculating the global warming potential for the PSA stand alone and the PSA membrane hybrid. For the system at hand, methane and carbon dioxide are the only gases for which GWPs are listed in the latest IPCC report [50], and hence are considered for the analysis. Reported GWP of methane is 21 and is 1 for carbon dioxide for a 10 year time horizon, which is also the time horizon selected for the LCA study. These GWP values are multiplied with the individual inventories (per kg of hydrogen) evaluated in the LCI section and then summed together to obtain the cumulative GWP for the data set.

Figure 6.9 depicts the value of cumulative GWP for the standalone PSA and the hybrid process, clearly indicating that the GWP is generally smaller for the hybrid process as compared to the standalone PSA system, represented in the

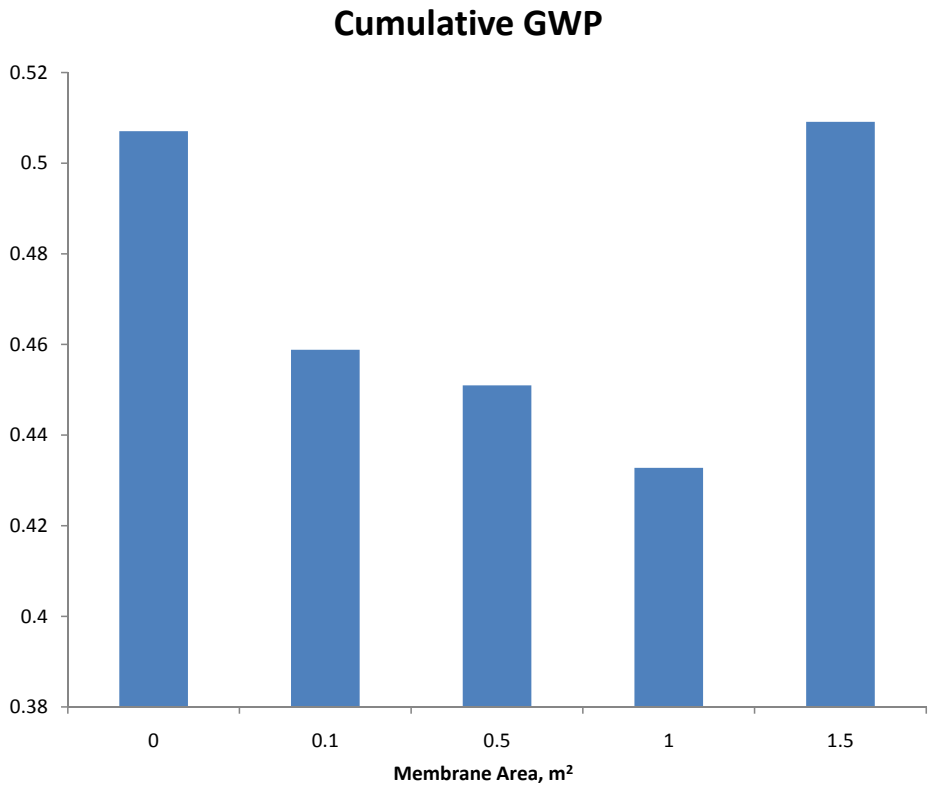

Figure 6.9: Variation of cumulative global warming potential with the membrane area of the hybrid PSA-membrane separation system

plot by the zero area value. The minimum value of GWP is found to be for a membrane area of 1 m^2.

6.5.6 Conclusions

A first-principles dynamic model based approach is chosen to design the membrane-PSA hybrid system. Preliminary investigation of standalone membrane module is conducted where membrane area and shell side pressure are varied to evaluate the membrane performance. It is found that increasing the area increases CO_2 recovery and reduces purity for both the upstream and downstream configurations. However, for the same value of area, the downstream configuration offers better CO_2 purity and recovery and is thus selected for integration with the PSA. Similar parametric study approach has been chosen to evaluate standalone PSA performance, and the results shows that PSA cycletime of 480 seconds offers the best possible performance. The results of standalone PSA and membranes studies in a way prepare the base case for designing the hybrid. In order to design the hybrid system, a simulation based approach is employed as compared to the traditional dynamic optimization which is found to be too time computationally intensive to be applied to the hybrid system. In this approach, membrane area and PSA cycletime are varied over a range and hybrid performance variables are calculated. It is found that using low membrane area increases PSA hydrogen product recovery by over 10 % as compared to the standalone PSA.

The designed hybrid process, like every chemical process also impacts the environment. An environmental impact analysis study is conducted to quantify the value of these impacts. This is compared with the stand alone PSA separation system achieving same hydrogen purity. Here, only emissions from the PSA process during the purge and blowdown operation are considered for the analysis as these emissions occur throughout the operating cycle of the plant. Global

warming potential is calculated for the cycletime optimized hybrid and the stand alone PSA as a function of membrane area and compared. The results show that cumulative GWP for the hybrid process is always less than the stand alone PSA system and thus the hybrid process environmental impact is less. The minimum GWP was obtained for the membrane area of 1 m^2.

Chapter 7

Conclusions and Future Research Directions

Pressure swing adsorption systems offers great flexibility at both design and operational stages, requiring careful selection of important decision variables. On the other hand, due to its inherent nonlinear nature and discontinuous operation, both design and control of PSA, especially incorporating the operational aspects, is a challenging task. The thesis is mainly focussed on the application of state of the art system engineering methodologies to tackle some of these challenges while employing a rigorous mathematical model.

7.1 Thesis Summary

7.1.1 Explicit/Multi-parametric MPC PSA Purity Control

Chapter 3 and Chapter 4 of the thesis present a detailed study on an important but relatively unexplored area of PSA control. One one hand, an advanced model

based controller for purity control appears to be an ideal choice as it provides optimal control action, while on other hand its design and validation, considering its highly nonlinear nature and inherently dynamic operation, present great challenges. This work employs a systematic and rigorous framework for accomplishing this task. The detailed controller formulation also includes important constraints on manipulative variable, adsorption time to ensure a PSA system cycle which is neither too fast as it can lead to severe wear and tear of important PSA components, or is too slow which can cause irreversible adsorption situation in reality.

Furthermore, as part of the system identification process, serious consideration has been given towards the design of the perturbation signal used to disturb the plant, as it plays a critical role in obtaining the true dynamic nature of the system. In this regard, two important features of the random pulse test signal, maximum pulse amplitude and its switching time, are investigated in detail. The maximum pulse amplitude is established by performing various hit and trial open loop simulations and a value of 3 seconds is finally selected, while three different values of switching time are selected leading to three best-fit reduced state space models of different sizes. It is important to note that the purpose of in-silico closed loop simulation is not only to find the best tuning parameters of the mp-MPC controller but also to simultaneously compare the effect of different optimal reduced linear models on the real time performance of the controller.

The work also demonstrates that, in contrast to the conventional PID controllers, an explicit MPC controller, powered with a predictive model and constraint handling feature in an optimization framework, provides twice as fast response time (for the step disturbance study) and also maintains the manipulative variable within the intended bounds, in response to the step and impulse disturbances considered in this study.

7.1.2 Simultaneous Design and Control Optimization of PSA Under Uncertainty

Following the work on the design of mp-MPC for the given PSA system, a detailed PSA optimization study is conducted, where design, operational and control aspects of PSA system are considered simultaneously in order to obtain PSA system with superior real time operability in the face of disturbances. The simultaneous approach followed here facilitates the incorporation of conflicting, design and control objective functions in an unified formulation while yielding an optimal PSA system which also obeys important operational constraints including product purity specifications.

To accomplish the task, the decomposition based algorithm of Mohideen et al. [98] is employed comprising three main steps of feed composition uncertainty discretization into three critical scenarios, then performing the multi-period dynamic optimization, and finally conducting the dynamic feasibility test. Another key feature of this study is the consideration of a variety of decision variables related to bed design and cyclic operation of PSA. In the context of cyclic operation, the time duration of PSA processing steps is also optimized.

As part of the work, two detailed comparison studies are also conducted. In the first comparative study, the design and control configuration obtained from the simultaneous approach followed here is compared with the traditional sequential approach, at nominal conditions. The results show that with the sequential approach, the actual recovery obtained in the presence of disturbances is around 60 %, which is much smaller than the 63 % recovery obtained at the optimal design conditions (with no disturbances). In contrast, the simultaneous approach provides almost 3 % extra real time recovery, in addition to providing better purity response. Furthermore, it is also found that the design obtained from

the simultaneous approach is slightly bigger in size with slower PSA cycles as compared to the design obtained from the sequential approach. In the next comparative study, a full scale mp-MPC is designed at the nominal conditions to observe any further benefits related to the model based controller. The results show improvement, albeit marginal, in the closed loop response with respect to the optimized PI controller considered in the study.

7.1.3 Design Heuristics for Hybrid PSA-Membrane Systems

The main motivation to integrate membrane separation system with the PSA assembly is to minimize the hydrogen loss through the off gas stream of PSA. To analyze the effect of various operating conditions on the CO_2 selective membrane system performance, detailed simulation studies are conducted on the stand alone membrane modules. In the upstream configuration, the membrane is subjected to feed conditions of the PSA system, in terms of inlet composition, operating pressure and temperature, while in the downstream configuration, the membrane module is subject to PSA off gas conditions. The results show that with the downstream configuration, both CO_2 recovery and purity in excess of 90 % are possible, which are significantly higher than the upstream case. For the hybrid PSA-membrane system design with downstream membrane configuration, key decision variables considered are the membrane area and the PSA cycle time. The results of simulation studies indicates that the hydrogen recovery first increase and then decreases with increasing membrane area with the best recovery of 65.5 %, obtained for membrane area of 0.1 m^2. The most important aspect of this study is that the recovery obtained here is almost 10 % higher than the optimal recovery achieved from a stand alone PSA system, providing strong motivation to

further study the effect of other important decision variables, such as membrane feed rate, adsorbent bed length and diameter etc, on the hybrid performance, for further benefits.

Furthermore, a brief LCA study is also conducted to quantify the environmental impact of the hybrid PSA-membrane separation system in comparison to the stand alone PSA system. Towards this purpose, the cumulative GWP potential is calculated for the net off gas leaving the separation system as a function of the membrane area for the cycle time optimized hybrid and stand lone PSA systems. The results indicates that the minimum value of GWP is achieved for membrane area of 1 m^2. This result also highlights the conflict between the design objective, hydrogen recovery and the environmental objective, GWP for choosing a suitable value of membrane area of the hybrid system under consideration.

7.2 Key contributions

7.2.1 Mathematical Model of PSA Operation

A key contribution of this work is the development of a detailed mathematical model of the PSA system, which functions as its virtual copy towards the purpose of PSA optimization and control studies. The distributed model incorporates rigorous formulation of the mass, energy, and momentum balances for the gas-solid system, including dispersive effects in the mass and heat transfer phenomenons. The intra-particle mass transfer rate is presented by linear driving force model, while the adsorption equilibrium characteristic is captured by multi-site Langmuir isotherms.

7.2.2 Explicit/Multi-Parametric MPC Controller of PSA

An explicit/multi-parametric MPC is designed for purity control of an industrial scale four bed PSA system, employing a rigorous framework comprising of four main steps towards formulation and testing of the controller. Since the original PDAE model cannot be used for control purposes, reduced (linear) models are obtained by the application of advanced system identification techniques. Furthermore, detailed comparative studies are also performed to test the mp-MPC controller performance with the standard (optimized) PID controllers.

7.2.3 Simultaneous Design and Control Optimization of PSA Under Uncertainty

An optimal design and control configuration of PSA separation system used for hydrogen purification purposes is obtained by employing the simultaneous design and control methodology. The unified design and control formulation considered in this work incorporates the complex interaction between the design objective, PSA recovery and the control objective, purity control in addition to taking into account the important PSA design, operational, controller constraints, and also the time variant and invariant disturbances in process conditions. Detailed comparison studies are also conducted to compare the design and control configuration obtained from the simultaneous with the sequential approach, and also to compare the closed loop performance from optimized PI with mp-MPC controller.

7.2.4 Design of a Hybrid PSA-Membrane Separation System

A novel hybrid separation system consisting of four bed, nine step PSA with CO_2 selective membrane module at its downstream has been designed to produce high

purity hydrogen of 99.99 % quality from a five component feed stream of CO, H_2, CO_2, CH_4, N_2. Here, the main design objective is to improve the overall operational hydrogen recovery, as compared to the stand alone PSA separation system. Furthermore, environmental impact of the designed hybrid is also calculated by evaluating its cumulative global warming potential.

7.3 Future Research Directions

7.3.1 PSA Control Improvements

In the future studies, it will be worthwhile to investigate the effect of off-gas tank dynamics on the purity controller performance, and also to include its own controller details with in the overall MIMO MPC controller formulation for PSA. The main purpose of the off-gas tank is to minimize the flow and pressure fluctuations resulting from the blowdown and purge steps of the PSA cycle. The off-gas tank controller gains further significance in scenarios where PSA is a part of a bigger reaction-separation system, such as the purification unit of the steam methane reforming process. Here, the controller objective is to ensure that the off-gas stream finally leaving the purification unit has steady flow and pressure characteristics.

Further studies should also be carried out to understand, if having multiple measurements within one PSA cycle (higher sampling frequency), actually improves the controller performance. Ultimately, the explicit/multi-parametric controller design should be made robust [121], to obtain better performance in the presence of modeling uncertainties and operational noises.

7.3.2 Enhancing Computational Efficiency of PSA Optimization

Due to PSA inherent feature of achieving only a CSS, detailed and computationally challenging, dynamic optimization procedures has to be used for design purposes in this study. This is in sharp contrast to other dynamic processes, where at steady state the time derivatives approaches zero and steady state optimization can be effectively employed without the need of calculating the CPU intensive, model sensitivities with respect to the decision variables through out the time horizon of operation. Dynamic optimization studies performed in Chapter 5 (see Table 5.10), shows that more than half of the CPU time is spent in the sensitivity calculations. It is important to note that for the optimization studies where no time variant decision variables are involved, which is usually the case for most PSA optimization problems, the objective function and constraints sensitivities with respect to time invariant decision variables are only required at the final time of the operation. Therefore, a possible way to accelerate the PSA optimization procedure is to calculate the sensitivity information only at the end (CSS) or towards the end. Furthermore, bypassing the sensitivities for most part of the time horizon would significantly enhance the robustness of the numerical optimization procedures, without compromising its rigorousness.

7.3.3 Simultaneous Design and Control of Process System With Model Based Controllers

In past, only few studies have incorporated a model based control such as MPC [25, 139] in the simultaneous design and control optimization framework. The controller moves in this case are obtained by solving an optimization problem, which poses further challenges to the solution of overall optimization formulation.

One important aspect of such a formulation is the requirement of two instances of dynamic models with different complexity in the same optimization problem. Here, the detailed model represents the real plant operation, while the reduced model is used for the MPC purposes. It is important to note that the reduced model represents dynamics between the control and manipulative variable set for the given design conditions only. During the numerical solution of dynamic optimization problem, each new iteration evaluates a new set of decision variables, which include process design variables as well. Therefore, employing the reduced model corresponding to the first iteration (or initial guess) in the subsequent iterations is not a suitable approach as it can lead to large inaccuracies related to the calculation of system dynamics, further leading to a faulty design. One possible way to resolve this is to embed the system identification procedures within the optimization framework, as depicted in Figure 7.1. Here, as the new decision variables are evaluated, the reduce model is also *refreshed* employing some of the system identification techniques mentioned in Chapter 5 of this thesis.

It is important to note that embedding MPC inside an other optimization problem also leads to bi-level dynamic optimization problems. Here, the role of multi-parametric programming based mp-MPC is quite profound, as it provides the governing control laws explicitly, eliminating the need of MPC related optimization problem in the framework. Consequently, the critical regions corresponding to the new version of reduced model needs to be re-evaluated as shown in Figure 7.1.

Another area of improvement is to incorporate the controller stability and robustness features in the step 2 of the PSA optimization under uncertainty procedure itself. The combination of ISE and dynamic feasibility test, as shown in this study appears to be an efficient methodology to handle time varying and invariant disturbances. In this context, ISE as a choice of controller performance

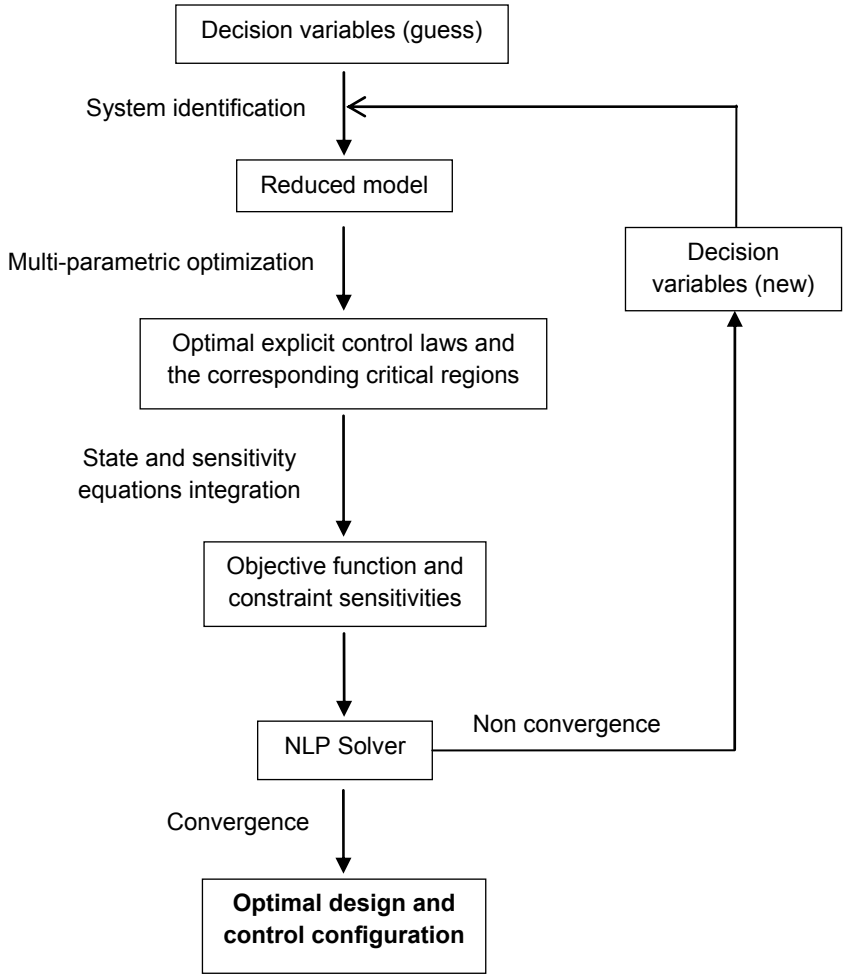

Figure 7.1: Dynamic optimization approach with embedded system identification step for simultaneous design and control with mp-MPC formulation

indicator, especially for MIMO [177] systems, does not cover all aspects of a controller response including the stability issue. In principle, solution of the controller synthesis problem can result in an optimal input trajectory which is oscillatory in nature. Embedding controller stability and robustness measures (in the form of additional constraints) in the controller synthesis formulation, even though is expected to complicate the overall design methodology, should be investigated to observe any benefits in terms of design with superior operability.

Publications From This Thesis

Journal Articles

1. Khajuria, H., Pistikopoulos, E. N., 2011. Dynamic modeling and explicit/multi–parametric mpc control of pressure swing adsorption systems. Journal of Process Control 21 (1), 151-163.

2. Khajuria, H., Pistikopoulos, E. N., (manuscript submitted). Optimization and control of pressure swing adsorption processes under uncertainty. AIChE Journal.

Conferences

1. Khajuria, H., Pistikopoulos, E. N., November 2009. An advanced MPC controller design for PSA operation. In: AIChE Annual Meeting. Nashville, TN.

2. Khajuria, H., Pistikopoulos, E. N., July 2010. An explicit/multi–parametric controller design for pressure swing adsorption system. In: Kothare, M., Tade, M., Wouwer, A. V., Smets, I. (Eds.), Proceedings of the 9^{th} International Symposium on Dynamics and Control of Process Systems (DYCOPS 2010). Leuven, Belgium, pp. 192-197.

3. Khajuria, H., Pistikopoulos, E. N., 2011. Integrated design and control of pressure swing adsorption systems. In: Pistikopoulos, E., Georgiadis, M., Kokossis, A. (Eds.), 21^{st} European Symposium on Computer-Aided Process Engineering (ESCAPE 2011). pp. 628-632.

4. Khajuria, H., Pistikopoulos, E. N., 2011. Simultaneous design and control of pressure swing adsorption processes. In: AIChE Annual Meeting.

Minneapolis, MN.

5. Khajuria, H., Pistikopoulos, E. N., 2012 (manuscript submitted). Optimization and control of pressure swing adsorption systems. In: CHEMICAL PROCESS CONTROL VIII. Savannah, Georgia, US.

Technical Reports (Hy2SEPS)

1. Khajuria, H., Pistikopoulos, E. N., 2008. D25:PSA separation system optimization and design part i. Tech. rep., HY2SEPS, EU Contract no: 019887.

2. Khajuria, H., Pistikopoulos, E. N., 2008. D27: Optimization and design of hybrid separation system. Tech. rep., HY2SEPS, EU Contract no: 019887.

3. Khajuria, H., Pistikopoulos, E. N., 2008. D30: Assessment of hybrid separation process sustainability. Tech. rep., HY2SEPS, EU Contract no: 019887.

Bibliography

[1] Adhikari, S., Fernando, S., 2006. Hydrogen membrane separation techniques. Industrial & Engineering Chemistry Research 45 (3), 875–881.

[2] Agarwal, A., Biegler, L. T., Zitney, S. E., 2009. Simulation and optimization of pressure swing adsorption systems using reduced-order modeling. Industrial & Engineering Chemistry Research 48 (5), 2327–2343.

[3] Agrawal, R., Auvil, S., Choe, J., Woodward, D., 1990. Membrane/cryogenic hybrid scheme for argon production from air. Gas Separation & Purification 4 (2), 75 – 80.

[4] Anderson, L. E., Gulati, M., Westgate, P. J., Kvam, E. P., Bowman, K., Ladisch, M. R., 1996. Synthesis and optimization of a new starch-based adsorbent for dehumidification of air in a pressure-swing dryer. Industrial & Engineering Chemistry Research 35 (4), 1180–1187.

[5] Asteasuain, M., Brandolin, A., Sarmoria, C., Bandoni, A., 2004. Simultaneous design and control of a semibatch styrene polymerization reactor. Industrial & Engineering Chemistry Research 43 (17), 5233–5247.

[6] Asteasuain, M., Sarmoria, C., Brandolin, A., Bandoni, A., 2007. Integration of control aspects and uncertainty in the process design of polymerization reactors. Chemical Engineering Journal 131 (1-3), 135 – 144.

[7] Ayoub, S., Tondeur, D., Latifi, M., 2011. New formulation of optimization-based simulation of a pressure swing adsorption process: Hybrid dynamic optimization. AIChE Journal 57 (5), 1367–1373.

[8] Ayres, R. U., Ayres, L. W., Martins, K., 1998. Exergy, waste accounting, and life-cycle analysis. Energy 23 (5), 355 – 363.

[9] Azizian, S., Bashiri, H., 2009. A new isotherm for multisite occupancy adsorption of binary gaseous mixtures. Langmuir 25 (4), 2309–2312.

[10] Baker, R. W., 2002. Future directions of membrane gas separation technology. Industrial & Engineering Chemistry Research 41 (6), 1393–1411.

[11] Bandermann, F., Harder, K.-B., 1982. Production of h2 via thermal decomposition of h2s and separation of h2 and h2s by pressure swing adsorption. International Journal of Hydrogen Energy 7 (6), 471 – 475.

[12] Bansal, V., Perkins, J., Pistikopoulos, E., Ross, R., van Schijndel, J., 2000. Simultaneous design and control optimisation under uncertainty. Computers & Chemical Engineering 24 (2-7), 261 – 266.

[13] Bansal, V., Perkins, J. D., Pistikopoulos, E. N., 2002. A case study in simultaneous design and control using rigorous, mixed-integer dynamic optimization models. Industrial & Engineering Chemistry Research 41 (4), 760–778.

[14] Bansal, V., Ross, R., Perkins, J. D., Pistikopoulos, E. N., 2000. The interactions of design and control: double-effect distillation. Journal of Process Control 10 (2-3), 219 – 227.

[15] Bansal, V., Sakizlis, V., Ross, R., Perkins, J. D., Pistikopoulos, E. N.,

2003. New algorithms for mixed-integer dynamic optimization. Computers & Chemical Engineering 27 (5), 647 – 668.

[16] Barton, P. I., Banga, J. R., Galn, S., 2000. Optimization of hybrid discrete/continuous dynamic systems. Computers & Chemical Engineering 24 (9-10), 2171 – 2182.

[17] Beccuti, A., Papafotiou, G., Frasca, R., Morari, M., june 2007. Explicit hybrid model predictive control of the dc-dcboost converter. In: Power Electronics Specialists Conference, 2007. PESC 2007. IEEE. pp. 2503 – 2509.

[18] Bernardo, P., Drioli, E., Golemme, G., 2009. Membrane gas separation: A review/state of the art. Industrial & Engineering Chemistry Research 48 (10), 4638–4663.

[19] Bird, R., Stewart, W., Lightfoot, E., 2007. Transport Phenomena (Revised Second Edition ed.). John Wiley & Sons.

[20] Bitzer, M., 2005. Model-based nonlinear tracking control of pressure swing adsorption plants. In: Meurer, T., Graichen, K., Gilles, E.-D. (Eds.), Control and Observer Design for Nonlinear Finite and Infinite Dimensional Systems. Vol. 322/2005 of Lecture Notes in Control and Information Sciences. Springer Berlin / Heidelberg, pp. 403–418.

[21] Bitzer, M., Zeitz, M., 2002. Design of a nonlinear distributed parameter observer for a pressure swing adsorption plant. Journal of Process Control 12 (4), 533 – 543.

[22] Bitzer, M., Zeitz, M., May 2002. Process control scheme for a 2-bed pressure swing adsorption plant. In: Grievink, J., Schijndel, J. V. (Eds.), European

Symposium on Computer Aided Process Engineering-12. Vol. 10. pp. 451–456.

[23] Bonjour, J., Chalfen, J.-B., Meunier, F., 2002. Temperature swing adsorption process with indirect cooling and heating. Industrial & Engineering Chemistry Research 41 (23), 5802–5811.

[24] Borrelli, F., Bemporad, A., Fodor, M., Hrovat, D., 2001. A hybrid approach to traction control. In: Di Benedetto, M., Sangiovanni-Vincentelli, A. (Eds.), Hybrid Systems: Computation and Control. Vol. 2034 of Lecture Notes in Computer Science. Springer Berlin / Heidelberg, pp. 162–174.

[25] Brengel, D., Seider, W., 1992. Coordinated design and control optimization of nonlinear processes. Computers & Chemical Engineering 16 (9), 861 – 886.

[26] Buzanowski, M. A., Yang, R. T., 1991. Approximations for intraparticle diffusion rates in cyclic adsorption and desorption. Chemical Engineering Science 46 (10), 2589 – 2598.

[27] Carter, J., Wyszynski, M., 1983. The pressure swing adsorption drying of compressed air. Chemical Engineering Science 38 (7), 1093 – 1099.

[28] Cavenati, S., Grande, C. A., Rodrigues, A. E., 2006. Separation of ch4/co2/n2 mixtures by layered pressure swing adsorption for upgrade of natural gas. Chemical Engineering Science 61 (12), 3893 – 3906.

[29] Chawankul, N., Budman, H., Douglas, P., 2005. The integration of design and control: Imc control and robustness. Computers & Chemical Engineering 29 (2), 261 – 271.

[30] Chawankul, N., Sandoval, L. R., Budman, H., Douglas, P. L., 2007. Integration of design and control: A robust control approach using mpc. The Canadian Journal of Chemical Engineering 85 (4), 433–446.

[31] Cho, S., Han, S., Kim, J., Park, J., Rhee, H., 2002. Adsorptive ethylene recovery from ldpe off-gas. Korean Journal of Chemical Engineering 19, 821–826.

[32] Chou, C., Huang, W.-C., 1994. Simulation of a four-bed pressure swing adsorption process for oxygen enrichment. Industrial & Engineering Chemistry Research 33 (5), 1250–1258.

[33] Chou, C.-T., Huang, W.-C., 1994. Incorporation of a valve equation into the simulation of a pressure swing adsorption process. Chemical Engineering Science 49 (1), 75 – 84.

[34] Chue, K. T., Kim, J. N., Yoo, Y. J., Cho, S. H., Yang, R. T., 1995. Comparison of activated carbon and zeolite 13x for co2 recovery from flue gas by pressure swing adsorption. Industrial & Engineering Chemistry Research 34 (2), 591–598.

[35] Connor, Denis, J., Doman, David, G., Jeziorowski, L., Keefer, Bowie, G., Larisch, B., McLean, C., Shaw, I., 2002. Rotary pressure swing adsorption apparatus. United States Patent and Trademark Office Granted Patent No US6406523.

[36] Cruz, P., Magalhes, F. D., Mendes, A., 2005. On the optimization of cyclic adsorption separation processes. AIChE Journal 51 (5), 1377 – 1395.

[37] Cuthrell, J. E., Biegler, L. T., 1987. On the optimization of differential-algebraic process systems. AIChE Journal 33 (8), 1257–1270.

[38] Dimitriadis, V. D., Pistikopoulos, E. N., 1995. Flexibility analysis of dynamic systems. Industrial & Engineering Chemistry Research 34 (12), 4451–4462.

[39] Ding, Y., LeVan, M. D., 2001. Periodic states of adsorption cycles iii. convergence acceleration for direct determination. Chemical Engineering Science 56 (17), 5217 – 5230.

[40] Douglas, J. M., 1988. Conceptual Design of Chemical Processes. McGraw-Hill.

[41] Dua, P., Doyle, F., Pistikopoulos, E., aug. 2006. Model-based blood glucose control for type 1 diabetes via parametric programming. Biomedical Engineering, IEEE Transactions on 53 (8), 1478 –1491.

[42] Dua, P., Doyle, F., Pistikopoulos, E., 2009. Multi-objective blood glucose control for type 1 diabetes. Medical and Biological Engineering and Computing 47, 343–352.

[43] Esteves, I. A. A. C., Mota, J. P. B., 2002. Simulation of a new hybrid membrane/pressure swing adsorption process for gas separation. Desalination 148 (1-3), 275 – 280.

[44] Esteves, I. A. A. C., Mota, J. P. B., 2007. Gas separation by a novel hybrid membrane/pressure swing adsorption process. Industrial & Engineering Chemistry Research 46 (17), 5723–5733.

[45] Farooq, S., Ruthven, D. M., Boniface, H. A., 1989. Numerical simulation of a pressure swing adsorption oxygen unit. Chemical Engineering Science 44 (12), 2809 – 2816.

[46] Fatehi, A., Loughlin, K., Hassan, M., 1995. Separation of methane–nitrogen mixtures by pressure swing adsorption using a carbon molecular sieve. Gas Separation & Purification 9 (3), 199 – 204.

[47] Feehery, W. F., Barton, P. I., 1998. Dynamic optimization with state variable path constraints. Computers & Chemical Engineering 22 (9), 1241 – 1256.

[48] Feng, X., Pan, C. Y., Ivory, J., Ghosh, D., 1998. Integrated membrane/adsorption process for gas separation. Chemical Engineering Science 53 (9), 1689 – 1698.

[49] Flores-Tlacuahuac, A., Biegler, L. T., 2007. Simultaneous mixed-integer dynamic optimization for integrated design and control. Computers & Chemical Engineering 31 (5-6), 588 – 600, eSCAPE-15 - Selected Papers from the 15th European Symposium on Computer Aided Process Engineering held in Barcelona, Spain, May 29-June 1, 2005.

[50] Forster, P., Ramaswamy, V., Artaxo, P., Berntsen, T., Betts, R., Fahey, D., Haywood, J., Lean, J., Lowe, D., Myhre, G., Nganga, J., Prinn, R., Raga, G., Schulz, M., Dorland, R. V., 2007. Changes in atmospheric constituents and in radiative forcing. In: Solomon, S., Qin, D., Manning, M., Chen, Z., Marquis, M., Averyt, K., M.Tignor, Miller, H. (Eds.), Climate Change 2007:The Physical Science Basis. Contribution of Working Group I to the Fourth Assessment Report of the Intergovernmental Panel on Climate Change. Cambridge University Press, Cambridge, United Kingdom and New York, NY, USA.

[51] Georgiadis, M. C., Kikkinides, E. S., Makridis, S. S., Kouramas, K., Pistikopoulos, E. N., 2009. Design and optimization of advanced materials

and processes for efficient hydrogen storage. Computers & Chemical Engineering 33 (5), 1077 – 1090, chemical Products: From conceptualization to commercialization.

[52] Georgis, D., Jogwar, S. S., Almansoori, A. S., Daoutidis, P., 2011. Design and control of energy integrated sofc systems for in situ hydrogen production and power generation. Computers & Chemical Engineering 35 (9), 1691 – 1704, energy Systems Engineering.

[53] Gomes, V. G., Hassan, M. M., 2001. Coalseam methane recovery by vacuum swing adsorption. Separation and Purification Technology 24 (1-2), 189 – 196.

[54] Gomes, V. G., Yee, K. W. K., 2002. Pressure swing adsorption for carbon dioxide sequestration from exhaust gases. Separation and Purification Technology 28 (2), 161 – 171.

[55] Goto, M., Sato, M., Kodama, A., Hirose, T., 1997. Application of supercritical fluid technology to citrus oil processing. Physica B: Condensed Matter 239 (1-2), 167 – 170, proceedings of the Workshop on Transition Metals and Compounds under Multiextreme Conditions.

[56] gPROMS, 2008. Process Systems Enterprise Ltd., gPROMS model developer guide. http://www.psenterprise.com/gproms/index.html.

[57] Grancharova, A., Johansen, T. A., Kocijan, J., 2004. Explicit model predictive control of gas-liquid separation plant via orthogonal search tree partitioning. Computers & Chemical Engineering 28 (12), 2481 – 2491.

[58] Grande, C. A., Rodrigues, A. E., 2005. Propane/propylene separation by

pressure swing adsorption using zeolite 4a. Industrial & Engineering Chemistry Research 44, 8815–8829.

[59] Hamid, M. K. A., Sin, G., Gani, R., 2010. Integration of process design and controller design for chemical processes using model-based methodology. Computers & Chemical Engineering 34 (5), 683 – 699, selected Paper of Symposium ESCAPE 19, June 14-17, 2009, Krakow, Poland.

[60] Han, S.-S., Park, J.-H., Kim, J.-N., Cho, S.-H., 2005. Propylene recovery from propylene/propane/nitrogen mixture by psa process. Adsorption 11, 621–624.

[61] Hart, J., Battrum, M. J., Thomas, W. J., 1990. Axial pressure gradients during the pressurization and depressurization steps of a psa gas separation cycle. Gas Separation & Purification 4 (2), 97 – 102.

[62] Hassan, M., Ruthven, D., Raghavan, N., 1986. Air separation by pressure swing adsorption on a carbon molecular sieve. Chemical Engineering Science 41 (5), 1333 – 1343.

[63] Hegrenæs, Ø., Gravdahl, J., Tøndel, P., june 2005. Attitude control by means of explicit model predictive control, via multi-parametric quadratic programming. In: American Control Conference, 2005. Proceedings of the 2005. pp. 901 – 906 vol. 2.

[64] Hegrenæs, Ø., Gravdahl, J. T., Tndel, P., 2005. Spacecraft attitude control using explicit model predictive control. Automatica 41 (12), 2107 – 2114.

[65] Ho, M. T., Allinson, G. W., Wiley, D. E., 2008. Reducing the cost of co2 capture from flue gases using pressure swing adsorption. Industrial & Engineering Chemistry Research 47 (14), 4883–4890.

[66] Hsiao-Kuo, Hsuen, 2000. An improved linear driving force approximation for intraparticle adsorption. Chemical Engineering Science 55 (17), 3475 – 3480.

[67] Jacobson, M. Z., Colella, W. G., Golden, D. M., 2005. Cleaning the air and improving health with hydrogen fuel-cell vehicles. Science 308 (5730), 1901–1905.

[68] Jiang, L., Biegler, L. T., Fox, V. G., 2003. Simulation and optimization of pressure-swing adsorption systems for air separation. AIChE Journal 49 (5), 1140–1157.

[69] Jiang, L., Fox, V. G., Biegler, L. T., November 2004. Simulation and optimal design of multiple-bed pressure swing adsorption systems. AIChE Journal 50 (11), 2904–2917.

[70] Johansen, T. A., Fuglseth, T. P., Tøndel, P., Fossen, T. I., 2008. Optimal constrained control allocation in marine surface vessels with rudders. Control Engineering Practice 16 (4), 457 – 464, special Section on Manoeuvering and Control of Marine Craft.

[71] Kaltschmitt, M., Reinhardt, G., Stelzer, T., 1997. Life cycle analysis of biofuels under different environmental aspects. Biomass and Bioenergy 12 (2), 121 – 134.

[72] Khajuria, H., Pistikopoulos, E. N., July 2010. An explicit/multi-parametric controller design for pressure swing adsorption system. In: Kothare, M., Tade, M., Wouwer, A. V., Smets, I. (Eds.), Proceedings of the 9^{th} International Symposium on Dynamics and Control of Process Systems (DYCOPS 2010). Leuven, Belgium, pp. 192–197.

[73] Khajuria, H., Pistikopoulos, E. N., 2011. Dynamic modeling and explicit/multi-parametric mpc control of pressure swing adsorption systems. Journal of Process Control 21 (1), 151 – 163.

[74] Kikkinides, E. S., Sikavitsas, V. I., Yang, R. T., 1995. Natural gas desulfurization by adsorption: Feasibility and multiplicity of cyclic steady states. Industrial & Engineering Chemistry Research 34 (1), 255–262.

[75] Kikkinides, E. S., Yang, R. T., 1991. Simultaneous sulfur dioxide/nitrogen oxide (nox) removal and sulfur dioxide recovery from flue gas by pressure swing adsorption. Industrial & Engineering Chemistry Research 30 (8), 1981–1989.

[76] Kikkinides, E. S., Yang, R. T., 1993. Gas separation and purification by polymeric adsorbents: flue gas desulfurization and sulfur dioxide recovery with styrenic polymers. Industrial & Engineering Chemistry Research 32 (10), 2365–2372.

[77] Kikkinides, E. S., Yang, R. T., Cho, S. H., 1993. Concentration and recovery of carbon dioxide from flue gas by pressure swing adsorption. Industrial & Engineering Chemistry Research 32 (11), 2714–2720.

[78] Kim, M.-B., Moon, J.-H., Lee, C.-H., Ahn, H., Cho, W., 2004. Effect of heat transfer on the transient dynamics of temperature swing adsorption process. Korean Journal of Chemical Engineering 21, 703–711.

[79] Ko, D., Siriwardane, R., Biegler, L. T., 2003. Optimization of a pressure-swing adsorption process using zeolite 13x for co2 sequestration. Industrial & Engineering Chemistry Research 42 (2), 339–348.

[80] Koroneos, C., Dompros, A., Roumbas, G., Moussiopoulos, N., 2004. Life cycle assessment of hydrogen fuel production processes. International Journal of Hydrogen Energy 29 (14), 1443 – 1450.

[81] Koros, W. J., Mahajan, R., 2000. Pushing the limits on possibilities for large scale gas separation: which strategies? Journal of Membrane Science 175 (2), 181 – 196.

[82] Krogstad, T., Gravdahl, J., Tøndel, P., june 2005. Explicit model predictive control of a satellite with magnetic torquers. In: Intelligent Control, 2005. Proceedings of the 2005 IEEE International Symposium on, Mediterrean Conference on Control and Automation. pp. 491 –496.

[83] Kumar, R., 1994. Pressure swing adsorption process: Performance optimum and adsorbent selection. Industrial & Engineering Chemistry Research 33 (6), 1600–1605.

[84] Kumar, R., Fox, V. G., Hartzog, D. G., Larson, R. E., Chen, Y. C., Houghton, P. A., Naheiri, T., 1994. A versatile process simulator for adsorptive separations. Chemical Engineering Science 49 (18), 3115 – 3125.

[85] Lee, C.-H., Yang, J., Ahn, H., 1999. Effects of carbon-to-zeolite ratio on layered bed H_2 psa for coke oven gas. AIChE Journal 45 (3), 535–545.

[86] Lenhoff, A. M., Morari, M., 1982. Design of resilient processing plants–i process design under consideration of dynamic aspects. Chemical Engineering Science 37 (2), 245 – 258.

[87] Lipták, B. G., 2006. Instrument engineers' handbook. Process control and optimization. Vol. 2. CRC Press.

[88] Ljung, L., 1987. System Identification: Theory for the User. PTR Prentice Hall.

[89] Ljung, L., 1994. Modeling of Dynamic Systems. PTR Prentice Hall.

[90] Luyben, M., Floudas, C., 1994. Analyzing the interaction of design and control–1. a multiobjective framework and application to binary distillation synthesis. Computers & Chemical Engineering 18 (10), 933 – 969, an International Journal of Computer Application in Chemical Engineering.

[91] Maciejowski, J. M., 2002. Predictive Control with Constraints. Pearson Education.

[92] Malcolm, A., Polan, J., Zhang, L., Ogunnaike, B. A., Linninger, A. A., 2007. Integrating systems design and control using dynamic flexibility analysis. AIChE Journal 53 (8), 2048–2061.

[93] Malek, A., Farooq, S., 1996. Comparison of isotherm models for hydrocarbon adsorption on activated carbon. AIChE Journal 42 (11), 3191–3201.

[94] Malek, A., Farooq, S., 1998. Hydrogen purification from refinery fuel gas by pressure swing adsorption. AIChE Journal 44 (9), 1985–1992.

[95] Martin, Pehnt, 2001. Life-cycle assessment of fuel cell stacks. International Journal of Hydrogen Energy 26 (1), 91 – 101.

[96] Mérel, J., Clausse, M., Meunier, F., 2006. Carbon dioxide capture by indirect thermal swing adsorption using 13x zeolite. Environmental Progress 25 (4), 327–333.

[97] Merel, J., Clausse, M., Meunier, F., 2008. Experimental investigation on co2 postcombustion capture by indirect thermal swing adsorption using 13x and 5a zeolites. Industrial & Engineering Chemistry Research 47 (1), 209–215.

[98] Mohideen, M. J., Perkins, J. D., Pistikopoulos, E. N., 1996. Optimal design of dynamic systems under uncertainty. AlChE Journal 42 (8), 2251–2272.

[99] Moon, J., Kim, S., Linninger, A. A., 2011. Integrated design and control under uncertainty: Embedded control optimization for plantwide processes. Computers & Chemical Engineering 35 (9), 1718 – 1724, energy Systems Engineering.

[100] Morari, M., 1983. Design of resilient processing plants–iii : A general framework for the assessment of dynamic resilience. Chemical Engineering Science 38 (11), 1881 – 1891.

[101] Na, B.-K., Lee, H., Koo, K.-K., Song, H. K., 2002. Effect of rinse and recycle methods on the pressure swing adsorption process to recover co2 from power plant flue gas using activated carbon. Industrial & Engineering Chemistry Research 41 (22), 5498–5503.

[102] Nikolic, D., Giovanoglou, A., Georgiadis, M. C., Kikkinides, E. S., 2008. Generic modeling framework for gas separations using multibed pressure swing adsorption processes. Industrial & Engineering Chemistry Research 47 (9), 3156–3169.

[103] Nikolić, D., Kikkinides, E. S., Georgiadis, M. C., 2009. Optimization of multibed pressure swing adsorption processes. Ind. Eng. Chem. Res. 48, 53885398.

[104] Nilchan, S., Pantelides, C., 1998. On the optimisation of periodic adsorption processes. Adsorption 4 (2), 113–147.

[105] Nishida, N., Ichikawa, A., 1975. Synthesis of optimal dynamic process sys-

tems by a gradient method. Industrial & Engineering Chemistry Process Design and Development 14 (3), 236–242.

[106] Nishida, N., Liu, Y. A., Ichikawa, A., 1976. Studies in chemical process design and synthesis ii. optimal synthesis of dynamic process systems with uncertainty. AIChE Journal 22 (3), 539–549.

[107] Nitta, T., Kuro-Oka, M., Katayama, T., 1984. An adsorption isotherm of multi-site occupancy model for heterogeneous surface. Journal of Chemical Engineering of Japan 17 (1), 45–52.

[108] Ogata, K., 1997. Modern control engineering. Prentice Hall.

[109] Olajossy, A., Gawdzik, A., Budner, Z., Dula, J., 2003. Methane separation from coal mine methane gas by vacuum pressure swing adsorption. Chemical Engineering Research and Design 81 (4), 474 – 482.

[110] Palazoglu, A., Arkun, Y., 1986. A multiobjective approach to design chemical plants with robust dynamic operability characteristics. Computers & Chemical Engineering 10 (6), 567 – 575.

[111] Panos, C., Kouramas, K., Georgiadis, M., Pistikopoulos, E., 2010. Dynamic optimization and robust explicit model predictive control of hydrogen storage tank. Computers & Chemical Engineering 34 (9), 1341 – 1347, selected papers from the 7th International Conference on the Foundations of Computer-Aided Process Design (FOCAPD, 2009, Breckenridge, Colorado, USA.

[112] Park, J.-H., Han, S.-S., Kim, J.-N., Cho, S.-H., 2004. Vacuum swing adsorption process for the separation of ethylene/ethane with $AgNO_3$/clay adsorbent. Korean Journal of Chemical Engineering 21, 236–245.

[113] Perkins, J. D., Walsh, S. P. K., 1996. Optimization as a tool for design/control integration. Computers & Chemical Engineering 20 (4), 315 – 323.

[114] Perry, R. H., Green, D. W., Maloney, J. O. (Eds.), 1997. Perry's chemical engineers' handbook. McGraw-Hill.

[115] Pezolt, D. J., Collick, S. J., Johnson, H. A., Robbins, L. A., 1997. Pressure swing adsorption for voc recovery at gasoline loading terminals. Environmental Progress 16 (1), 16–19.

[116] Pistikopoulos, E. N., August 2009. Perspectives in multiparametric programming and explicit model predictive control. AIChE Journal 55 (8), 1918 – 1925.

[117] Pistikopoulos, E. N., Bozinis, N. A., Dua, V., Perkins, J. D., Sakizlis, V., 2004. Improved process control. European Patent EP1399784.

[118] Pistikopoulos, E. N., Bozinis, N. A., Dua, V., Perkins, J. D., Sakizlis, V., 2008. Process control using co-ordinate space. United States Patent and Trademark Office Granted Patent No US7433743.

[119] Pistikopoulos, E. N., Dua, V., Bozinis, N. A., Bemporad, A., Morari, M., 2000. On-line optimization via off-line parametric optimization tools. Computers & Chemical Engineering 24 (2-7), 188 – 188.

[120] Pistikopoulos, E. N., Georgiadis, M. C., Dua, V., 2007. Mulit-Parametric Programming: Theory, Algorithms, and Applications. Vol. 1. Wiley-VCH.

[121] Pistikopoulos, E. N., Georgiadis, M. C., Dua, V., 2007. Multi-parametric Model-Based Control: Theory and Applications. Vol. 2. Wiley-VCH.

[122] POP, 2009. Parametric optimization solutions (ParOS) Ltd., parametric optimization programming (POP) toolbox. www.parostech.co.uk.

[123] Qin, S. J., Badgwell, T. A., 2003. A survey of industrial model predictive control technology. Control Engineering Practice 11 (7), 733 – 764.

[124] Rawlings, J., 2000. Tutorial overview of model predictive control. IEEE Control Systems Magazine 20 (3), 38–52.

[125] Rawlings, J. B., Mayne, D. Q., 2009. Model Predictive Control: Theory and Design. Nob Hill Publishing.

[126] Rege, S. U., Yang, R. T., 2002. Propane/propylene separation by pressure swing adsorption: sorbent comparison and multiplicity of cyclic steady states. Chemical Engineering Science 57 (7), 1139 – 1149.

[127] Rege, S. U., Yang, R. T., Qian, K., Buzanowski, M. A., 2001. Air-prepurification by pressure swing adsorption using single/layered beds. Chemical Engineering Science 56 (8), 2745 – 2759.

[128] Reynolds, S. P., Ebner, A. D., Ritter, J. A., 2005. New pressure swing adsorption cycles for carbon dioxide sequestration. Adsorption 11, 531–536.

[129] Ribeiro, A. M., Grande, C. A., Lopes, F. V., Loureiro, J. M., Rodrigues, A. E., 2008. A parametric study of layered bed psa for hydrogen purification. Chemical Engineering Science 63 (21), 5258 – 5273.

[130] Ricardez-Sandoval, L., Douglas, P., Budman, H., 2011. A methodology for the simultaneous design and control of large-scale systems under process parameter uncertainty. Computers & Chemical Engineering 35 (2), 307 – 318.

[131] Ricardez-Sandoval, L. A., Budman, H. M., Douglas, P. L., 2010. Simultaneous design and control: A new approach and comparisons with existing methodologies. Industrial & Engineering Chemistry Research 49 (6), 2822–2833.

[132] Ritter, J. A., Yang, R. T., 1991. Pressure swing adsorption: experimental and theoretical study on air purification and vapor recovery. Industrial & Engineering Chemistry Research 30 (5), 1023–1032.

[133] Rodrigues, A. E., Dias, M. M., 1998. Linear driving force approximation in cyclic adsorption processes: Simple results from system dynamics based on frequency response analysis. Chemical Engineering and Processing 37 (6), 489 – 502.

[134] Rodrigues, A. E., Loureiro, J. M., LeVan, M. D., 1991. Simulated pressurization of adsorption beds. Gas Separation & Purification 5 (2), 115 – 124.

[135] Romero-Hernandez, O., Pistikopoulos, E. N., Livingston, A. G., 1998. Waste treatment and optimal degree of pollution abatement. Environmental Progress 17 (4), 270–277.

[136] Rota, R., Wankat, P. C., 1990. Intensification of pressure swing adsorption processes. AIChE Journal 36 (9), 1299–1312.

[137] Ruthven, D. M., Farooq, S., Knaebel, K. S., 1994. Pressure Swing Adsorption. Wiley-VCH.

[138] Sakizlis, V., Perkins, J. D., Pistikopoulos, E. N., 2003. Parametric controllers in simultaneous process and control design optimization. Industrial & Engineering Chemistry Research 42 (20), 4545–4563.

[139] Sakizlis, V., Perkins, J. D., Pistikopoulos, E. N., 2004. Recent advances in optimization-based simultaneous process and control design. Computers & Chemical Engineering 28 (10), 2069 – 2086, special Issue for Professor Arthur W. Westerberg.

[140] Sato, M., Goto, M., Kodama, A., Hirose, T., 1998. New fractionation process for citrus oil by pressure swing adsorption in supercritical carbon dioxide. Chemical Engineering Science 53 (24), 4095 – 4104.

[141] Seader, J. D., 1998. Separation process principles. John Wiley & Sons, Inc.

[142] Seborg, D. E., Edgar, T. F., Mellichamp, D. A., 1989. Process Dynamics and Control. John Wiley & Sons.

[143] Seider, W. D., Seader, J., Lewin, D. R., 1999. Product and process design principles, 2nd Edition. John Wiley & Sons, Inc.

[144] Sereno, C., Rodrigues, A., 1993. Can steady-state momentum equations be used in modelling pressurization of adsorption beds? Gas Separation & Purification 7 (3), 167 – 174.

[145] Sircar, S., 1996. Production of oxy-rich air by rpsa for combustion use. Adsorption 2, 323–326.

[146] Sircar, S., 2002. Pressure swing adsorption. Industrial & Engineering Chemistry Research 41 (6), 1389–1392.

[147] Sircar, S., Hanley, B. F., 1995. Production of oxygen enriched air by rapid pressure swing adsorption. Adsorption 1, 313–320.

[148] Sircar, S., Hufton, J., 2000. Why does the linear driving force model for adsorption kinetics work? Adsorption 6, 137–147.

[149] Sircar, S., Waldron, W. E., Rao, M. B., Anand, M., 1999. Hydrogen production by hybrid smr-psa-ssf membrane system. Separation and Purification Technology 17 (1), 11 – 20.

[150] Skogestad, S., Morari, M., 1987. Effect of disturbance directions on closed-loop performance. Industrial & Engineering Chemistry Research 26 (10), 2029–2035.

[151] Smith, O. J., Westerberg, A. W., 1991. The optimal design of pressure swing adsorption systems. Chemical Engineering Science 46 (12), 2967 – 2976.

[152] Söderström, T., Stoica, P., 1989. System Indentification. Prentice Hall.

[153] Stefanis, S. K., Livingston, A., Pistikopoulos, E. N., 2001. Life cycle optimization. In: Wiley Encyclopedia of Electrical and Electronics Engineering. John Wiley & Sons, Inc.

[154] Stewart, A. B., Henzler, G. W., Leavitt, F. W., Notaro, F., Kane, M. S., February 2000. Psa apparatus and process using adsorbent mixtures. U.S. Patent Number US006027548A.

[155] Takamura, Y., Narita, S., Aoki, J., Hironaka, S., Uchida, S., 2001. Evaluation of dual-bed pressure swing adsorption for co2 recovery from boiler exhaust gas. Separation and Purification Technology 24 (3), 519 – 528.

[156] Todd, R. S., Webley, P. A., 2002. Limitations of the ldf/equimolar counterdiffusion assumption for mass transport within porous adsorbent pellets. Chemical Engineering Science 57 (19), 4227 – 4242.

[157] Torre, V. D. L., Fox, V. G., Bandoni, J. A., Biegler, L. T., 2005. Model

predictive controller for periodic adsorption processes. In: ENPROMER, 2^{nd} Mercosur Congress on Chemical Engineering 2005.

[158] Ulrich, G. D., 1984. A guide to chemical engineering process design and economics. John Wiley & Sons, Inc.

[159] Vassiliadis, V. S., Sargent, R. W. H., Pantelides, C. C., 1994. Solution of a class of multistage dynamic optimization problems. 1. problems without path constraints. Industrial & Engineering Chemistry Research 33 (9), 2111–2122.

[160] Vassiliadis, V. S., Sargent, R. W. H., Pantelides, C. C., 1994. Solution of a class of multistage dynamic optimization problems. 2. problems with path constraints. Industrial & Engineering Chemistry Research 33 (9), 2123–2133.

[161] Vinson, D. R., 2006. Air separation control technology. Computers & Chemical Engineering 30 (10-12), 1436 – 1446.

[162] Wakao, N., Funazkri, T., 1978. Effect of fluid dispersion coefficients on particle-to-fluid mass transfer coefficients in packed beds : Correlation of sherwood numbers. Chemical Engineering Science 33 (10), 1375 – 1384.

[163] Wakao, N., Kaguei, S., Funazkri, T., 1979. Effect of fluid dispersion coefficients on particle-to-fluid heat transfer coefficients in packed beds : Correlation of Nusselt numbers. Chemical Engineering Science 34 (3), 325 – 336.

[164] Walas, S. M., 1995. Chemical Process Equipment: Selection and Design. Butterworth-Heinemann Ltd.

[165] Waldron, W., Sircar, S., 2000. Parametric study of a pressure swing adsorption process. Adsorption 6 (2), 179–188.

[166] Wang, H., Goto, M., Sasaki, M., Hirose, T., 2004. Separation of α-tocopherol and squalene by pressure swing adsorption in supercritical carbon dioxide. Industrial & Engineering Chemistry Research 43 (11), 2753–2758.

[167] Warmuziński, K., Tańczyk, M., 1997. Multicomponent pressure swing adsorption part i. modelling of large-scale psa installations. Chemical Engineering and Processing 36 (2), 89 – 99.

[168] WEN, C. Y., YU, Y. H., 1966. A generalized method for predicting the minimum fluidization velocity. AIChE Journal 12 (3), 610–612.

[169] Westgate, P. J., Ladisch, M. R., 1993. Air drying using corn grits as the sorbent in a pressure swing adsorber. AIChE Journal 39 (4), 720–723.

[170] Whysall, M., Wagemans, L. J. M., April 2001. Very large-scale pressure swing adsorption processes. U.S. Patent Number 6210466B1.

[171] Yang, J., Lee, C.-H., 1998. Adsorption dynamics of a layered bed psa for H_2 recovery from coke oven gas. AIChE Journal 44 (6), 1325–1334.

[172] Yang, J., Lee, C.-H., Chang, J.-W., 1997. Separation of hydrogen mixtures by a two-bed pressure swing adsorption process using zeolite 5a. Industrial & Engineering Chemistry Research 36 (7), 2789–2798.

[173] Yang, J., Park, M.-W., Chang, J.-W., Ko, S.-M., Lee, C.-H., 1998. Effects of pressure drop in a psa process. Korean Journal of Chemical Engineering 15, 211–216.

[174] Yang, R. T., 1997. Gas Separation by Adsorption Processes. Imperial College Press.

[175] Yang, R. T., Doong, S. J., 1985. Gas separation by pressure swing adsorption: A pore-diffusion model for bulk separation. AIChE Journal 31 (11), 1829–1842.

[176] Yang, S.-I., Choi, D.-Y., Jang, S.-C., Kim, S.-H., Choi, D.-K., 2008. Hydrogen separation by multi-bed pressure swing adsorption ofsynthesis gas. Adsorption 14, 583–590.

[177] Yuan, Z., Chen, B., Zhao, J., 2011. An overview on controllability analysis of chemical processes. AIChE Journal 57 (5), 1185–1201.

[178] Zhang, R., Ritter, J. A., 1997. New approximate model for nonlinear adsorption and diffusion in a single particle. Chemical Engineering Science 52 (18), 3161 – 3172.

[179] Zhang, W. X., Yahiro, H., Mizuno, N., Iwamoto, M., Izumi, J., 1993. Silver ion-exchanged zeolites as highly effective adsorbents for removal of nox by pressure swing adsorption. Journal of Materials Science Letters 12, 1197–1198.

[180] Zhang, W. X., Yahiro, H., Mizuno, N., Izumi, J., Iwamoto, M., 1993. Removal of nitrogen monoxide on copper ion-exchanged zeolites by pressure swing adsorption. Langmuir 9 (9), 2337–2343.

[181] Zhu, L. Q., Tu, J. L., Shi, Y. J., 1991. Separation of CO—CO2—N_2 gas mixture for high-purity CO by pressure swing adsorption. Gas Separation & Purification 5 (3), 173 – 176.

[182] Zhu, Y., 2001. Multivariable System Identification for Process Control. Elsevier/Pergamon.

Appendix A

Derivation of The Energy Balance Equation

The overall energy energy balance assuming adiabatic bed conditions can be expressed as,

$$E_{accumulation} = E_{input} - E_{output} + E_{generation} \tag{A.1}$$

Here, the accumulation term represents the difference in the system energy levels between the time t and $t + \Delta t$, and can be mathematically represented as,

$$E_{accmulation} = E_{system}\big|_{t+\Delta t} - E_{system}\big|_{t} \tag{A.2}$$

The system energy value, under the assumption of negligible kinetic and potential energy effects can further be decomposed between the contributions from the gas phase, adsorbed phase, adsorbent phase and the bed walls as shown below,

$$E_{system}\big|_{t} = E_{gasphase}\big|_{t} + E_{adsorbedphase}\big|_{t} + E_{adsorbent}\big|_{t} + E_{wall}\big|_{t} \tag{A.3}$$

$$E_{gasphase}\Big|_t = (\epsilon_b + (1-\epsilon_b)\epsilon_p)\left[\sum_{i=1}^{N_{comp}} C_i C_{vi}\right] T A_{bed}\Delta z \tag{A.4}$$

$$E_{adsorbedphase}\Big|_t = \left[\sum_{i=1}^{N_{comp}} \overline{Q}_i C_{p_i}\right] T\rho_s(1-\epsilon_b) A_{bed}\Delta z \tag{A.5}$$

$$E_{adsorbent}\Big|_t = (1-\epsilon_b)\rho_s C_{p_s} T A_{bed}\Delta z \tag{A.6}$$

$$E_{wall}\Big|_t = D_{R_1}\rho_w C_{p_w} T\Delta z \tag{A.7}$$

The input and output term represents the amount of thermal energy entering and leaving the system in the axial direction for the lumped system under consideration, and can be represented as,

$$E_{input} = \left[\sum_{i=1}^{N_{comp}} C_i C_{p_i}\right] U T A_{bed}\Delta t\Big|_z \tag{A.8}$$

$$E_{output} = \left[\sum_{i=1}^{N_{comp}} C_i C_{p_i}\right] U T A_{bed}\Delta t\Big|_{z+\Delta z} \tag{A.9}$$

The amount of heat generated due to adsorption and desorption phenomena is expressed by the generation term shown below

$$E_{generation} = (1-\epsilon_b)\rho_s\left[\sum_{i=1}^{N_{comp}} (-\Delta H_i)\frac{\partial \overline{Q}_i}{\partial t}\right] A_{bed}\Delta z\Delta t \tag{A.10}$$

Putting equations A.4 to A.10 together along with $t + \Delta t$ counterparts of equations A.4, A.5, A.6, A.7 in Eq. A.1 and dividing the whole equation by $A_{bed}\Delta z\Delta t$ we get

$$
\begin{aligned}
&\epsilon_t \frac{\partial}{\partial t}\left(T\sum_{i=1}^{N_{comp}} C_i C_{vi}\right) + (1-\epsilon_b)\rho_s C_{p_s}\frac{\partial T}{\partial t} \\
&+\rho_s(1-\epsilon_b)\frac{\partial}{\partial t}\left(T\sum_{i=1}^{N_{comp}} \overline{Q}_i C_{p_i}\right) + D_{R_2}\rho_w C_{p_w}\frac{\partial T}{\partial t} \\
&+\frac{\partial}{\partial z}\left(UT\sum_{i=1}^{N_{comp}} C_i C_{p_i}\right) - (1-\epsilon_b)\rho_s\left[\sum_{i=1}^{N_{comp}}(-\Delta H_i)\frac{\partial \overline{Q}_i}{\partial t}\right] \\
&=\lambda\frac{\partial^2 T}{\partial z^2}
\end{aligned}
\tag{A.11}
$$

Here, ϵ_t and D_{R_2} are defined as

$$
\epsilon_t = \epsilon_b + (1-\epsilon_b)\epsilon_p \tag{A.12}
$$

$$
D_{R_2} = \left(1+\frac{\Delta d_w}{D}\right)^2 - 1 \tag{A.13}
$$

Next, we perform differentiation by parts on the first five terms of Eq. A.11 to separate the T differential terms from the rest to get the following equation,

$$
\begin{aligned}
&\left[\epsilon_t\frac{\partial}{\partial t}\sum_{i=1}^{N_{comp}} C_i C_{p_i} + \frac{\partial}{\partial z}\left(U\sum_{i=1}^{N_{comp}} C_i C_{p_i}\right) + (1-\epsilon_b)\rho_s\frac{\partial}{\partial t}\sum_{i=1}^{N_{comp}}\overline{Q}_i C_{p_i}\right] T \\
&\left[\epsilon_t\sum_{i=1}^{N_{comp}} C_i C_{v_i} + (1-\epsilon_b)\rho_s C_{p_s}\right]\frac{\partial T}{\partial t} \\
&+\left[\rho_s(1-\epsilon_b)\sum_{i=1}^{N_{comp}}\overline{Q}_i C_{p_i} + D_{R_2}\rho_w C_{p_w}\right]\frac{\partial T}{\partial t} \\
&-\left[U\sum_{i=1}^{N_{comp}} C_i C_{p_i}\right]\frac{\partial T}{\partial z} + \epsilon_t RT\frac{\partial C}{\partial t} - (1-\epsilon_b)\rho_s\sum_{i=1}^{N_{comp}}(-\Delta H_i)\frac{\partial \overline{Q}_i}{\partial t} \\
&=\lambda\frac{\partial^2 T}{\partial z^2}
\end{aligned}
\tag{A.14}
$$

Next, mass balance equation Eq. 3.3 is multiplied with individual C_p and summed over

$$\epsilon_t \frac{\partial}{\partial t} \sum_{i=1}^{N_{comp}} C_i C_{p_i} + \frac{\partial}{\partial z} \left(U \sum_{i=1}^{N_{comp}} C_i C_{p_i} \right) + (1-\epsilon_b)\rho_s \frac{\partial}{\partial t} \sum_{i=1}^{N_{comp}} \overline{Q}_i C_{p_i} = \epsilon_b D_z \frac{\partial}{\partial z} \sum_{i=1}^{N_{comp}} C y_i \tag{A.15}$$

Combining equations A.15 and A.16, and neglecting the mass dispersion term in the Eq. A.15 gives the final form of energy balance as

$$\begin{aligned} &\left[\epsilon_t \sum_{i=1}^{N_{comp}} C_i C_{v_i} + (1-\epsilon_b)\rho_s C_{p_s} \right] \frac{\partial T}{\partial t} \\ &+ \left[\rho_s (1-\epsilon_b) \sum_{i=1}^{N_{comp}} \overline{Q}_i C_{p_i} + D_{R_2} \rho_w C_{p_w} \right] \frac{\partial T}{\partial t} \\ &- \left[U \sum_{i=1}^{N_{comp}} C_i C_{p_i} \right] \frac{\partial T}{\partial z} + \epsilon_t RT \frac{\partial C}{\partial t} - (1-\epsilon_b)\rho_s \sum_{i=1}^{N_{comp}} (-\Delta H_i) \frac{\partial \overline{Q}_i}{\partial t} \\ &= \lambda \frac{\partial^2 T}{\partial z^2} \end{aligned} \tag{A.16}$$